

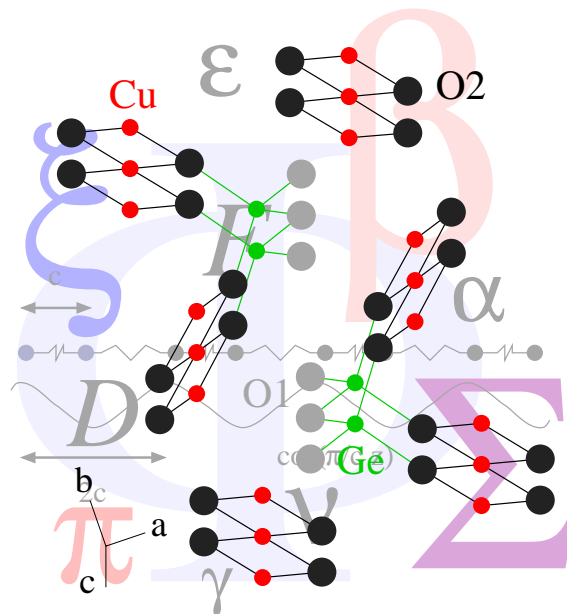
The spin-Peierls Transition in CuGeO_3

DISSERTATION

zur Erlangung des akademischen Grades eines
Doktors der Naturwissenschaften
des Fachbereichs Physik
der Universität Dortmund

vorgelegt von

Ralph Werner



Dortmund
1999

Copyright ©1999 Ralph Werner.
All rights reserved.

Publications based on excerpts from the thesis:

Chapter 6: R. Werner and C. Gros, Phys. Rev. B **57**, 2897 (1998).

Chapter 5: C. Gros and R. Werner, Phys. Rev. B **58**, R14677 (1998).

Chapter 2: R. Werner, C. Gros, and M. Braden, Phys. Rev. B **59**, 14356 (1999).

Printed as manuscript. Typset using L^AT_EX.

Dedicated to Liesel and Wendelin Werner

Acknowledgements

This work in its present form was made possible by the support I enjoyed in many ways. This is also true for the time before the beginning of the thesis. Many opportunities and experiences I was able to live through were made possible or supported through the efforts of others.

Most important is the psychological backup and the motivation especially in times when progress is rough. It is difficult for me to find here the right expressions of gratitude for all those involved. I hope I have been and will be able to show my appreciation at appropriate times.

I must thus content myself to underline the technical support which I enjoyed in the past three years. The intensive supervision of Prof. Gros in the course of the thesis led to the successful publication of many of the results presented here. His encouragement and support of the attendance of national and international conferences contributed largely to my education and motivation.

The atmosphere within the group of the chairs of theoretical condensed matter physics in Dortmund is an excellent basis for effective research and studying. Both Prof. Keiter and Prof. Weber were always available for clarifying and stimulating discussions. Prof. Stolze has been a constant source of valuable references in literature and scientific advice.

I will not list all the other members of the department who rendered with advice, support, discussion, and spreading good mood the institute a pleasant place to work at. I must mention though the instructive discussions with Nguyen Tri Lan on path integrals and with Stefan Feldkemper on the microscopic coupling constants.

I also do not attempt to give a list of people outside of Dortmund who I profited from through discussion, collaboration, and opportunities to present own results. These relations also were an important source of motivation and instructive beyond my own area of research which I am very thankful for.

I thank J. Drewniok and S. Kretzer for proofreading parts of the manuscript and T. Becker for illumination.

Contents

1	Introduction	1
1.1	Basic concept of structural phase transitions	1
1.2	The spin-Peierls transition	4
1.3	CuGeO ₃	5
1.4	Summary of the thesis	7
2	Lattice dynamics and spin-phonon coupling	12
2.1	Peierls-active phonon modes	13
2.2	Spin-phonon coupling term	17
2.2.1	Next nearest neighbor spin-phonon coupling	19
2.2.2	Coupling to bond angles and lengths	20
2.3	Normal-mode coupling constants	21
2.3.1	Ginzburg criterion	21
2.3.2	Mean-field approach	23
2.3.3	Values	24
2.4	Microscopic coupling constants	25
2.5	Static distortion	26
2.5.1	Dimerization	26
2.5.2	Pressure	28
2.5.3	Thermal expansion and spontaneous strain	29
2.6	Coupling constants for real-space normal coordinates	31
2.7	Discussion of χ_0	33
2.8	Summary	34
3	Partition function	35
3.1	Bose coherent states	36
3.2	Ordered phase	38
3.3	Fourier transform to Matsubara frequencies	40
3.3.1	Discrete transformation	41
3.3.2	Partition function of the unperturbed phonon system	43
3.3.3	Continuous transformation and problems involved	44

4	Mappings and approximations	47
4.1	Integrating out phonon degrees of freedom: effective spin models	47
4.1.1	Static limit	47
4.1.2	Static saddle point	49
4.1.3	Short remark on incommensurate ordering	50
4.1.4	Effective spin model with long range interaction	51
4.1.5	Limiting cases	52
4.1.6	Equivalence of dimer and distortion fields	54
4.2	Spin degrees of freedom: cumulant expansion	56
4.2.1	Random Phase Approximation (RPA)	56
4.2.2	Ordered phase	60
4.2.3	Static limit, mean-field results, and stability	62
4.3	Approaches to the spin system	65
4.3.1	Spinless Fermions	65
4.3.2	Dimer-dimer correlation function	67
4.3.3	Quantum criticality in CuGeO_3	69
5	Phonon dynamics	71
5.1	Normal-coordinate propagator in RPA	71
5.2	Phonon softening versus central peak	74
5.2.1	Isotropic case	75
5.2.2	Conduction electrons	77
5.2.3	Ising and XY limit	80
5.3	Application to CuGeO_3	81
5.3.1	Applicability of RPA	82
5.3.2	Magneto-elastic modes	85
5.3.3	Conclusions	87
6	Effective Ising model	88
6.1	Effective real-space mean-field dimer partition function	88
6.2	Mapping on an effective Ising model	90
6.2.1	Inclusion of the finite soliton width	92
6.2.2	Excitation energies	93
6.2.3	Landau expansion	94
6.3	Application to CuGeO_3	94
6.3.1	Self-consistency equation	96
6.3.2	Thermodynamics	96
6.3.3	Singlet-triplet gap	99
6.3.4	Conclusions	101
6.4	Appendix: discussion of related topics	101
6.4.1	Derivation from an electronic model	101
6.4.2	Critique: RPA versus Ising	102

Contents	iii
----------	-----

6.4.3 The Ising-Landau approach	103
---	-----

Bibliography	106
---------------------	------------

Chapter 1

Introduction

Structural phase transitions are an important area of research in solid state physics. An overview is given by Bruce and Cowley [1]. They are characterized by a spontaneous breaking of the lattice symmetry. Below the critical temperature the lattice undergoes a distortion enlarging the unit cell. Consequently such transitions are not only experimentally accessible through thermodynamic methods probing anomalies due to the critical behavior at the phase transition but also by spectroscopic methods such as X-ray or neutron diffraction. The interesting fact about CuGeO_3 is that a large number of different experimental methods have been applied. As I try to show with this work the number of data available made it possible to achieve a consistent understanding of the spin-Peierls transition in CuGeO_3 . Yet, a number of quantities are still controversial within certain boundaries. Where possible I try to propose approaches suited for further clarification.

In the introduction I wish to discuss the general physical concepts of structural phase transitions and the spin-Peierls transition as well as the fundamental experimental results showing the presence of such a phenomenon in CuGeO_3 . An overview of the thesis is given in section 1.4.

1.1 Basic concept of structural phase transitions

In a purely harmonic lattice no phase transition occurs. But no crystal is purely harmonic as can be seen from the presence of thermal expansion [2]. The harmonicity of a crystal lattice is induced by the many particle wave function including all electrons and atomic cores leading to potential wells binding the atoms to the fixed lattice sites. The standard approach to obtain a model describing a structural phase transition is to first identify those electronic degrees of freedom responsible for the anharmonicities in the binding potential. This will usually involve those electronic degrees of freedom close to the Fermi surface since they are the easiest to excite. They are described by some appropriate Hamiltonian H_e .

All the other electronic degrees of freedom contribute to the harmonic potential for the atoms. The atomic degrees of freedom are then described as decoupled harmonic

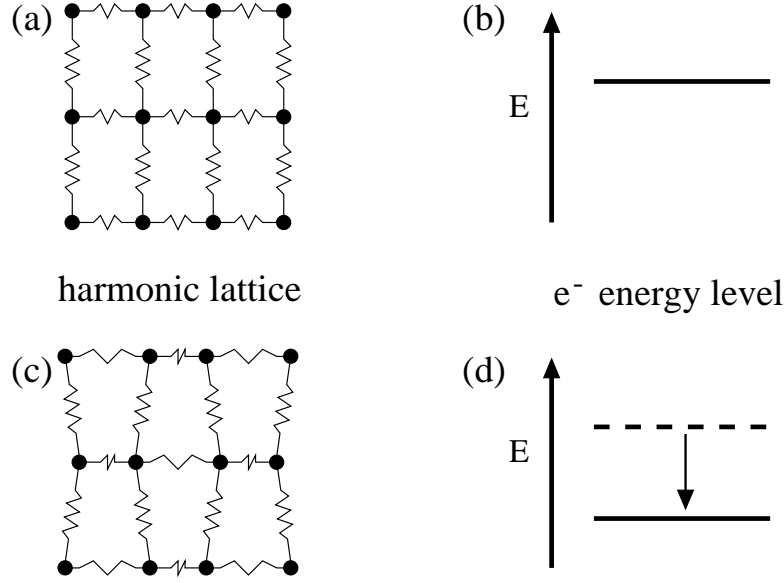


Figure 1.1: (a) *Harmonic lattice with linear restoring forces indicated by the zig-zag lines.* (b) *Energy level of the electronic system H_e .* (c) *Lattice distortion lowering the electronic energy via the coupling term (1.2) as shown in (d).*

oscillators.

$$H_p = \sum_q \Omega_q b_q^\dagger b_q \quad (1.1)$$

Ω_q is the eigenenergy of the quantum state q , b_q^\dagger and b_q are bosonic creation and annihilation operators. Such a model is derived explicitly from a microscopic picture for the relevant degrees of freedom in CuGeO_3 in section 2.1. The separated electronic degrees of freedom described by the Hamiltonian H_e usually couple to the harmonic degrees of freedom via their density operator $\hat{\rho}_e = \hat{\rho}_e^\dagger$.

$$H_{ep} = \sum_q [g_q b_q^\dagger + g_q^* b_q] \hat{\rho}_e(q) \quad (1.2)$$

g_q is a coupling constant.

The coupling term (1.2) is responsible for the anharmonic effects leading to a symmetry-broken ground state. figure 1.1 shows in part (a) a harmonic lattice with linear restoring forces indicated by the zig-zag lines. Part (b) shows the energy level of the electronic system H_e . A certain lattice distortion as depicted in figure 1.1 (c) may lower the electronic energy via the coupling term (1.2). If the resulting electronic energy gain shown in figure 1.1 (d) overcompensates the elastic energy loss, the ground state of the system is indeed distorted. In table 1.1 I give a list of different structural phase transitions with their relevant electronic degrees of freedom.

Another important feature of structural phase transitions is the appearance of spectral weight in the phononic structure factor for vanishing excitation energies when approaching

Phenomenon	Electronic degrees of freedom	Example for model used
Ferroelectrica	Coulomb energy of electronic dipoles	Ising model [1]
Jahn-Teller effect	Locally degenerate energy level	Ising model [3]
Peierls transition	Conduction band electrons	Phonon induced effective coulomb interaction (see section 4.1.5)
Spin-Peierls transition	Magnetic exchange	Heisenberg chains coupled to phonons

Table 1.1: *Different mechanism leading to structural phase transitions and their relevant electronic degrees of freedom.*

the phase transition. Such low energy excitations are responsible for the critical behavior of thermodynamic observables such as the specific heat and are connected to the appearance of Goldstone bosons at symmetry breaking phase transitions [4]. The lattice distortion below the structural phase transition enlarges the unit cell. The Brillouin zone is reduced accordingly giving rise to new acoustical modes at the zone centers of the reduced Zones. Those can be identified as the Goldstone modes corresponding to the reduced translational invariance of the lattice.

When approaching the transition from the high temperature phase there are usually precursors of the transition. They are either seen in the softening of a phonon mode or by the appearance of a central peak [1]. Typically one associates them with displacive and order-disorder transitions, respectively, even though there is no strict formal distinction between displacive and order-disorder transitions. I present in chapter 5 results showing that the random phase approximation (RPA) treatment of the spin- or electron-phonon coupling includes both scenarios. The central peak is shown to be caused by a new spin- or electron-phonon coupled mode growing soft.

I must note at this point that a description of the lattice by a harmonic part and a relevant electronic system which are coupled usually is not sufficient to describe all anharmonic effects. The thermal expansion, which also does not occur in harmonic systems, usually is described via the Grüneisen parameter in the so called quasi-harmonic approximation [2]. Still, it is possible to experimentally distinguish the quasi-harmonic effects from those driving the phase transition [5, 6]. For a close discussion in the case of CuGeO_3 see section 2.5.3.

1.2 The spin-Peierls transition

In the spin-Peierls transition the driving electronic degree of freedom is the unpaired spin of localized electrons coupled via the magnetic superexchange between ionic sites. If the exchange is spatially strongly anisotropic and of short range, the spin degrees of freedom are well described by the Hamiltonian of the nearest neighbor Heisenberg chain.

$$H_s^{\text{NN}} = J \sum_l \mathbf{S}_l \cdot \mathbf{S}_{l+\hat{z}} \quad (1.3)$$

The sum is taken over all magnetic ions, \mathbf{S}_l are the usual spin 1/2 vectorial operators with components

$$S_l^\alpha = \frac{1}{2} (c_{l\uparrow}^\dagger, c_{l\downarrow}^\dagger) \underline{\sigma}^\alpha \begin{pmatrix} c_{l\uparrow} \\ c_{l\downarrow} \end{pmatrix}, \quad (1.4)$$

where $c_{l\sigma}^\dagger$ and $c_{l\sigma}$ are fermionic creation and annihilation operators and $\underline{\sigma}^\alpha$ are the Pauli matrices with $\alpha \in \{x, y, z\}$. The chains run in z direction as shown in the schematic representation of such a chain in a crystal in figure 1.2 (a). The open circles indicate the moment carrying ions.

The spin model (1.3) is formed of independent chains as shown in figure 1.2 (b). It is Bethe ansatz solvable [7, 8] and ground state [9, 10], excitation spectrum [11], and thermodynamics [12] can be calculated.

An alternating lattice distortion as shown in figure 1.2 (c) will change the geometry of the superexchange path leading to an alternation in the magnetic exchange integral $J(1 \pm \delta_J)$. For antiferromagnetic exchange, i.e., $J > 0$ in equation (1.3), the consequence is a fundamental change in the physics of the spin system. The spectrum develops a gap and the ground state energy is lowered [13, 14, 15, 16]. A simple physical picture is that the stronger bonds $J(1 + \delta_J)$ form spin singlets requiring a finite energy to be excited to one of the triplet states. By analogy of the Heisenberg chain to an eight-vertex model [17] Black and Emery found the ground state to scale as $\delta_J^{4/3} / |\ln \delta_J|$ [18], which has been confirmed by numerical studies for $\delta_J < 0.05$ [15]. Above that value the logarithmic correction appears not to be present any more [16].

The lowering of the magnetic energy will overcompensate the elastic energy loss $\sim \delta_J^2$, so that indeed an ordered ground state is expected. As the temperature is raised, thermal excitations will break up singlet states leading to local relaxations of the lattice. As these relaxations become too numerous the ordering of the distortion will lose its coherence and a transition to a high temperature disordered phase occurs.

The spin-Peierls transition can thus be classified by an alternating lattice distortion, the opening of a gap in the magnetic spectrum, and quasi one-dimensional magnetic behavior in the disordered phase.

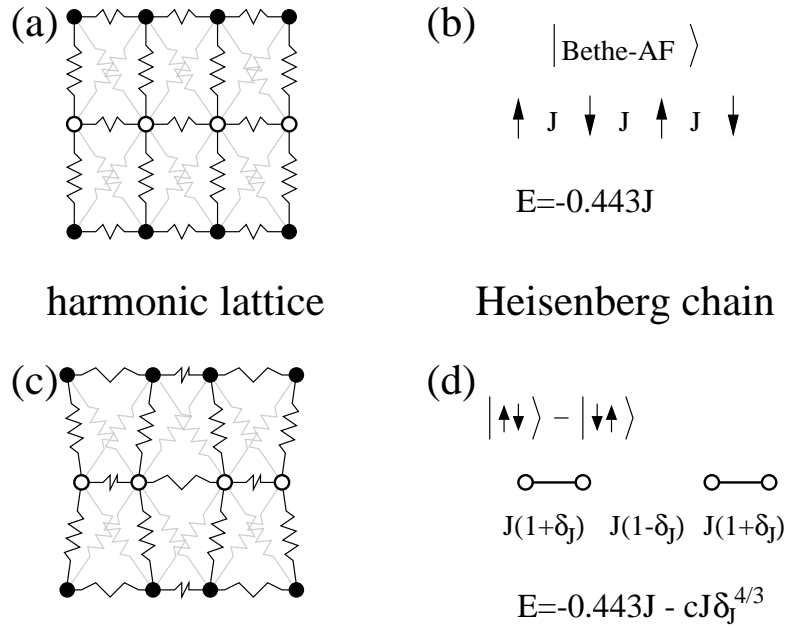


Figure 1.2: (a) Harmonic lattice with a chain of ions carrying magnetic moments (open circles). (b) Antiferromagnetic spin chain with exchange J and ground state energy E . (c) Spin-Peierls lattice distortion leading to the magnetic exchange alternation. (d) Alternating spin chain. Bond lines indicate the formation of singlets, referred to as dimerization. E is — up to logarithmic corrections — the lowered ground state energy.

1.3 CuGeO₃

In 1993 Hase and co-workers [19] measured the magnetic susceptibility of CuGeO₃ and found an exponential drop below ~ 14 K indicating the opening of a spin gap. Neutron scattering experiments confirmed the opening of a gap in the magnetic spectrum [20] and showed the quasi one-dimensionality via the strongly anisotropic dispersion of the magnetic excitations [21]. At the same time the appearance of spontaneous strain was observed [20] which couples to the square of an alternating lattice order parameter [1]. The consistence of the strain coupling to the spin-Peierls order parameter has been shown latter very nicely [5]. The appearance of superlattice reflections in inelastic neutron scattering experiments has been observed shortly after [22] indicating the quadrupling of the unit cell.

The magnetic susceptibility has been shown to be well described by a Heisenberg chain with next nearest neighbor interaction [23, 24].

$$H_s = J \sum_l \mathbf{S}_l \cdot \mathbf{S}_{l+\hat{z}} + J_2 \sum_l \mathbf{S}_l \cdot \mathbf{S}_{l+2\hat{z}} \quad (1.5)$$

The exchange integrals J and J_2 denote nearest neighbor (NN) and next nearest neighbor (NNN) interaction, respectively. This confirms the quasi one-dimensional character of the material as well as the magnetic spectrum measured by Arai and co-workers [25]. The inverse correlation length measured by Schoeffel *et al.* [26] also shows dominant correlations

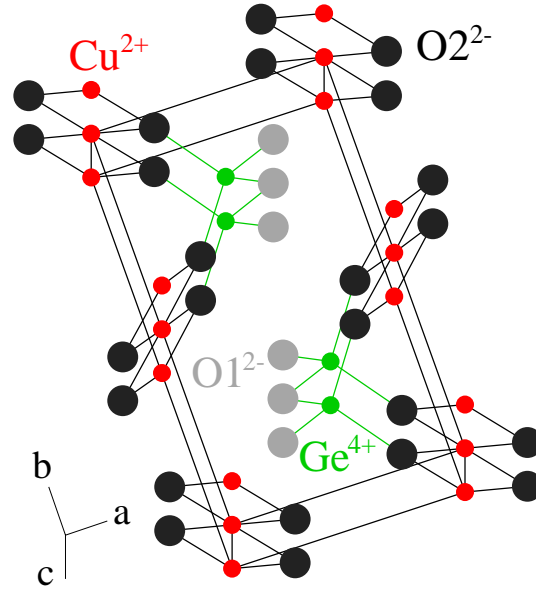


Figure 1.3: Crystal structure of CuGeO_3 . The crystal is constructed of CuO_2 ribbons connected via GeO_4 tetrahedra. The Cu^{2+} ions in $3d^9$ configuration form antiferromagnetic spin $1/2$ chains in c direction. There are two different types of O^{2-} ions shown in black (O_2) and gray (O_1). The Ge^{4+} ions connect adjacent CuO_2 ribbons. The lattice parameters of the orthorhombic unit cell are $a = 4.8 \text{ \AA}$, $b = 8.4 \text{ \AA}$, and $c = 2.9 \text{ \AA}$.

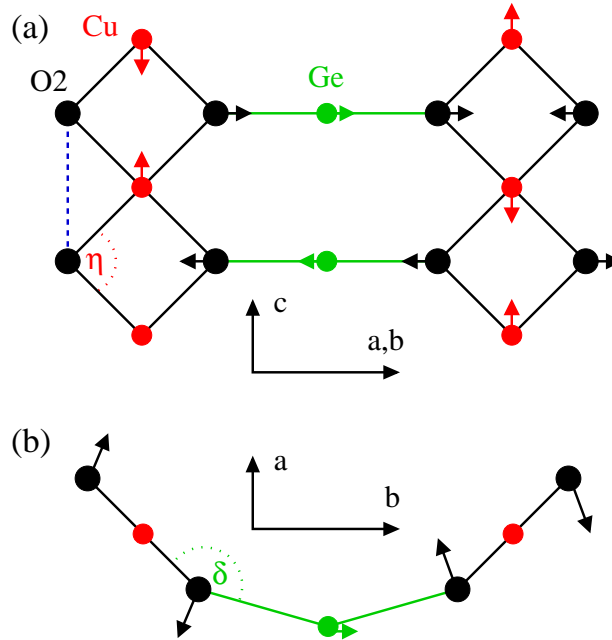


Figure 1.4: (a) Projection of the CuO_2 ribbons in the a/b - c plane. (b) Projection in the a - b plane. The nearest neighbor superexchange path is $\text{Cu-O}_2\text{-Cu}$ via the angle $\eta \sim 99^\circ$, the dashed line indicates the next nearest neighbor superexchange path. The arrows show the distortion in the ordered phase [40]. The values are given in table 1.2.

$ r_{\text{Cu}}^c $	$ r_{\text{Ge}}^b $	$ r_{\text{O}_2}^a $	$ r_{\text{O}_2}^b $
0.0056 Å	0.0008 Å	0.0095 Å	0.0065 Å
$\Delta\eta$	$\Delta\delta$	$\Delta\overline{\text{CuO}_2}$	$\Delta\overline{\text{GeO}_2}$
0.4°	0.8°	0.0029 Å	0.0008 Å

Table 1.2: *Ionic elongations and alternation of the angels* $\Delta\eta = \eta_{\text{max}} - \eta_{\text{min}}$, $\Delta\delta = \delta_{\text{max}} - \delta_{\text{min}}$ and *bond lengths* $\Delta\overline{\text{CuO}_2} = (\overline{\text{CuO}_2})_{\text{max}} - (\overline{\text{CuO}_2})_{\text{min}}$, $\Delta\overline{\text{GeO}_2} = (\overline{\text{GeO}_2})_{\text{max}} - (\overline{\text{GeO}_2})_{\text{min}}$ in the ordered phase as taken from references [40] and [44]. The distortions are three orders of magnitude smaller than the lattice constants.

along the crystallographic c axis. The magnetic spectrum in the gaped phase obtained by neutron scattering [21, 27, 28, 29, 30] and Raman scattering experiments [31, 32, 33] can also be described by one-dimensional models [34, 23, 35, 36, 37, 38, 39]. Thus CuGeO_3 qualifies as a spin-Peierls substance.

The crystal structure is shown in figure 1.3 [40] and has been determined already back in 1967 [41]. The space group is $Pbmm$. The crystal is constructed of CuO_2 ribbons connected via GeO_4 tetrahedra. The Cu^{2+} ions are in $3d^9$ configuration and carry a spin 1/2 [42]. They form antiferromagnetic spin chains along the c axis. The lattice parameters of the orthorhombic unit cell are $a = 4.8$ Å, $b = 8.4$ Å, and $c = 2.9$ Å. In figure 1.4 (a) the projection of the CuO_2 ribbons in the a/b - c plane is shown. The Cu-O-Cu superexchange path via the angle $\eta \sim 99^\circ$ leads to a much smaller antiferromagnetic exchange than in materials with collinear Cu-O-Cu configurations due to the orthogonality of the oxygen p_x and p_y orbitals [43, 40]. The dashed line in figure 1.4 (a) shows the next nearest neighbor superexchange path. Comparison of numerical results with the experimentally observed susceptibility gives values of $J = 150$ K for $J_2/J = 0.24$ [23] and $J = 160$ K for $J_2/J = 0.36$ [24]. The correct value of J_2/J is still controversial. A discussion including the relevance of the parameters for the here presented work is given in section 2.7.

The distortion of the lattice in the ordered phase is indicated by the arrows in figure 1.4 (a) and (b). Chapter 2 is dedicated to the detailed description of the alternation of the exchange integral J resulting from the alternation of the superexchange path geometry. The ionic displacements involve four degrees of freedom quantified in table 1.2 together with the corresponding alternation of the angles δ and η and the alternation of the bond lengths $\overline{\text{CuO}_2}$ and $\overline{\text{GeO}_2}$ relevant for the superexchange path. The modulation of the distortion in reciprocal space is $\mathbf{q}_0 = (\pi/a, 0, \pi/c)$, the space group in the ordered phase is $Bbcm$ [40].

1.4 Summary of the thesis

The overall structure of the thesis is to first derive an appropriate model for the description of the spin-Peierls phenomenon using the example of CuGeO_3 in chapter 2. I verify the

applicability of the model regarding static effects using simple standard many-particle methods. I then turn to the formulation of a field-theoretical approach to the partition function in chapter 3. The partition function contains all the information of the system. In chapter 4 I use the formulation of the partition function to discuss a series of approximations used for the description of spin- and electron-phonon coupled systems. Next the effect of the spin-phonon coupling on the phonon dynamics is studied in chapter 5. Finally the topic of thermodynamics in the ordered phase is addressed via a phenomenological model in chapter 6.

Lattice dynamics and spin-phonon coupling

Starting from the microscopic structure of CuGeO_3 an appropriate Hamiltonian for the description of the spin-phonon coupled system is derived using standard harmonic theory. It is possible to limit the spin-phonon coupling term on the description of the relevant degrees of freedom determined spectroscopically. These are the in real space the four elongations of the ions in the lattice involved in the spin-Peierls distortion. In reciprocal space they are given by the four Peierls-active phonon modes that form an irreducible subgroup of the 30 modes in CuGeO_3 at the high symmetry point of the Brillouin zone that corresponds to the spin-Peierls modulation.

Application of the Ginzburg criterion shows the critical region to be of the order of 3K around the transition justifying the application of RPA and mean-field theories. Using RPA results, mean field theory, and the polarization vectors, the coupling constants of the four Peierls-active phonon modes to the spin chains are determined. They are found to be of the order of $J/10$ to $J/2$. The coupling of the mode with the polarization pattern closest to the spin-Peierls distortion is dominant.

The explicit derivation of the Hamiltonian gives directly a relation between the coupling constants for the in real-space degrees of freedom and the reciprocal-space degrees of freedom. I thus obtain the values of the parameters describing the coupling of the spin system to the linear ionic displacements, the bond lengths, and the angles between bonds. The coupling to the Cu-O-Cu angle η is clearly dominant. From the coupling constants the effect of static lattice distortions on the spin system can be predicted. The effect has been studied experimentally by measuring the pressure dependence of the magnetic properties and the magnetic field dependence of the lattice parameters. The theoretical values are consistent with various experimental results. The thermal expansion of the c axis shows an anomaly in CuGeO_3 which can be understood in terms of the microscopic coupling constants. The effect of spontaneous strain appearing at the phase transition is shown to be small compared with the spin-Peierls distortion.

I explicitly make predictions for the alternation of the magnetic exchange, which is discussed rather controversially in the literature. The value obtained is rather large and about $J/10$. A rigorous lower boundary for the exchange alternation of $J/25$ rules out a number of results obtained from models approximating the phonons as a static distortion. Some physical quantities might be influenced significantly by the dynamics of the phonons. I show the connection of the reciprocal-space Hamiltonian to one-dimensional real-space

models which are used in the literature to study the effect of dynamical phonons on the spin system.

A serious problem for the quantitative study of spin-Peierls materials is the analysis of the underlying spin system. I discuss in which way the connected uncertainties might influence the results presented.

Partition function

I derive a path-integral representation for the partition function of the spin-phonon coupled Hamiltonian using Bose coherent states. It is a preliminary chapter discussing technical details of the derivation of the representation of the partition function used in the subsequent chapters. The transformation to the Fourier representation introducing Matsubara frequencies is discussed in detail. The emphasis lies on the problems involved when taking the continuum limit of the Trotter times initially defined on a discrete lattice. The outcome is essentially that the application of the continuum limit is practical if the necessary care is applied.

Mappings and approximations

A rigorous determination of the partition function derived in chapter 3 is not possible. Mappings to other representations or limiting cases allow some insight into the physics and the interdependence of problems.

Applying a static approximation to the partition function directly yields the model where a static lattice distortion couples to the spin system. The ground state properties of the resulting alternating-exchange spin model have been studied intensively. Finite temperature density matrix renormalization group studies (DMRG) give access to the thermodynamical properties. Within the model entropy and magnetic susceptibility of CuGeO_3 can be well described predicting a next nearest neighbor frustration of $J_2/J = 0.35$. I discuss briefly the problems and discrepancies involved in these approaches. In this context the incommensurate phase appearing in an external field in CuGeO_3 finds mentioning.

The phonon fields introduced by the introduction of the Bose coherent states can be integrated out yielding an effective spin model with dynamical (frequency or time dependent) interaction. Such interactions are well known in theories for electron-phonon coupling. Examples are conventional superconductivity and Peierls transitions. When the spin system is Ising-like the interaction is static and corresponding effective models studied in the literature are readily reproduced. Re-introducing Bose fields via a Hubbard-Stratonovich transformation shows that phonon fields and spin-pair or dimer fields are identical up to an arbitrary scaling factor.

The integration of the spin degrees of freedom is the most difficult problem. I introduce a cumulant expansion up to second order in the dimer operators and in the phonon fields yielding an effective action. In the disordered phase the (dynamical) saddle point solutions

obtained from minimizing the effective action are identical to the real poles of the normal-coordinate propagator used in chapter 5 to describe the dynamics of the spin-phonon coupled system. The RPA equation for the transition temperature is derived as it is used in chapter 2.

The introduction of shifted phonon fields allows an equivalent second-order cumulant expansion in the ordered phase as in the disordered case. I derive the stability conditions. Comparing results from the literature show the expansion to be stable. The broken translational invariance in the ordered phase and the resulting loss of conservation of momentum leads to a coupling of Brillouin zone center phonons to zone boundary phonons via the dimer-dimer correlation function. The static saddle point yields the mean-field equation relating the macroscopic occupation of the Peierls-active phonon modes and the coupling constants. This is used in chapter 2 to determine the values of the latter. I propose a method for estimating the importance of Gaussian fluctuations.

Finally I discuss the approaches used in the literature for solving of the spin part of the systems and present results for the correlation functions. I discuss the limits of the approximations used. Indications of quantum criticality in CuGeO_3 are shown by probing the scale invariance of the magnetic excitation spectrum.

Phonon dynamics

The influence of the spin-phonon coupling on the lattice dynamics is studied by regarding the normal-coordinate propagator. The latter is derived via a standard perturbative approach in RPA.

First limiting the description to a single mode coupling to the spin system I show that within the bosonization approach to the dimer-dimer correlation function a *soft phonon* occurs only if for the phonon frequency of the unperturbed system $\hbar\Omega_{\mathbf{q}_0} < 2.2 k_B T_{\text{SP}}$ is valid. T_{SP} is the transition temperature, \hbar is Planck's constant divided by 2π , and k_B is Boltzmann's constant. A soft phonon is characterized by a renormalization of the frequency of the eigenmode of the system due to the coupling to the spin-degrees of freedom such that the frequency is lowered with decreasing temperature. The frequency vanishes at the phase transition. For larger phonon frequencies $\Omega_{\mathbf{q}_0}$ even phonon hardening may occur and the transition is driven by a new magneto-elastic mode leading to a so called *central peak*. This result does not depend on the specific electronic system as can be seen by considering conduction electrons in a half-filled cosine band coupling to the phonon. The relevant density-density correlation function is then described by the Lindhard formula. For a band width of $2J$ and a transition temperature of $J/(10 k_B)$ a soft phonon is obtained for $\hbar\Omega_{\mathbf{q}_0} < 0.8J$. Results for the XY model are in qualitative agreement.

Generalization to four phonon modes shows CuGeO_3 in the central peak regime and the calculated temperature dependence of the Peierls-active phonon modes is in good agreement with experiment. A central peak of a width ~ 0.2 meV is predicted at T_{SP} . Good agreement is found between theory and experiment for the pre-transitional Peierls-fluctuations justifying the RPA approach.

Effective Ising model

In an alternative approach I map the elementary excitations (solitons) of the dimerized chain on an effective Ising model. Phonon induced interchain coupling then introduces a linear binding potential between a pair of soliton and anti-soliton, leading to a finite transition temperature. I evaluate, as a function of temperature, the order parameter, the singlet-triplet gap, the specific heat, and the susceptibility and compare with experimental data on CuGeO_3 . CuGeO_3 is found close to a first-order phase transition. Introducing the experimentally determined soliton width to the description a rough quantitative agreement with experiment is obtained. The famous scaling law $\sim \delta^{2/3}$ of the triplet gap can be interpreted as a simple consequence of the linear binding potential between pairs of solitons and anti-solitons in dimerized spin chains.

Finally I discuss effects from magnetic interchain coupling, the connection between the real-space Ising model and RPA, and I give a derivation of the Ising-like Landau-Ginzburg approach often used in the literature for the description of quasi one-dimensional systems.

Chapter 2

Lattice dynamics and spin-phonon coupling

Braden *et al.* [44] acquired detailed data on the phonon dispersions in CuGeO_3 . Using a shell model they have determined the polarization pattern of the lattice-vibrational eigenmodes. It is then possible to identify the four modes with the symmetry of the spin-Peierls lattice distortion. Limiting myself to those relevant degrees of freedom I derive in this chapter the appropriate Hamiltonian for CuGeO_3 by treating the lattice with the standard harmonic theory. Including the spin-phonon coupling mean-field like, I calculate the microscopic coupling constants between the lattice and the spin chains. It is then possible to predict the effect of structural changes on the spin system, namely the antiferromagnetic exchange J . The latter has been subject to various experimental [45, 46, 47, 48, 49] and theoretical studies [23, 34, 35, 43, 40, 38, 50].

As has been motivated in the introduction, the microscopic three-dimensional Hamiltonian I have to consider consists of three parts.

$$H = H_s + H_p + H_{sp} \quad (2.1)$$

I recall that the Heisenberg spin Hamiltonian given in equation (1.5) is

$$H_s = J \sum_l \mathbf{S}_l \cdot \mathbf{S}_{l+\hat{z}} + J_2 \sum_l \mathbf{S}_l \cdot \mathbf{S}_{l+2\hat{z}}, \quad (2.2)$$

where the exchange integrals J and J_2 denote nearest neighbor (NN) and next nearest neighbor (NNN) interaction, respectively.

Further I distinguish the phonon part

$$H_p = \sum_{\substack{\mathbf{n} \\ \nu, \alpha}} \frac{(p_{\mathbf{n}, \nu}^\alpha)^2}{2m_\nu} + \sum_{\substack{\mathbf{n}, \mathbf{n}' \\ \nu, \nu', \alpha, \alpha'}} \Phi_{\mathbf{n}, \mathbf{n}', \nu, \nu'}^{\alpha, \alpha'} r_{\mathbf{n}, \nu}^\alpha r_{\mathbf{n}', \nu'}^{\alpha'} \quad (2.3)$$

describing the lattice vibrations in harmonic approximation, where $\mathbf{r}_{\mathbf{n}, \nu} = (r_{\mathbf{n}, \nu}^x, r_{\mathbf{n}, \nu}^y, r_{\mathbf{n}, \nu}^z)$ are the deviations from the ionic equilibrium positions.

Finally the spin-phonon coupling term reads

$$H_{sp} = \sum_l \Delta J_{l,l+\hat{z}} \mathbf{S}_l \cdot \mathbf{S}_{l+\hat{z}} + \sum_l \Delta J_{l,l+2\hat{z}} \mathbf{S}_l \cdot \mathbf{S}_{l+2\hat{z}}. \quad (2.4)$$

The energy scale $\Delta J_{l,l+\hat{z}}$ is a function of the variation of the magnetic exchange integral with the atomic displacements $g_{l,\nu}^\alpha = \partial J / \partial r_{l,\nu}^\alpha$ to be discussed in section 2.2. The NNN term $\Delta J_{l,l+2\hat{z}}$ is a function of $\partial J_2 / \partial r_{l,\nu}^\alpha$.

The indices used are $\mathbf{n} = (n_x, n_y, n_z) \in \mathcal{Z}^3$ running over all unit cells of the three-dimensional crystal, the Cu-site index $\mathbf{l} = (l_x, l_y, l_z) \in \mathcal{Z}^3$ (2 Cu sites per unit cell), and the unit vectors $\hat{x} = (1, 0, 0)$, $\hat{y} = (0, 1, 0)$, and $\hat{z} = (0, 0, 1)$ to nearest neighbor unit cells in the corresponding direction. The index ν labels the 10 atoms within a unit cell as shown in figure 2.1 and $\alpha \in \{x, y, z\}$ is the vectorial component of the indexed quantity in the respective three-dimensional space.

In section 2.1 I briefly summarize the diagonalization of the phonon Hamiltonian (2.3) followed by the discussion of the symmetry of the four Peierls-active phonon modes, including refined data for their polarization vectors. Using these symmetries I transform in section 2.2 the microscopic spin-phonon coupling Hamiltonian (2.4) to normal coordinates in reciprocal space. This procedure yields relations between the different linear, angular and normal-mode coupling constants. Using RPA results and mean-field theory in section 2.3 I obtain numerical values for the normal-mode coupling constants which then can be converted to the real-space coupling constants. The resulting dependence of the magnetic exchange on static distortion of the lattice is discussed in section 2.5 and compared with values from the literature. Finally I derive an effective one-dimensional model to give coupling constants consistent with frequently applied theoretical approaches. The consistency of the different results gives a *à posteriori* justification of the mean-field approach.

2.1 Peierls-active phonon modes

In the standard treatment of harmonic lattice dynamics the initial problem of $3 \cdot N \cdot N_{\text{ion}}$ degrees of freedom (N number of unit cells, N_{ion} number of ions in the unit cell) is transformed into reciprocal space by Fourier transformation, where N wave vectors fulfil the periodic boundary condition [51]. For any fixed wave vector one obtains a $3 \cdot N_{\text{ion}}$ -dimensional problem which may be diagonalized, resulting in a set of $3 \cdot N_{\text{ion}}$ eigenmodes labelled by $\lambda \in \{1, \dots, 3N_{\text{ion}}\}$. On that purpose the displacement and momentum operators are decomposed into eigenmode contributions introducing normal coordinates Q and conjugate momenta P .

$$\mathbf{r}_{\mathbf{n},\nu} =: \frac{1}{\sqrt{N}} \sum_{\mathbf{q}} e^{i\mathbf{q}\mathbf{R}_{\mathbf{n}}} \sum_{\lambda} \frac{\mathbf{e}_{\nu}(\lambda, \mathbf{q})}{\sqrt{m_{\nu}}} Q_{\lambda, \mathbf{q}} \quad (2.5)$$

$$\mathbf{p}_{\mathbf{n},\nu} =: \frac{1}{\sqrt{N}} \sum_{\mathbf{q}} e^{i\mathbf{q}\mathbf{R}_{\mathbf{n}}} \sum_{\lambda} \mathbf{e}_{\nu}(\lambda, \mathbf{q}) \sqrt{m_{\nu}} P_{\lambda, \mathbf{q}} \quad (2.6)$$

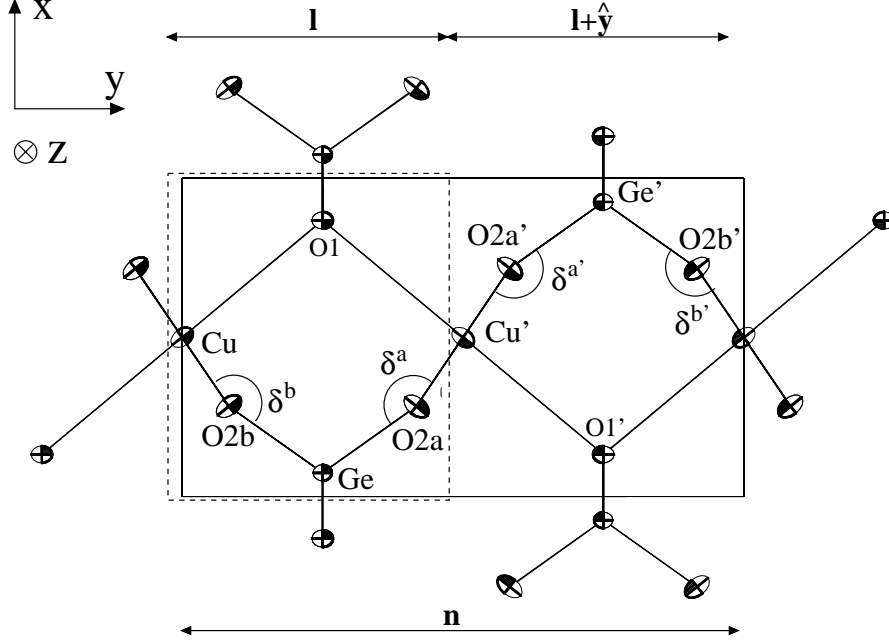


Figure 2.1: Projection of the unit cell of CuGeO_3 on the x - y plane. The oxygen atoms are distinguished into $O1$, $O2a$, and $O2b$, the atoms of the second formula unit are labelled with a prime. Each unit cell contains two Cu chains in z direction (positive z direction is into the plane). The broken lines show the reduced unit cell introduced in section 2.2. \mathbf{n} is the index for the whole cells, \mathbf{l} indexes the reduced cells.

The vectors \mathbf{R}_n designate the coordinates of the unit cell origins. m_ν is the mass of the ν -th atom and \mathbf{e}_ν are polarization vectors. Note that I use a non-standard definition for \mathbf{R}_n and $\mathbf{e}_\nu(\lambda, \mathbf{q})$ which will simplify the interpretation of the polarization vectors at high symmetry points in the Brillouin zone. Further transformation to boson creation and annihilation operator representation via

$$Q_{\lambda, \mathbf{q}} = \sqrt{\frac{\hbar}{2\Omega_{\lambda, \mathbf{q}}}} \left(b_{\lambda, -\mathbf{q}}^\dagger + b_{\lambda, \mathbf{q}} \right) \quad (2.7)$$

and

$$P_{\lambda, \mathbf{q}} = i\sqrt{\frac{\hbar\Omega_{\lambda, \mathbf{q}}}{2}} \left(b_{\lambda, -\mathbf{q}}^\dagger - b_{\lambda, \mathbf{q}} \right) \quad (2.8)$$

yields the Hamiltonian usually used in the theoretical treatment of the lattice vibrations.

$$H_p = \sum_{\lambda, \mathbf{q}} \hbar\Omega_{\lambda, \mathbf{q}} \left(b_{\lambda, \mathbf{q}}^\dagger b_{\lambda, \mathbf{q}} + \frac{1}{2} \right) \quad (2.9)$$

λ	1	2	3	4
$\Omega_\lambda/(2\pi)$	3.12 THz	6.53 THz	11.1 THz	24.6 THz
$u e_{\text{Cu}}^z(\lambda)/\sqrt{m_{\text{Cu}}}$	0.0095	-0.4790	0.7412	-0.0888
$u e_{\text{Ge}}^y(\lambda)/\sqrt{m_{\text{Ge}}}$	-0.4330	-0.5325	-0.3698	-0.2605
$u e_{\text{O2b}}^x(\lambda)/\sqrt{m_{\text{O2}}}$	-0.6212	0.6581	0.3382	-0.7932
$u e_{\text{O2b}}^y(\lambda)/\sqrt{m_{\text{O2}}}$	-0.8620	0.1339	0.2021	0.8723

Table 2.1: *Frequencies and polarization of the Peierls-active T_2^+ phonon modes at room temperature. The global prefactor is given by $u^2 = (8.26 \pm 0.02) \cdot 10^{-26}$ kg. The notation is $e_\nu^z(\lambda, \mathbf{q}_0) \equiv e_\nu^z(\lambda)$.*

With the experimentally determined phonon modes $\Omega_{\lambda, \mathbf{q}}$ and shell model calculations it is possible to determine the components of the polarization vectors $\mathbf{e}_\nu(\lambda, \mathbf{q})$ [44]. At the wave vector of the Peierls instability $\mathbf{q}_0 = (\pi/a, 0, \pi/c)$ four of the 30 modes correspond to the irreducible representation with the symmetry of the lattice distortion in the spin-Peierls phase, T_2^+ in the notation of reference [52]. $a = 4.8 \text{ \AA}$, $b = 8.5 \text{ \AA}$, and $c = 2.9 \text{ \AA}$ are the lengths of the unit cell in x , y , and z direction, respectively.

Adapting the lattice dynamical model presented in reference [44] a special effort was made for the description of the spin-Peierls relevant modes by the introduction of additional force constants [53]. The T_2^+ modes are characterized by displacements of the Cu ions along c , of the O2 sites along a and b , and of the Ge ions along b . The polarization patterns of the four modes as obtained by the shell model are represented in figure 2.2 and given together with their frequencies in table 2.1. The highest T_2^+ mode corresponds to a Ge-O bond stretching vibration thereby explaining its elevated frequency. The three T_2^+ modes at lower energies possess a common element which consists in the rotation of the O2-O2 edges of the CuO_4 plaquettes in the x - y plane around the c axis. However, only for the lowest mode this twisting of the CuO_2 ribbons describes the main character of the polarization pattern. The modes at 11 and at 6.5 THz show in addition a modulation of the lengths of the O2-O2 edges and a Cu shift parallel c . For the 11 THz mode the displacements of the Cu ions modulate the O2-Cu bond distance. The 6.5 THz mode is characterized by a strong modulation of the Cu-O2-Cu bond angle (see figure 2.2) which is essential for the magnetic interaction.

For later use I define the Matrix \mathbf{M} with the elements given by $e_\nu^\alpha(\lambda, \mathbf{q}_0)/\sqrt{m_\nu}$ extracted from table 2.1.

$$\mathbf{M} = \begin{pmatrix} 0.03 & -1.67 & 2.58 & -0.31 \\ -1.51 & -1.85 & -1.29 & -0.91 \\ -2.16 & 2.29 & 1.18 & -2.76 \\ -3.00 & 0.47 & 0.70 & 3.04 \end{pmatrix} \frac{10^{12}}{\sqrt{\text{kg}}} \quad (2.10)$$

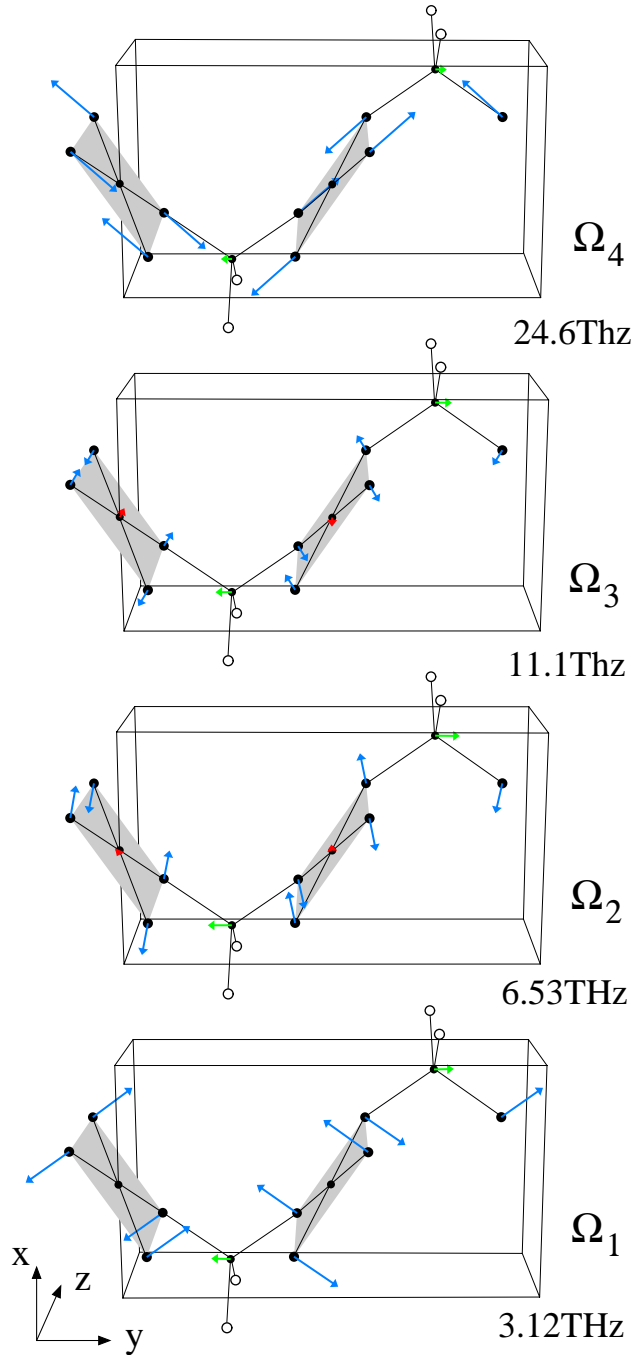


Figure 2.2: Geometry of the T_2^+ eigenmodes as given by the polarization patterns in table 2.1. The shaded areas are the CuO_4 plaquettes which form the Cu chains in z direction. The Cu atoms are in the center of each plaquette, the corners are formed by O2 ions. The O1 atoms are represented by the open circles with the Ge ions in between them. (Compare with the x - y projection given in figure 2.1.) Note that the O2 elongations are in the x - y plane, the (small) Cu displacements are along the z axis while the Ge displacements are along y .

The static distortion in the spin-Peierls phase at $T = 4$ K also has been determined [40]. I define a corresponding four-dimensional vector.

$$\langle \mathbf{r} \rangle_{T=4\text{K}} = \begin{pmatrix} \langle r_{\text{Cu}}^z \rangle \\ \langle r_{\text{Ge}}^y \rangle \\ \langle r_{\text{O2b}}^x \rangle \\ \langle r_{\text{O2b}}^y \rangle \end{pmatrix} = 10^{-2} \begin{pmatrix} 0.57 \\ 0.08 \\ -0.95 \\ -0.65 \end{pmatrix} \text{Å} \quad (2.11)$$

2.2 Spin-phonon coupling term

In the spin-phonon coupling term (2.4) I focus on the NN part for reasons that will become obvious at the end of the section. I include the relevant displacements of the ions directly involved in the Cu-Cu superexchange path determining J and only those coupling constants where the ions actually show displacements in the Peierls-active modes. The apex ‘‘O1’’ atoms are not displaced by those modes at the appropriate wave vector \mathbf{q}_0 . I have to consider two copper ions in adjacent unit cells along the c direction, two germanium sites, and two oxygen atoms surrounding a Cu-Cu bond. The notation introduced is shown in figure 2.1, the two ‘‘O2’’ oxygen atoms per formula unit are denoted ‘‘O2a’’ and ‘‘O2b’’. There are two formula units per unit cell which I distinguish by a prime.

The relevant coupling constants for the linear atomic elongations are shown in table 2.2. The effective spin-phonon coupling Hamiltonian is

$$\begin{aligned} H_{sp}^{\text{NN}} &= \sum_{\mathbf{n}} \left[g_{\text{Cu}}^z (r_{\text{Cu},\mathbf{n}}^z - r_{\text{Cu},\mathbf{n}+\hat{z}}^z) - g_{\text{Ge}}^y (r_{\text{Ge}',\mathbf{n}-\hat{y}}^y - r_{\text{Ge},\mathbf{n}}^y) \right. \\ &\quad \left. - g_{\text{O2b}}^x (r_{\text{O2b}',\mathbf{n}-\hat{y}}^x - r_{\text{O2b},\mathbf{n}}^x) - g_{\text{O2b}}^y (r_{\text{O2b}',\mathbf{n}-\hat{y}}^y - r_{\text{O2b},\mathbf{n}}^y) \right] \mathbf{S}_{\mathbf{n}} \cdot \mathbf{S}_{\mathbf{n}+\hat{z}} \\ &+ \sum_{\mathbf{n}} \left[g_{\text{Cu}}^z (r_{\text{Cu}',\mathbf{n}}^z - r_{\text{Cu}',\mathbf{n}+\hat{z}}^z) - g_{\text{Ge}}^y (r_{\text{Ge},\mathbf{n}}^y - r_{\text{Ge}',\mathbf{n}}^y) \right. \\ &\quad \left. + g_{\text{O2a}}^x (r_{\text{O2a},\mathbf{n}}^x - r_{\text{O2a}',\mathbf{n}}^x) + g_{\text{O2a}}^y (r_{\text{O2a},\mathbf{n}}^y - r_{\text{O2a}',\mathbf{n}}^y) \right] \mathbf{S}'_{\mathbf{n}} \cdot \mathbf{S}'_{\mathbf{n}+\hat{z}}. \quad (2.12) \end{aligned}$$

The two sums correspond to the two Cu chains running through each unit cell.

The symmetry of the Hamiltonian (2.12) allows for some simplifications. First of all I use the equivalence of coupling to the O2a and O2b displacements (see figure 2.1).

$$g_{\text{O2}}^x = g_{\text{O2b}}^x = g_{\text{O2a}}^x \quad (2.13)$$

$$g_{\text{O2}}^y = g_{\text{O2b}}^y = -g_{\text{O2a}}^y \quad (2.14)$$

From the symmetry of the T_2^+ modes (see figure 2.2) one can see that the O2- y components are in phase, i.e., $r_{\text{O2a},\mathbf{n}}^y = r_{\text{O2b},\mathbf{n}}^y = r_{\text{O2},\mathbf{n}}^y$, while the x components exhibit an anti-phase shift: $-r_{\text{O2a},\mathbf{n}}^x = r_{\text{O2b},\mathbf{n}}^x = r_{\text{O2},\mathbf{n}}^x$.

$$\begin{array}{l}
\overline{\overline{g_{\text{Cu}}^z}} = \frac{\partial J}{\partial r_{\text{Cu},\mathbf{n}}^z} = -\frac{\partial J}{\partial r_{\text{Cu},\mathbf{n}+\hat{z}}^z} = \frac{\partial J'}{\partial r_{\text{Cu}',\mathbf{n}}^z} \\
g_{\text{Ge}}^y = \frac{\partial J}{\partial r_{\text{Ge},\mathbf{n}}^y} = -\frac{\partial J}{\partial r_{\text{Ge}',\mathbf{n}-\hat{y}}^y} = -\frac{\partial J'}{\partial r_{\text{Ge},\mathbf{n}}^y} \\
g_{\text{O2a}}^{x,y} = \frac{\partial J'}{\partial r_{\text{O2a},\mathbf{n}}^{x,y}} = -\frac{\partial J'}{\partial r_{\text{O2a}',\mathbf{n}}^{x,y}} = -\frac{\partial J'}{\partial r_{\text{O2a}',\mathbf{n}-\hat{y}}^{x,y}} \\
\overline{\overline{g_{\text{O2b}}^{x,y}}} = \frac{\partial J}{\partial r_{\text{O2b},\mathbf{n}}^{x,y}} = -\frac{\partial J}{\partial r_{\text{O2b}',\mathbf{n}}^{x,y}} = -\frac{\partial J}{\partial r_{\text{O2b}',\mathbf{n}-\hat{y}}^{x,y}}
\end{array}$$

Table 2.2: Definition of the coupling constants for linear atomic elongations. The two Cu chains running through each unit cell are distinguished by a prime (see figure 2.1). J' is the magnetic coupling constant along the Cu' chains.

As indicated in figure 2.1 I then cut the unit cell along the y axis in half separating the ions labelled “prime” from those without a label.

$$r_{\nu',\mathbf{n}}^\alpha \rightarrow -r_{\nu,\mathbf{n}+\hat{y}/2}^\alpha \quad (2.15)$$

$$\mathbf{S}'_{\mathbf{n}} \cdot \mathbf{S}'_{\mathbf{n}+\hat{z}} \rightarrow \mathbf{S}_{\mathbf{n}+\hat{y}/2} \cdot \mathbf{S}_{\mathbf{n}+\hat{y}/2+\hat{z}} \quad (2.16)$$

The change of sign of the coordinates accounts for the anti-phase elongation of the two types of ions in the Peierls-active modes at the wave vector of the instability $\mathbf{q}_0 = (\pi/a, 0, \pi/c)$. Resummation $\mathbf{n} \rightarrow \mathbf{l}$ over all the new cells, i.e., twice as many with a new cell length $b/2$ in y direction, yields

$$\begin{aligned}
H_{sp}^{\text{NN}} = \sum_{\mathbf{l}} \left[g_{\text{Cu}}^z (r_{\text{Cu},\mathbf{l}}^z - r_{\text{Cu},\mathbf{l}+\hat{z}}^z) + g_{\text{Ge}}^y (r_{\text{Ge},\mathbf{l}-\hat{y}}^y + r_{\text{Ge},\mathbf{l}}^y) \right. \\
\left. + g_{\text{O2}}^x (r_{\text{O2},\mathbf{l}-\hat{y}}^x + r_{\text{O2},\mathbf{l}}^x) + g_{\text{O2}}^y (r_{\text{O2},\mathbf{l}-\hat{y}}^y + r_{\text{O2},\mathbf{l}}^y) \right] e^{i\pi l_y} \mathbf{S}_{\mathbf{l}} \cdot \mathbf{S}_{\mathbf{l}+\hat{z}}. \quad (2.17)
\end{aligned}$$

The overall change of sign in the first sum with respect to the second in equation (2.12) has been incorporated in the phase factor $e^{i\pi l_y}$. This change of sign translates into the anti-phase shift of the spin-Peierls ordering between neighboring Cu chains in y direction.

Now I substitute the displacements $r_{\nu,\mathbf{l}}^\alpha$ with the \mathbf{q} -space normal coordinates (2.5). For clarity I introduce the abbreviation

$$Y_{-\mathbf{q}}^{(1)} := \sum_{\mathbf{l}} e^{i\mathbf{q}\mathbf{R}_{\mathbf{l}}} e^{i\pi l_y} \mathbf{S}_{\mathbf{l}} \cdot \mathbf{S}_{\mathbf{l}+\hat{z}} \quad (2.18)$$

for the Fourier transform of the nearest neighbor spin-spin correlation operator.

$$H_{sp}^{\text{NN}} = \frac{1}{\sqrt{N}} \sum_{\mathbf{q}} Y_{-\mathbf{q}}^{(1)} \sum_{\lambda} \sqrt{\frac{2\Omega_{\lambda,\mathbf{q}}}{\hbar}} g_{\lambda,\mathbf{q}} Q_{\lambda,\mathbf{q}} \quad (2.19)$$

Here the effective normal-mode coupling constants

$$\boxed{\begin{aligned} \sqrt{\frac{2\Omega_{\lambda,\mathbf{q}}}{\hbar}} g_{\lambda,\mathbf{q}} &:= (1 - e^{iq_z c}) g_{\text{Cu}}^z \frac{e_{\text{Cu}}^z(\lambda, \mathbf{q})}{\sqrt{m_{\text{Cu}}}} \\ &+ (e^{-iq_y b/2} + 1) \left(g_{\text{Ge}}^y \frac{e_{\text{Ge}}^y(\lambda, \mathbf{q})}{\sqrt{m_{\text{Ge}}}} + g_{\text{O}_2}^x \frac{e_{\text{O}_2}^x(\lambda, \mathbf{q})}{\sqrt{m_{\text{O}_2}}} + g_{\text{O}_2}^y \frac{e_{\text{O}_2}^y(\lambda, \mathbf{q})}{\sqrt{m_{\text{O}_2}}} \right) \end{aligned}} \quad (2.20)$$

were introduced. Note that in the literature the coupling constants often are given with respect to normal coordinates, i.e., set $g_{\text{normal}} = \sqrt{(2\Omega_{\lambda,\mathbf{q}})/\hbar} g_{\lambda,\mathbf{q}}$ in equation (2.19). In equation (2.25) the transition temperature then is $T_{\text{SP}} \sim g_{\text{normal}}^2/\Omega^2$, consistent with the result of Cross and Fisher [14].

The next step is to transform the normal coordinates to boson creation and annihilation operator representation via equation (2.7).

$$\boxed{H_{sp}^{\text{NN}} = \frac{1}{\sqrt{N}} \sum_{\mathbf{q}} Y_{-\mathbf{q}}^{(1)} \sum_{\lambda} g_{\lambda,\mathbf{q}} (b_{\lambda,-\mathbf{q}}^{\dagger} + b_{\lambda,\mathbf{q}})} \quad (2.21)$$

This is the representation usually used in theoretical approaches to spin-phonon coupling. Since the polarization vectors are known for \mathbf{q}_0 (table 2.1), equation (2.20) defines the relation between the coupling to the linear atomic deviations g_{ν}^{α} (table 2.2) and the normal-mode coupling constants $g_{\lambda,\mathbf{q}}$.

2.2.1 Next nearest neighbor spin-phonon coupling

The Cu-O2-O2-Cu NNN superexchange path is shown by the dashed line in figure 1.4 on page 6. The NNN exchange term $J_2 \mathbf{S}_i \cdot \mathbf{S}_{i+2\hat{z}}$ leads to a magneto-elastic coupling equivalent to the one for the NN exchange shown in equation (2.17). Including all ionic linear elongations contributing to the NNN superexchange path the prefactors in the resulting reciprocal space coupling constants — compare equation (2.20) — then are $(1 - e^{2iq_z c})$ for the Cu part and $(1 + e^{iq_z c})$ for the other ions. The coupling of the J_2 term vanishes at the wave vector of the instability $\mathbf{q}_0 = (\pi/a, 0, \pi/c)$ and does thus not directly influence the spin-Peierls transition. Away from \mathbf{q}_0 the \mathbf{q} dependence of the polarization vectors is difficult to handle since then all 13 modes of an irreducible representation of lower symmetry couple to the spin system [44]. Any quantitative inclusion of the NNN spin-phonon coupling term is thus difficult. In most of this work I limit the discussion to the vicinity of \mathbf{q}_0 where this contribution can be disregarded.

θ	η	δ	d_{Cu}	d_{Ge}
$ \partial\theta^\kappa/\partial r_{\text{Cu}}^z $	0.11 $\frac{\pi}{\text{\AA}}$	0	0.76	0
$ \partial\theta^\kappa/\partial r_{\text{Ge}}^y $	0	0.11 $\frac{\pi}{\text{\AA}}$	0	0.82
$ \partial\theta^\kappa/\partial r_{\text{O2}}^x $	0.21 $\frac{\pi}{\text{\AA}}$	0.29 $\frac{\pi}{\text{\AA}}$	0.54	0.57
$ \partial\theta^\kappa/\partial r_{\text{O2}}^y $	0.14 $\frac{\pi}{\text{\AA}}$	0.32 $\frac{\pi}{\text{\AA}}$	0.36	0.82
θ_0	0.55 π	0.89 π	1.93 \AA	1.73 \AA

Table 2.3: Linear coefficients of the expansion of the angles and bond lengths as a function of the linear atomic elongations, as defined in equation (2.22). The variables $\kappa \in \{a, a', b, b'\}$ and $\theta^\kappa \in \{\eta^\kappa, \delta^\kappa, d_{\text{Cu}}^\kappa, d_{\text{Ge}}^\kappa\}$ are introduced in the text. The last line holds the experimental equilibrium angles and bond lengths [40] ($\theta^\kappa = \theta_0 + \Delta\theta^\kappa$, $\Delta\theta^\kappa$ is defined in equation (2.22)).

2.2.2 Coupling to bond angles and lengths

The two lower Peierls-active modes essentially vary the angles $\eta^\kappa = \angle(\text{Cu-O}2\kappa\text{-Cu})$ and $\delta^\kappa = \angle(\text{O}2\kappa'\text{-O}2\kappa\text{-Ge})$. Together with the bond lengths $d_{\text{Cu}}^\kappa = \overline{\text{Cu-O}2\kappa}$ and $d_{\text{Ge}}^\kappa = \overline{\text{Ge-O}2\kappa}$ they represent the natural set of coordinates of the lattice vibrations in the irreducible group of the T_2^+ modes. The index $\kappa \in \{a, a', b, b'\}$ was introduced to label the position on the different oxygen atoms in the unit cell.

Introducing the variable $\theta^\kappa \in \{\eta^\kappa, \delta^\kappa, d_{\text{Cu}}^\kappa, d_{\text{Ge}}^\kappa\}$ I can write

$$\Delta J_{l,l+z} = \sum_{\{\theta^\kappa\}} \frac{\partial J}{\partial \theta_n^\kappa} \Delta \theta_n^\kappa = \sum_{\{\theta^\kappa\}} g_\theta \sum_\nu \frac{\partial \theta_n^\kappa}{\partial r_{\nu,n}^\alpha} r_{\nu,n}^\alpha. \quad (2.22)$$

Here I defined the coupling constants $g_\theta = (\partial J)/(\partial \theta_n^\kappa)$, which are independent of κ . For reasons of translational invariance I can drop the unit cell index \mathbf{n} . The linear coefficients of the Taylor expansions $(\partial \theta^\kappa)/(r_\nu^\alpha)$ at the different positions κ in the unit cell all yield the same numerical coefficients but with varying signs. The absolute values of the coefficients are given in table 2.3.

Considering all the relevant bonds and angles and using the decomposition (2.22) I can set up a spin-phonon Hamiltonian similar to (2.12) in the previous section. By a simple comparison of the coefficients I obtain the transformation matrix between the angular and bond length coupling constants and the linear atomic deviation coupling constants.

$$\begin{pmatrix} g_{\text{Cu}}^z \\ g_{\text{Ge}}^y \\ g_{\text{O2}}^x \\ g_{\text{O2}}^y \end{pmatrix} = \begin{pmatrix} -0.22 \frac{\pi}{\text{\AA}} & 0 & -1.52 & 0 \\ 0 & -0.11 \frac{\pi}{\text{\AA}} & 0 & 0.82 \\ 0.21 \frac{\pi}{\text{\AA}} & 0.29 \frac{\pi}{\text{\AA}} & -1.08 & 0.57 \\ -0.14 \frac{\pi}{\text{\AA}} & 0.32 \frac{\pi}{\text{\AA}} & 0.72 & -0.82 \end{pmatrix} \begin{pmatrix} g_\eta \\ g_\delta \\ g_{\text{Cu}}^d \\ g_{\text{Ge}}^d \end{pmatrix} \quad (2.23)$$

Together with equation (2.20) I now can determine all coupling constants if any four of the them are known.

2.3 Normal-mode coupling constants

I now numerically determine the four normal-mode coupling constants. In chapter 5 I shown the RPA approach by Cross and Fisher [14] to the Hamiltonian

$$\begin{aligned}
 H = & J \sum_l \mathbf{S}_l \cdot \mathbf{S}_{l+\hat{z}} + J_2 \sum_l \mathbf{S}_l \cdot \mathbf{S}_{l+2\hat{z}} \\
 & + \sum_{\lambda, q} \hbar \Omega_{\lambda, q} \left(b_{\lambda, q}^\dagger b_{\lambda, q} + \frac{1}{2} \right) \\
 & + \frac{1}{\sqrt{N}} \sum_q Y_{-q}^{(1)} \sum_\lambda g_{\lambda, q} \left(b_{\lambda, -q}^\dagger + b_{\lambda, q} \right)
 \end{aligned} \tag{2.24}$$

to satisfactorily describes the dynamics of the Peierls-active Phonon modes. It consists of the Heisenberg chain (2.2), the harmonic phonon part (2.9) and the spin-phonon coupling term (2.21) all discussed above. The expression for the critical temperature T_{SP} of the spin-Peierls transition is derived in section 4.2.1. Using the approach of Cross and Fisher [14] to the corresponding dimer-dimer correlation function discussed in section 4.3.2, the expression involving the four Peierls-active modes I have to consider herein ($\Omega_{\lambda, q_0} \equiv \Omega_\lambda$, $g_{\lambda, q_0} \equiv g_\lambda$, [54]) is:

$$k_B T_{\text{SP}} = \left(\frac{2g_1^2}{\hbar\Omega_1} + \frac{2g_2^2}{\hbar\Omega_2} + \frac{2g_3^2}{\hbar\Omega_3} + \frac{2g_4^2}{\hbar\Omega_4} \right) \chi_0. \tag{2.25}$$

k_B is Boltzmann's constant. The factor $\chi_0 \approx 0.5$ is a contribution of the static dimer-dimer correlation function at the appropriate wave vector. Its value is controversial and I have adopted a mean of the proposed values. Please refer to the discussion in section 2.7 for the details.

2.3.1 Ginzburg criterion

The Ginzburg criterion gives an estimate of the temperature range of the critical region in which fluctuations suppress the applicability of mean-field approaches (or RPA). It is obtained through comparing the theoretical correction of Gaussian fluctuations to the specific heat

$$C_p - C_{p,0} = \frac{abc}{16\pi} \frac{T_{\text{SP}}^2}{(T - T_{\text{SP}})^2} \frac{k_B}{\xi_a \xi_b \xi_c} \tag{2.26}$$

with the experimental jump in the specific heat at the transition [55]. The correlation lengths ξ_a , ξ_b , and ξ_c along the respective crystallographic axes can be obtained from fits

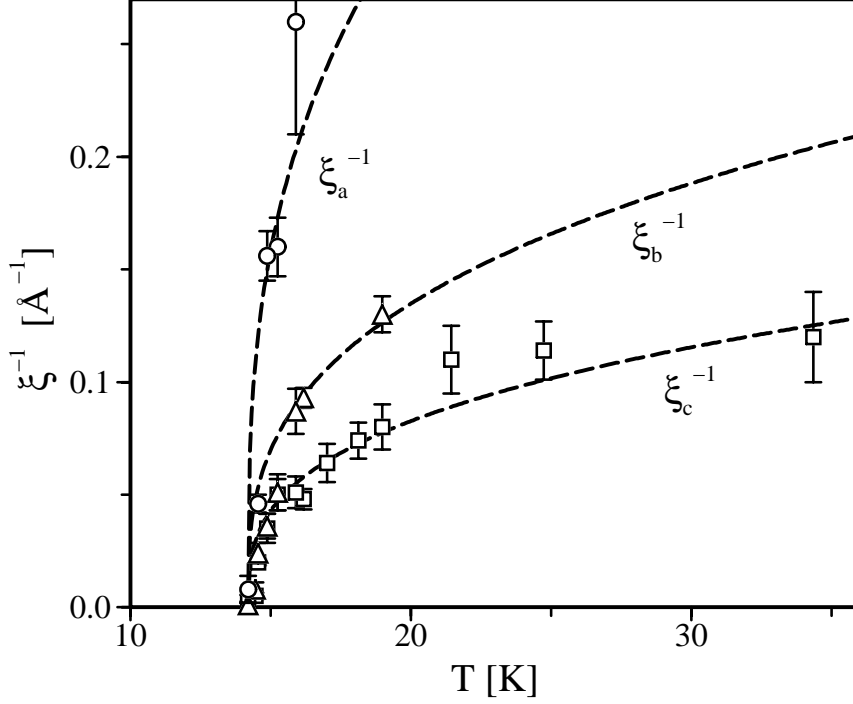


Figure 2.3: Correlation length from diffusive X-ray scattering experiments by Schoeffel *et al.* [26] along the three crystallographic axes. The broken lines are the fits given in equations (2.27), (2.28), and (2.29).

to the diffuse X-ray data from Schoeffel *et al.* [26] as shown in figure 2.3.

$$\xi_a \approx 0.50 a [(T - T_{\text{SP}})/T_{\text{SP}}]^{-\frac{1}{3}} \quad (2.27)$$

$$\xi_b \approx 0.65 b [(T - T_{\text{SP}})/T_{\text{SP}}]^{-\frac{1}{3}} \quad (2.28)$$

$$\xi_c \approx 3.06 c [(T - T_{\text{SP}})/T_{\text{SP}}]^{-\frac{1}{3}} \quad (2.29)$$

The specific heat jump at T_{SP} has been determined by Lasjaunias *et al.* [56] to be $\Delta C_{\text{exp}} = 0.73 k_{\text{B}}$ per unit cell volume. Requiring $C_p - C_{p,0} \ll \Delta C_{\text{exp}}$ I find the Ginzburg criterion to be

$$(T - T_{\text{SP}}) \gg 0.03 T_{\text{SP}} = 0.4 \text{ K}. \quad (2.30)$$

In accordance with the mean-field approach to the susceptibility by Klümper *et al.* [57] I conclude that beyond a region of 3-4 K around T_{SP} the mean-field theory is reliable.

2.3.2 Mean-field approach

The transition temperature given for CuGeO₃ with 14.1 K, one parameter is fixed through equation (2.25). As I shall discuss now, the others can be estimated from the polarization vectors of the Peierls-active phonon modes and the static distortion in the dimerized phase at 4 K also given by Braden *et al.* [40]. For the fixed wave vector of the Peierls instability \mathbf{q}_0 I can derive from expressions (2.5) and (2.7) a relation between a static lattice distortion $\langle r_\nu^\alpha \rangle$ and the expectation values of the displacement of the eigenmodes out of the harmonic equilibrium $\langle b_{\lambda, \mathbf{q}_0} \rangle$.

$$\langle r_\nu^\alpha \rangle = \frac{\langle r_{\mathbf{q}_0, \nu}^\alpha \rangle}{\sqrt{N}} = \sum_\lambda \frac{e_\nu^\alpha(\lambda, \mathbf{q}_0)}{\sqrt{Nm_\nu}} \sqrt{\frac{2\hbar}{\Omega_{\lambda, \mathbf{q}_0}}} \langle b_{\lambda, \mathbf{q}_0} \rangle \quad (2.31)$$

In section 4.1.1 I show that the expectation values $\langle b_{\lambda, \mathbf{q}_0} \rangle$ are real. The real-space displacements $\langle r_\nu^\alpha \rangle$ are real anyway. This is consistent with the fact that in this representation the polarization vectors $e_\nu^\alpha(\lambda, \mathbf{q}_0)$ are real.

Introducing the canonical transformation

$$\tilde{b}_{\lambda, \mathbf{q}} = b_{\lambda, \mathbf{q}} + \frac{1}{\sqrt{N}} \frac{g_{\lambda, \mathbf{q}}}{\hbar\Omega_{\lambda, \mathbf{q}}} Y_{\mathbf{q}}^{(1)} \quad (2.32)$$

for the Bose annihilation and creation operators $b_{\lambda, \mathbf{q}}$, where $Y_{\mathbf{q}}^{(1)}$ was defined by (2.18), the Hamiltonian (2.24) decouples into

$$H = J \sum_l \mathbf{S}_l \cdot \mathbf{S}_{l+\hat{z}} - \frac{1}{N} \sum_{\lambda, \mathbf{q}} \frac{|g_{\lambda, \mathbf{q}}|^2}{\hbar\Omega_{\lambda, \mathbf{q}}} Y_{-\mathbf{q}}^{(1)} Y_{\mathbf{q}}^{(1)} + \sum_{\lambda, \mathbf{q}} \hbar\Omega_{\lambda, \mathbf{q}} \left(\tilde{b}_{\lambda, \mathbf{q}}^\dagger \tilde{b}_{\lambda, \mathbf{q}} + \frac{1}{2} \right). \quad (2.33)$$

The operators $\tilde{b}_{\lambda, \mathbf{q}}$ do not satisfy Bose commutation relations and since $[Y_{-\mathbf{q}}^{(1)}, \tilde{b}_{\lambda, \mathbf{q}}]_- \neq 0$ the solution of this Hamiltonian is not at all evident. But in a mean-field like approach I can assume $\langle \tilde{b}_{\lambda, \mathbf{q}} \rangle = 0$ so that from (2.32) follows

$$\langle b_{\lambda, \mathbf{q}} \rangle = -\frac{1}{\sqrt{N}} \frac{g_{\lambda, \mathbf{q}}}{\hbar\Omega_{\lambda, \mathbf{q}}} \langle Y_{\mathbf{q}}^{(1)} \rangle. \quad (2.34)$$

This relation is derived in detail in section 4.2.3. The mean-field ansatz is reasonable here, since I am interested in temperatures of 4K which is far from the critical region and the dimerization is as good as saturated [27].

g_1/k_B	g_2/k_B	g_3/k_B	g_4/k_B
-15 K	58 K	-30 K	-12 K

Table 2.4: Normal-mode coupling constants for the four Peierls-active phonon modes at \mathbf{q}_0 as determined by equation (2.35).

2.3.3 Values

With expressions (2.32) and (2.34) I am left with a set of linear equations. The values of the frequencies Ω_λ are given in table 2.1, the polarization vectors $e_\nu^\alpha(\lambda, \mathbf{q}_0)$ enter via the Matrix \mathbf{M} defined in equation (2.10), and $\langle \mathbf{r} \rangle_{T=4K}$ is given in equation (2.11).

$$\langle \mathbf{r} \rangle_{T=4K} = -\frac{\langle Y_{\mathbf{q}_0}^{(1)} \rangle}{N} \sqrt{\frac{2}{\hbar}} \mathbf{M} \begin{pmatrix} g_1/\sqrt{\Omega_1^3} \\ g_2/\sqrt{\Omega_2^3} \\ g_3/\sqrt{\Omega_3^3} \\ g_4/\sqrt{\Omega_4^3} \end{pmatrix} \quad (2.35)$$

The solution of the equations gives the coupling constants as a function of $N/\langle Y_{\mathbf{q}_0}^{(1)} \rangle$. The latter is then determined by the critical temperature $T_{SP} = 14.1$ K via equation (2.25).

$$\frac{\langle Y_{\mathbf{q}_0}^{(1)} \rangle}{N} = \frac{1}{N} \sum_l (-1)^{l_x+l_y+l_z} \langle \mathbf{S}_l \cdot \mathbf{S}_{l+\hat{z}} \rangle = 0.59 \quad (2.36)$$

For a spin 1/2 system with two Cu chains per unit cell I have $\langle Y_{\mathbf{q}_0}^{(1)} \rangle/N \leq 0.75$ where 0.75 is reached in the fully dimerized state. In the uniform Heisenberg case $\langle Y_{\mathbf{q}_0}^{(1)} \rangle/N = 0$.

In table 2.4 I show the calculated coupling constants of the spin system to the Peierls-active eigenmodes of the lattice at the wave vector of the instability \mathbf{q}_0 . The signs are such that all contributions in the spin-phonon coupling term in the Hamiltonian (2.24) are negative when the phonon modes are macroscopically occupied as determined via equation (2.32) in section 2.5.1. The mode at $\Omega_2/(2\pi) = 6.5$ THz is dominant, by its symmetry it essentially varies the angles η . This will be reflected in the corresponding coupling constant discussed below. The values are rather large compared with the magnetic exchange of $J \sim 150$ K. This is what is expected intuitively since the spin system has to overcompensate the elastic energy of a rather rigid lattice. The two lowest Peierls-active eigenmodes with $\hbar\Omega_1/k_B = 150$ K and $\hbar\Omega_2/k_B = 320$ K have energies of the order of J .

Note that the influence of the lowest mode at $\Omega_1/(2\pi) = 3.1$ THz on the transition temperature is as important as that of $\Omega_3/(2\pi) = 11$ THz because of the frequencies in the denominator of equation (2.25).

$g_{\text{Cu}}^z/k_{\text{B}}$	$g_{\text{Ge}}^y/k_{\text{B}}$	$g_{\text{O}_2}^x/k_{\text{B}}$	$g_{\text{O}_2}^y/k_{\text{B}}$
-890 K/Å	-110 K/Å	400 K/Å	-91 K/Å

Table 2.5: Coupling constants for the linear atomic displacements calculated via equation (2.37) using the values for g_λ from table 2.4.

g_η/k_{B}	g_δ/k_{B}	$g_{\text{Cu}}^d/k_{\text{B}}$	$g_{\text{Ge}}^d/k_{\text{B}}$
15 K/deg	1.5 K/deg	180 K/Å	-96 K/Å

Table 2.6: Coupling constants for the angles and bond lengths calculated via equation (2.23) using the values for g_ν^α from table 2.5.

2.4 Microscopic coupling constants

The numerical values of the normal-mode coupling constants thus given, the microscopic coupling constants can be determined. Using the matrix (2.10) I rewrite expression (2.20) for $\mathbf{q} = \mathbf{q}_0$ as

$$\mathbf{M}^T \begin{pmatrix} g_{\text{Cu}}^z \\ g_{\text{Ge}}^y \\ g_{\text{O}_2}^x \\ g_{\text{O}_2}^y \end{pmatrix} = \frac{1}{\sqrt{2\hbar}} \begin{pmatrix} g_1 \sqrt{\Omega_1} \\ g_2 \sqrt{\Omega_2} \\ g_3 \sqrt{\Omega_3} \\ g_4 \sqrt{\Omega_4} \end{pmatrix}, \quad (2.37)$$

and compute the coupling to the linear atomic elongations. Then I calculate the angular and bond length couplings using equation (2.23). The resulting values are given in table 2.5 and table 2.6, respectively.

The results allow for some immediate conclusions:

- The coupling to the angle η , i.e., g_η , is the dominant contribution.
- The signs of the coupling constants are correct, J increases with increasing angles and decreasing O2-Ge bond length. The positive value of g_{Cu}^d may indicate that a ferromagnetic contribution of the exchange is weakened more than the antiferromagnetic contribution when stretching the O2-Cu bond. This would be consistent with the net ferromagnetic exchange of the O2-Cu plaquettes without the germanium side group predicted by Geertsma and Khomskii [43].
- Variation of the coupling constants shows g_1 to couple mainly to the angles δ , g_2 to η , and g_3 and g_4 to be almost entirely bond stretching [44]. While the results for g_η and g_δ are robust under variation of the parameters, the values of g_{Cu}^d and g_{Ge}^d are less fixed within the accuracy of our approach.

Method [Reference]	$\frac{\partial J}{J\partial\eta^\kappa}$	$\frac{\partial J}{J\partial\delta^\kappa}$
Harm. theory and mean-field [here]	10 % $\frac{1}{\text{deg}}$	1 % $\frac{1}{\text{deg}}$
Microscopic superexchange [43]	≥ 8 % $\frac{1}{\text{deg}}$	≥ 0.3 % $\frac{1}{\text{deg}}$
Microscopic superexchange [40]	22 % $\frac{1}{\text{deg}}$	0.6 % $\frac{1}{\text{deg}}$
Pressure vs. magnetostriction [50]	> 3 % $\frac{1}{\text{deg}}$	> 0.3 % $\frac{1}{\text{deg}}$

Table 2.7: Variation of J with the variation of the angles. Note that in our notation there are two angles η^κ and two angles δ^κ contributing each to the Cu-Cu superexchange path (see figure 2.1).

- From magnetostriction data Büchner *et al.* [50] expect the influence of the Cu-O2-Cu angle η on the magnetic exchange to be of the order of $2\partial J/(J\partial\eta^\kappa) \approx 10$ % per degree and for the O2-O2-Ge angle their value is $2\partial J/(J\partial\delta^\kappa) \approx 1$ %. For $J/k_B = 150$ K I obtain about twice the values (see table 2.7).
- Comparing g_{Ge}^d and g_{Ge}^y shows the effect of the Ge elongation on the magnetic exchange to be due mainly to the stretching of the O2-Ge bond. The contribution of the Ge side group to the magnetic exchange should depend on the O2-O2-Ge angle as $J_{\text{side}} \sim \cos \delta$. Therefore, the angle $\delta^\kappa \approx 160^\circ = 0.89\pi$ being close to π , the angular dependence of J on δ is quite small in spite of the large entire side-group effect, which is of similar magnitude as that of the CuO_4 plaquette elongation [43, 40].
- Two groups analyzed the structural dependence of the superexchange within similar microscopic models. Geertsma and Khomskii [43] obtained $J/k_B = 135$ K and found $2\partial J_{\text{geo}}/(J\partial\eta^\kappa) \approx 16$ % and $2\partial J_{\text{geo}}/(J\partial\delta^\kappa) \approx 0.6$ % per degree. These values only account for the “geometrical” contribution and are thus lower bounds. Braden *et al.* [40] found $J/k_B = 160$ K and gave $2\partial J/(J\partial\eta^\kappa) \approx 44$ % and $2\partial J/(J\partial\delta^\kappa) \approx 1.1$ % per degree. The agreement between the microscopic models is affected by the choice of the parameters and the number of orbitals taken into consideration.

A summary of the values obtained with the different approaches is given in table 2.7.

2.5 Static distortion

The microscopic coupling constants given, I can directly calculate the effect of static distortions of the lattice geometry on the magnetic exchange.

2.5.1 Dimerization

Using the static displacements of the ions in the spin-Peierls phase at $T = 4$ K [40], one may calculate the alternation of the magnetic exchange usually used in mean-field approaches

$\langle b_{1,\mathbf{q}_0} \rangle / \sqrt{N}$	$\langle b_{2,\mathbf{q}_0} \rangle / \sqrt{N}$	$\langle b_{3,\mathbf{q}_0} \rangle / \sqrt{N}$	$\langle b_{4,\mathbf{q}_0} \rangle / \sqrt{N}$
0.061	-0.11	0.034	0.006

Table 2.8: Macroscopic occupation of the Peierls-active T_2^+ phonon modes in the ordered phase at 4 K as given by equation (2.32).

to the spin-phonon coupling, i.e.,

$$H_{\text{MF}} = J \sum_{l_z} (1 + (-1)^{l_z} \delta_J) \mathbf{S}_{l_z} \cdot \mathbf{S}_{l_z+1}. \quad (2.38)$$

This is achieved by substituting in the spin-phonon coupling term (2.17) the atomic displacements by their expectation values $r_{\nu,l}^\alpha \rightarrow (-1)^{l_z+l_x} \langle r_\nu^\alpha \rangle_{T=4\text{K}}$ and comparing the resulting $\langle H_{sp}^{\text{NN}} \rangle_{T=4\text{K}}$ with equation (2.38). Equivalently one can calculate $\langle H_{sp}^{\text{NN}} \rangle_{T=4\text{K}}$ by using the static angular and bond length deviations [40] yielding the same results.

I find $\delta_J J/k_B = 17$ K or $\delta_J \approx 0.11$ ($J/k_B = 150$ K). By solving the system of linear equations defined by equation (2.32) for $\mathbf{q} = \mathbf{q}_0$, the expectation values $\langle b_{\lambda,\mathbf{q}_0} \rangle / \sqrt{N}$ have been determined as given in table 2.8. The elastic energy per unit cell of the spin-Peierls distortion at $T \sim 4$ K then is given by

$$\frac{\langle H_p \rangle}{N k_B} = \sum_{\lambda} \frac{\hbar \Omega_{\lambda,\mathbf{q}_0}}{N k_B} \langle b_{\lambda,\mathbf{q}_0} \rangle^2 = 5 \text{ K}. \quad (2.39)$$

This energy loss has to be compensated by the spin system. Considering that the maximum gain of magnetic energy is reached in the fully dimerized case with $0.375 \delta_J J$ per Cu ion, I find a lower boundary for the dimerization of $\delta_J > 0.044$. Including a NNN term in equation (2.38) with $J_2/J = 0.241$ as studied by Chitra *et al.* [35] using a density matrix renormalization group (DMRG) approach I find $\delta_J \geq 0.078$.

Our result is within a factor of two of the values obtained by using $\partial J/\partial \eta$ and $\partial J/\partial \delta$ obtained from the magnetostriction results [50] and from the microscopic models [43, 40]. All other published estimates of the dimerization result from an analysis of the magnetic excitation spectra observed by inelastic neutron or Raman scattering. Most of these estimates are based on the static dimerized Hamiltonian (2.38) [23, 34] and yield dimerization values much smaller than the one reported here (see table 2.9). Augier and Poilblanc [58] as well as Wellein *et al.* [59] extend the static model by coupling to dynamical phonons which reduces the magnetic gap by lowering the effective lattice distortion acting on the spin system [50]. The derivation of their model and the significance of the phonon dynamics are closer discussed in section 2.6. Introducing interchain coupling may further suppress the spin gap [60]. For an extensive discussion see reference [38].

All methods incorporate more or less crude approximations to the real physical situation leaving the question of the true value of δ_J unanswered. Our lower boundary should be

Method [Reference]	δ_J
Harmonic theory and mean-field [here]	0.11
Macroscopic occupation of T_2^+ modes [here]	>0.04
Microscopic superexchange [43, 40]	0.07 to 0.2
Dynamic phonons and experimental gap [50]	~ 0.05
Static phonons and experimental gap [23, 34]	0.01 to 0.03
Coupled chains [38]	0.01 to 0.12

Table 2.9: Exchange alternation in $J[1 + (-1)^{l_z} \delta_J]$ in equation (2.38).

θ	η	δ	d_{Cu}	d_{Ge}
$\frac{\partial \theta^\kappa}{\partial p}$	$-0.16 \frac{\text{deg}}{\text{GPa}}$	$-1.3 \frac{\text{deg}}{\text{GPa}}$	$-0.0012 \frac{\text{\AA}}{\text{GPa}}$	$-0.0033 \frac{\text{\AA}}{\text{GPa}}$
$\frac{\partial J_\theta}{\partial p}$	$-2.5 \frac{k_{\text{B}}\text{K}}{\text{GPa}}$	$-1.9 \frac{k_{\text{B}}\text{K}}{\text{GPa}}$	$-0.22 \frac{k_{\text{B}}\text{K}}{\text{GPa}}$	$0.32 \frac{k_{\text{B}}\text{K}}{\text{GPa}}$

Table 2.10: Linear pressure gradients of angles and bond lengths from experimental data in reference [62] (top) and the resulting theoretical pressure gradients $\partial J_\theta/\partial p = (\partial J/\partial \theta)(\partial \theta/\partial p)$ (bottom). The values for $\partial J/\partial \theta$ are given in table 2.6.

rather reliable though. The values obtained in the different approaches are given in table 2.9 for comparison.

2.5.2 Pressure

Bräuninger *et al.* [61] and Braden *et al.* [62] have investigated the pressure dependence of the angles and bond lengths in CuGeO_3 under hydrostatic pressure. The linearity of the pressure dependence is reasonable for pressures < 2 GPa. The values for the pressure gradients obtained from reference [62] are shown in table 2.10.

Regarding the partial derivative of the exchange integral $\partial J_\theta/\partial p = (\partial J/\partial \theta)(\partial \theta/\partial p)$ I find immediately the pressure gradients of the different angular and bond length contributions to J as given in table 2.10. Considering all four contributions, I obtain the total variation of the antiferromagnetic exchange.

$$\frac{\partial J}{\partial p} = 2 \frac{\partial J_\eta}{\partial p} + 2 \frac{\partial J_\delta}{\partial p} + 2 \frac{\partial J_{\text{Ge}}}{\partial p} + 4 \frac{\partial J_{\text{Cu}}}{\partial p} = -9 \frac{k_{\text{B}}\text{K}}{\text{GPa}} \quad (2.40)$$

For $J/k_{\text{B}} = 150$ K this value corresponds to $\partial J/(J\partial p) \approx -6$ % per GPa. The pressure dependence of the magnetic susceptibility is directly related to the magnetostriction. A value of $-\partial \chi/(\chi \partial p) \sim \partial J/(J\partial p) \approx -8$ % per GPa was obtained after averaging the uniaxial components [47, 48, 24]. Takahashi *et al.* [45] have measured the pressure dependence

Method [Reference]	$\frac{\partial J}{J\partial p}$
Harmonic theory and mean-field [here]	-6 % $\frac{1}{\text{GPa}}$
Susceptibility via magnetostriction [47, 48]	-8 % $\frac{1}{\text{GPa}}$
Curie-Weiss fit to the susceptibility [45]	-7 % $\frac{1}{\text{GPa}}$
Fit to the triplet dispersion [46]	-8 to -10 % $\frac{1}{\text{GPa}}$

Table 2.11: *Variation of J with pressure.*

of the Curie constant C by fitting a Curie-Weiss law to the high temperature tail of the magnetic susceptibility. Assuming $C \sim 1/J$ one can estimate a value of about $\partial J/(J\partial p) \approx -7$ % per GPa. Nishi and coworkers [46] compared fits to the dispersion of the lowest triplet excitations at different pressures. They assume the ratio between the exchange J and next nearest neighbor exchange J_2 with a value of $J_2/J \approx 0.25$ not to alter under pressure and find $\partial J/(J\partial p) \approx -10$ % per GPa. In contrast to that Fabricius *et al.* [24] find J_2 not to alter under pressure. Then the result from Nishi's analysis is corrected to $\partial J/(J\partial p) \approx -8$ % per GPa. A newer analysis by Nishi and coworkers [49] yields at ambient pressure $J_2/J = 0.166$ which is increased to $J_2/J = 0.180$ at 2 GPa.

A summary of the values is given in table 2.11 showing their consistency. It must be stressed that the values extracted from the experiments are subject to corrections from the explicit pressure dependence of J_2 which is still controversial [63].

2.5.3 Thermal expansion and spontaneous strain

In a harmonic lattice the coefficients of linear thermal expansion $\alpha = (\partial L)/(L\partial T)_p$ vanish. Here L is the length of the crystal in a given spatial direction. Anharmonic contributions result in temperature dependent phonon frequencies which in turn yield finite values for α . The coefficient of thermal expansion is linked to the specific heat via the (temperature dependent) Grüneisen parameter. This implies in the limiting cases $T \rightarrow 0$: $\alpha \sim T^3$ and $T \gg \Theta_D$: $\alpha \sim \text{constant}$, where Θ_D is the Debye temperature [2].

The thermal expansion in CuGeO_3 can be attributed to two effects: the usual anharmonic behavior described above and anomalies due to the spin-phonon coupling [6, 64]. The coefficient of linear thermal expansion of the c axis in CuGeO_3 has a negative sign between T_{SP} and $T \sim 200$ K. The expansion of the c axis enlarges J via the angle η . The spin system then gains energy when the temperature is lowered to $T \sim J$ by driving the anomaly [65]. A rough quantitative estimate can be extracted from the analysis of the temperature dependence of the herein considered bond lengths and angles given by Braden *et al.* [6] Their temperature dependence between 295 K and 20 K is close to linear and presented in table 2.12. Summing up the different contributions equivalently to equation (2.40) yields $\partial J/(J\partial T) \approx -2.6$ % per 250 K ($J/k_B = 150$ K). This effect is a superposition of the normal thermal expansion with positive $\partial J_{\text{norm}}/(J\partial T)$ and the anomalous effect at

θ	η	δ	d_{Cu}	d_{Ge}
$\frac{\partial \theta^\kappa}{\partial T}$	$-0.2 \frac{\text{deg}}{250\text{K}}$	$0.6 \frac{\text{deg}}{250\text{K}}$	$0.0002 \frac{\text{\AA}}{250\text{K}}$	$-0.002 \frac{\text{\AA}}{250\text{K}}$
$\frac{\partial J_\theta}{\partial T}$	$-3.1 \frac{k_{\text{B}}\text{K}}{250\text{K}}$	$0.9 \frac{k_{\text{B}}\text{K}}{250\text{K}}$	$0.04 \frac{k_{\text{B}}\text{K}}{250\text{K}}$	$0.2 \frac{k_{\text{B}}\text{K}}{250\text{K}}$

Table 2.12: *Experimental linear temperature gradients of angles and bond lengths from reference [6] (top) and the resulting theoretical contributions to the temperature dependence of J (bottom) between 20 K and 295 K.*

	C_{11}	C_{22}	C_{33}	C_{12}	C_{13}	C_{23}
Exp. [$10^{11} \frac{\text{dyn}}{\text{cm}^2}$]	7.4	2.1	33.2	-	-	-
Theory [$10^{11} \frac{\text{dyn}}{\text{cm}^2}$]	8.2	5.0	34.6	3.0	4.0	2.2

Table 2.13: *Experimental uniaxial elastic constants from reference [66] (top) and the theoretical elastic constants obtained from the shell model (bottom).*

low temperature which can be estimated by $\partial J_{\text{an}}/(J\partial T) \leq 2\partial J_\eta/(J\partial T) = -4.1\%$ per 250 K.

As the crystal undergoes the spin-Peierls transition spontaneous strain appears along all three orthorhombic directions [5, 64]. The strain couples different T_2^+ modes [1]. Here I show the resulting corrections to equation (2.35) to be unimportant. The elastic energy per unit cell related to the spontaneous strain at $T \sim 4$ K can be estimated from the elastic constants. The diagonal elastic constants C_{ii} were taken from the ultra-sound study by Poirier *et al.* [66], and off-diagonal terms C_{ij} were calculated with the lattice dynamical model [53] as shown in table 2.13 using standard notation [2]. With the values for the strain ϵ_i given by Winkelmann *et al.* [64] I find

$$\frac{E_{\text{strain}}}{k_{\text{B}}} = \frac{a \cdot b \cdot c}{2k_{\text{B}}} \sum_{i,j=1,2,3} \epsilon_i C_{ij} \epsilon_j = 7 \cdot 10^{-4} \text{ K}. \quad (2.41)$$

Note that the strain components $\epsilon_4 = \epsilon_5 = \epsilon_6$ vanish, since the orthorhombicity is conserved. The elastic energy involved in the strain is four orders of magnitude smaller than the elastic energy of the dimerization given in equation (2.39).

Note that the components of the spontaneous strain [64] have the opposite sign compared with the anomalies of the thermal expansion [44] discussed above. The spontaneous strain may thus be interpreted as a relaxation of the latter when the spin system changes its character at the spin-Peierls transition. A possible origin is the coupling via the spin system as discussed in section 4.2.2. The relaxation is of the order of 1%.

λ	1	2	3	4
$g_\lambda^{\text{Cu}}/k_B$	-0.5 K	17 K	-20 K	1.6 K
$g_\lambda^{\text{loc}}/k_B$	-7.2 K	12 K	4.8 K	-7.5 K

Table 2.14: Coupling constants to real-space normal modes obtained from equation (2.43) and equation (2.44).

2.6 Coupling constants for real-space normal coordinates

In order to obtain real-space expressions I use the Fourier representation of the Bose operators

$$b_{\lambda,q} = \frac{1}{\sqrt{N}} \sum_l e^{-iqR_l} b_{\lambda,l}. \quad (2.42)$$

For simplicity I neglect the wave vector dependence of the frequencies $\Omega_\lambda = \Omega_{\lambda,q_0}$ and of the polarization vectors $e_\nu^\alpha(\lambda) = e_\nu^\alpha(\lambda, \mathbf{q}_0)$. The coupling constants g_{λ,q_0} in equation (2.20) then are be divided into

$$\sqrt{\frac{2\Omega_\lambda}{\hbar}} g_\lambda^{\text{Cu}} = g_{\text{Cu}}^z \frac{e_{\text{Cu}}^z(\lambda)}{\sqrt{m_{\text{Cu}}}}, \quad (2.43)$$

$$\sqrt{\frac{2\Omega_\lambda}{\hbar}} g_\lambda^{\text{loc}} = g_{\text{Ge}}^y \frac{e_{\text{Ge}}^y(\lambda)}{\sqrt{m_{\text{Ge}}}} + g_{\text{O}_2}^x \frac{e_{\text{O}_2}^x(\lambda)}{\sqrt{m_{\text{O}_2}}} + g_{\text{O}_2}^y \frac{e_{\text{O}_2}^y(\lambda)}{\sqrt{m_{\text{O}_2}}}. \quad (2.44)$$

Transforming the Hamiltonian (2.24) via (2.42) I obtain in real space

$$\begin{aligned} H_{\text{r}} = & \sum_{\lambda,l} \hbar\Omega_\lambda \left(b_{\lambda,l}^\dagger b_{\lambda,l} + \frac{1}{2} \right) + J \sum_l \mathbf{S}_l \cdot \mathbf{S}_{l+1} \\ & + \sum_{\lambda,l} (-1)^{l_y} \left[g_\lambda^{\text{Cu}} \left(b_{\lambda,l}^\dagger + b_{\lambda,l} - b_{\lambda,l+\hat{z}}^\dagger - b_{\lambda,l+\hat{z}} \right) \right. \\ & \left. + g_\lambda^{\text{loc}} \left(b_{\lambda,l}^\dagger + b_{\lambda,l} + b_{\lambda,l+\hat{y}}^\dagger + b_{\lambda,l+\hat{y}} \right) \right] \mathbf{S}_l \cdot \mathbf{S}_{l+\hat{z}}. \end{aligned} \quad (2.45)$$

The coupling constants are given in table 2.14. This result implies that the oxygen and germanium displacements are of the same importance for the spin-phonon coupling as the copper elongation.

Motivated by the symmetry of the Peierls-active phonon modes an effective one-dimensional model can be obtained by restricting the sum to a single chain. The Fourier transform of the one-dimensional model derived from equation (2.45) shows the different

$\sqrt{\langle (r_{\text{Cu}}^z)^2 \rangle}$	$\sqrt{\langle (r_{\text{Ge}}^y)^2 \rangle}$	$\sqrt{\langle (r_{\text{O}_2}^x)^2 \rangle}$	$\sqrt{\langle (r_{\text{O}_2}^y)^2 \rangle}$
0.029 Å	0.035 Å	0.048 Å	0.053 Å

Table 2.15: Zero point motion of the ions obtained by neglecting the dispersion of the T_2^+ modes via equation (2.48).

q dependences ($q \equiv q_z$) of the copper term and the local term.

$$\begin{aligned}
H_{1\text{D}} &= \sum_{\lambda, q} \hbar \Omega_{\lambda} \left(b_{\lambda, q}^{\dagger} b_{\lambda, -q} + \frac{1}{2} \right) + J \sum_{l_z} \mathbf{S}_{l_z} \cdot \mathbf{S}_{l_z+1} \\
&+ \sum_{\lambda, q} \frac{g_{1\text{D}}(q)}{\sqrt{N}} \left(b_{\lambda, -q}^{\dagger} + b_{\lambda, q} \right) \sum_{l_z} e^{iqR_{l_z}} \mathbf{S}_{l_z} \cdot \mathbf{S}_{l_z+1}
\end{aligned} \tag{2.46}$$

Here I defined the one-dimensional coupling constant

$$g_{1\text{D}}(q) = (1 - e^{iqc})g_{\lambda}^{\text{Cu}} + 2g_{\lambda}^{\text{loc}}. \tag{2.47}$$

Several studies [65, 58, 59, 67, 50, 68, 69] have been carried out using real-space Hamiltonians in the form of (2.45) reduced to a one-dimensional model. Usually a single mode Hamiltonian only keeping the local term is considered, i.e., in their notation $2g_1^{\text{loc}} \equiv g$ while the other coupling constants are set to zero. Considering g_2^{Cu} , g_2^{loc} , and g_1^{loc} being of the same order of magnitude this simplification should only yield qualitative results.

Yet, these treatments include the dynamics of the phonons. The significance of the latter can be estimated from the size of the zero point motion of the ions. Without the negligible contribution from the macroscopic occupation (section 2.5.1, table 2.8) the fluctuations of the T_2^+ modes at $T = 0$ can be obtained from equation (2.5) using the approximation of dispersionless phonons introduced above.

$$\langle (r_{\nu}^{\alpha})^2 \rangle = \frac{1}{N} \sum_{\mathbf{n}} \langle (r_{\nu \mathbf{n}}^{\alpha})^2 \rangle_{T=0} = \sum_{\lambda} \left(\frac{e_{\nu}^{\alpha}(\lambda)}{\sqrt{m_{\nu}}} \right)^2 \frac{\hbar}{2\Omega_{\lambda}} \tag{2.48}$$

The resulting values are given in table 2.15. They are consistent with the values of the total zero point fluctuations obtained from the shell model and the neutron scattering experiments presented in reference [6]. The zero point fluctuations are thus a factor of 5 to 10 larger than the static distortions as given in equation (2.11).

On the other hand the Ginzburg criterion discussed in section 2.3.1 and the consistency of our results with experimental ones justify our mean-field approach. In accordance to that Klümper *et al.* [57] show that a variety of physical quantities can be obtained correctly in a mean-field picture. For the derivation of their model and a discussion see section 4.1.2. It is beyond the scope of this work but certainly an interesting question addressed to future studies which quantities are sensitive to the zero point fluctuations and why. In section 4.2.3 I propose a model to include Gaussian fluctuations within a pathintegral approach.

2.7 Discussion of χ_0

The approach by Cross and Fisher [14, 70] gave a value of $\chi_0 \approx 0.26$. This value is independent of J because of the scale invariance at $q_z = \pi/c$. The scaling hypothesis is applicable close to the critical point of the spin chain, i.e., in the limit $T \rightarrow 0$. Recent DMRG results obtained by Klümper *et al.* [57, 63] show a strong temperature dependence of $\chi_0(T/J)$. For $J_2 = 0$ and $J = 120$ K they find $\chi_0(T_{\text{SP}}/J) \approx 0.28$, for $J_2/J = 0.241$ and $J = 150$ K the parameter attains $\chi_0(T_{\text{SP}}/J) \approx 0.56$, whereas for $J_2/J = 0.35$ and $J = 160$ K they find $\chi_0(T_{\text{SP}}/J) \approx 1$.

The exact value of J_2 in CuGeO_3 has not yet been determined. Fits to the susceptibility for $T > T_{\text{SP}}$ indicate an overcritical J_2 [23, 24], but fits to the four-spinon continuum seen by Raman scattering [71] indicate an undercritical J_2 . In favour of an undercritical J_2 is also the small binding energy of the singlet bound-state for $T < T_{\text{SP}}$, as seen by Raman experiments [33, 39]. Interchain coupling will reduce the value of χ_0 because of an enhancement of antiferromagnetic correlations [60].

As can be seen from equation (2.25) our coupling constants scale as $g_\lambda \sim \sqrt{\chi_0}^{-1}$. From the above results follows $1 < \sqrt{\chi_0}^{-1} < 1.9$ and I adapt the mean value of $\chi_0 = 0.5$ for our calculations. This value is close to the result for $J_2/J = 0.241$. Within the accuracy of our approach I can use $J = 150$ K as given by Castilla *et al.* [34]. The choice of χ_0 is justified a posteriori by the agreement of the results in the literature. Also note that including a NNN term with $J_2/J = 0.24$ in equation (2.38) with $\delta_J = 0.1$ and using exact diagonalization gives a value of $\sum_{l_z} (-1)^{l_z} \langle \mathbf{S}_{l_z} \cdot \mathbf{S}_{l_z+1} \rangle / N = 0.57$ per two Cu ions in agreement with the value given in equation (2.36).

Applying hydrostatic pressure the transition temperature grows at a rate of 4.8 K/GPa [45]. In our approach T_{SP} is given by equation (2.25) and depends on the coupling constants g_{λ, q_0} , the frequencies Ω_{λ, q_0} , and the factor χ_0 . The coupling constants g_{λ, q_0} in turn depend on the linear derivatives of the magnetic exchange g_ν^α and the polarization vectors, as given in equation (2.20). In a harmonic lattice the phonon frequencies and polarization vectors are independent of pressure. It seems very unlikely that the Peierls-active modes exhibit extremely large negative Grüneisen parameters which would be needed in order to describe the increase of T_{SP} upon pressure via the pressure dependence of the phonon frequencies. The linear coupling constants g_ν^α also are independent of pressure, and since the lattice distortions are rather small [61, 62] I do not expect higher order contributions to play a crucial role. I must thus conclude the value of χ_0 to be strongly pressure dependent.

Together with the pressure dependence of J_2/J discussed by Fabricius *et al.* [24], this can explain the shift of T_{SP} [63]. When introducing interchain coupling, prefactors and the functional dependence of the spin-spin correlation function are also altered [72]. The compressibility of the crystal is largest in b direction so that the alternation of the interchain coupling under pressure is another possible origin of the pressure dependence of χ_0 and T_{SP} .

2.8 Summary

In this chapter I have given a detailed analysis of the microscopic magneto-elastic coupling in CuGeO_3 which may be easily transferred to other systems. The comparison of several theoretical and experimental approaches yields a satisfactory consistency. Numbers have been given in table 2.7 for the angular dependence of the magnetic exchange, in table 2.9 for the dimerization, and in table 2.11 for the pressure dependence of the magnetic exchange. The quantitative agreement of course is limited by the uncertainties within experiments and theoretical techniques. Coupling constants for effective one-dimensional real-space model Hamiltonians accessible to numerical studies are given in table 2.14. I have discussed the applicability of static models (section 2.5.1 and 2.6) and I was able to explain qualitatively the c axis anomaly of the thermal expansion (section 2.5.3).

Chapter 3

Partition function

The trace over the phonon states can be transformed to Gaussian integrals introducing Bose coherent states. The pathintegral representation allows for a representation of the partition function

$$Z = \mathbf{Tr} \exp \{-\beta H\}, \quad (3.1)$$

from which it is possible to derive explicitly a number of effective models and approximations used to study spin-phonon coupled systems. $\beta = 1/(k_B T)$ is the inverse temperature, k_B is Boltzmann's constant. In this chapter I discuss the derivation of the representation and its Fourier transformation and turn to applications in chapter 4.

In the previous chapter 2 it has been shown that the appropriate Hamiltonian for the description for a spin-Peierls system can be derived microscopically (see page 21). For clarity I repeat here the expressions given in previous chapters. The appropriate three dimensional Hamiltonian for a spin-Peierls system consists of three parts

$$H = H_p + H_s + H_{sp}. \quad (3.2)$$

The three dimensional harmonic phonon part

$$H_p = \sum_{\lambda, q} \hbar \Omega_{\lambda, q} b_{\lambda, q}^\dagger b_{\lambda, q} \quad (3.3)$$

includes the all relevant modes λ . In the case of CuGeO_3 we have $\lambda \in \{1, \dots, 4\}$, as discussed in chapter 2 and in references [44] and [73]. Here the Hamiltonian is shifted by its ground state contribution $\sum_{\lambda, q} \hbar \Omega_{\lambda, q}/2$.

In this chapter I generalize the spin part to anisotropic nearest neighbor antiferromagnetic exchange in order to be able to tune between the limiting cases of the XY and Ising model. The anisotropic spin 1/2 Heisenberg Hamiltonian with next nearest neighbor frustration for the spin chains running in z direction is

$$\begin{aligned} H_s = & J \sum_l \left[\frac{1}{2} (S_l^+ S_{l+\hat{z}}^- + S_l^- S_{l+\hat{z}}^+) + \frac{J_z}{J} S_l^z S_{l+\hat{z}}^z \right] \\ & + J_2 \sum_l \left[\frac{1}{2} (S_l^+ S_{l+2\hat{z}}^- + S_l^- S_{l+2\hat{z}}^+) + \frac{J_{2,z}}{J_2} S_l^z S_{l+2\hat{z}}^z \right], \end{aligned} \quad (3.4)$$

where J_z and J are the nearest-neighbor- S^z and -transversal spin-component exchange integrals, respectively. J_2 and $J_{2,z}$ are the corresponding next nearest neighbor exchange integrals. The transversal part has been rewritten in spin raising and lowering operators. The index \mathbf{l} runs over all magnetic ions, \hat{z} is a unit vector in z direction.

The spin-phonon coupling term from equation (2.21) on page 19 is modified to

$$H_{sp} = \frac{1}{\sqrt{N}} \sum_{\mathbf{q}} Y_{-\mathbf{q}} \sum_{\lambda} g_{\lambda,\mathbf{q}} \left(b_{\lambda,-\mathbf{q}}^{\dagger} + b_{\lambda,\mathbf{q}} \right). \quad (3.5)$$

The Fourier transform of the anisotropic electronic operator

$$Y_{-\mathbf{q}} := \sum_{\mathbf{l}} \frac{e^{i\mathbf{q}\mathbf{R}_{\mathbf{l}} + i\pi l_y}}{2} [S_{\mathbf{l}}^+ S_{\mathbf{l}+\hat{z}}^- + S_{\mathbf{l}}^- S_{\mathbf{l}+\hat{z}}^+ + 2\gamma S_{\mathbf{l}}^z S_{\mathbf{l}+\hat{z}}^z]. \quad (3.6)$$

was introduced. I have defined the ratio $\gamma = J_z/J$. Since $Y_{-\mathbf{q}}$ consist of local spin-pair operators I will refer to it as a dimer operator. In the isotropic limit, where $J = J_z$ or $\gamma = 1$, equation (3.6) becomes equation (2.18) where $Y_{-\mathbf{q}}^{(1)}$ was defined.

I have not included the next nearest neighbor contribution for the reasons discussed on page 19. The next nearest neighbor contribution vanish at the wave vector of the spin-Peierls distortion $\mathbf{q}_0 = (\pi/a, 0, \pi/c)$, which most of this thesis is focused on. I will discuss its effect qualitatively where necessary.

3.1 Bose coherent states

The Bose coherent states are defined as [74]

$$|\Phi\rangle = \exp \left\{ \sum_{\mathbf{q}} (\phi_{\mathbf{q}} b_{\mathbf{q}}^{\dagger} - \phi_{\mathbf{q}}^* b_{\mathbf{q}}) \right\} |0\rangle \quad (3.7)$$

with the closure relation

$$1 = \left[\prod_{\mathbf{q}} \int_{\mathcal{C}} \frac{d\phi_{\mathbf{q}}^* d\phi_{\mathbf{q}}}{2\pi i} \right] |\Phi\rangle \langle \Phi|. \quad (3.8)$$

Here q runs over a set of quantum numbers. The matrix elements of any normal ordered operator functional $A\{b_{\mathbf{q}}^{\dagger}, b_{\mathbf{q}}\}$ are

$$\langle \Phi | A\{b_{\mathbf{q}}^{\dagger}, b_{\mathbf{q}}\} | \Phi' \rangle = A\{\phi_{\mathbf{q}}^*, \phi_{\mathbf{q}}\} e^{-\sum_{\mathbf{q}} [\frac{1}{2}|\phi_{\mathbf{q}}|^2 + \frac{1}{2}|\phi'_{\mathbf{q}}|^2 + \phi_{\mathbf{q}}^* \phi'_{\mathbf{q}}]}. \quad (3.9)$$

The trace in the partition function (3.1) is divided into a spin part \mathbf{Tr}_s and phonon part \mathbf{Tr}_p . I introduce the Trotter parameter $t = \tau/\epsilon$ where $\epsilon = \beta/M$. Expressing the phonon trace in terms of coherent states using equation (3.8) the partition function is written as

$$Z = \lim_{\epsilon \rightarrow 0} \mathbf{Tr}_s \left[\prod_{\lambda,\mathbf{q}} \int_{\mathcal{C}} \frac{d\phi_{\lambda,\mathbf{q}}^* d\phi_{\lambda,\mathbf{q}}}{2\pi i} \right] \langle \Phi | \prod_{t=1}^M e^{-\epsilon H} | \Phi \rangle. \quad (3.10)$$

I introduce $M - 1$ closure relations (3.8) between every pair of time slices. Normal ordering of the terms $\exp\{\epsilon H\} = : \exp\{\epsilon H\} : + O(\epsilon^2)$ yields an error negligible in the limit $\epsilon \rightarrow 0$ [4]. The Bose operators can then be traced out using equation (3.9) for every time slice. I introduce the shorthand

$$\lim_{\epsilon \rightarrow 0} \left[\prod_{\lambda, \mathbf{q}, t} \int_{\mathcal{C}} \frac{d\phi_{\lambda, \mathbf{q}}^*(t) d\phi_{\lambda, \mathbf{q}}(t)}{2\pi i} \right] = \int [\mathcal{D}\phi] \quad (3.11)$$

and write

$$Z = \lim_{\epsilon \rightarrow 0} \mathbf{Tr}_s \int [\mathcal{D}\phi] \prod_{\lambda, \mathbf{q}, t} e^{-\phi_{\lambda, \mathbf{q}}^*(t+1) [\phi_{\lambda, \mathbf{q}}(t+1) - \phi_{\lambda, \mathbf{q}}(t)] - \epsilon \Omega_{\lambda, \mathbf{q}} \phi_{\lambda, \mathbf{q}}^*(t+1) \phi_{\lambda, \mathbf{q}}(t)} \prod_{\lambda, \mathbf{q}, t} \exp \left\{ -\epsilon \frac{g_{\lambda, \mathbf{q}}}{\sqrt{N}} [\phi_{\lambda, -\mathbf{q}}^*(t+1) + \phi_{\lambda, \mathbf{q}}(t)] Y_{-\mathbf{q}} - \epsilon H_s \right\}. \quad (3.12)$$

The notation has been chosen such that the trace imposes the boundary condition $\phi_{\lambda, \mathbf{q}}(M+1) \equiv \phi_{\lambda, \mathbf{q}}(1)$ for the Bose fields.

Now the spin-phonon coupling can be treated as a perturbation with respect to the spin system by introducing the time dependence of $Y_{-\mathbf{q}}$ in the interaction representation.

$$Y_{-\mathbf{q}}(t) = e^{ctH_s} Y_{-\mathbf{q}} e^{-ctH_s}. \quad (3.13)$$

The second line of equation (3.12) can be factorized inducing an error of order ϵ^2 negligible for $\lim_{\epsilon \rightarrow 0}$. Then one can transform

$$\begin{aligned} & \prod_{\lambda, \mathbf{q}, t} \exp \left\{ -\epsilon \frac{g_{\lambda, \mathbf{q}}}{\sqrt{N}} [\phi_{\lambda, -\mathbf{q}}^*(t+1) + \phi_{\lambda, \mathbf{q}}(t)] Y_{-\mathbf{q}} \right\} e^{-\epsilon H_s} \\ &= \prod_{\lambda, \mathbf{q}, t} e^{ctH_s} \exp \left\{ -\epsilon \frac{g_{\lambda, \mathbf{q}}}{\sqrt{N}} [\phi_{\lambda, -\mathbf{q}}^*(t+1) + \phi_{\lambda, \mathbf{q}}(t)] Y_{-\mathbf{q}}(t) \right\} e^{-\epsilon(t+1)H_s} \\ &= e^{-\beta H_s} \prod_{\lambda, \mathbf{q}, t} \exp \left\{ -\epsilon \frac{g_{\lambda, \mathbf{q}}}{\sqrt{N}} [\phi_{\lambda, -\mathbf{q}}^*(t+1) + \phi_{\lambda, \mathbf{q}}(t)] Y_{-\mathbf{q}}(t) \right\}. \end{aligned} \quad (3.14)$$

When writing the product over t as a sum in the exponent the discrete time ordering operator T_t has to be introduced. The partition function becomes

$$Z = \lim_{\epsilon \rightarrow 0} \mathbf{Tr}_s e^{-\beta H_s} T_t \int [\mathcal{D}\phi] e^{-\epsilon \sum_{\lambda, \mathbf{q}, t} \mathcal{L}_{\epsilon}[\phi^* \phi Y]}. \quad (3.15)$$

The discrete imaginary time Lagrangian is given by

$$\mathcal{L}_\epsilon = \phi_{\lambda,\mathbf{q}}^*(t+1) \left[\frac{\phi_{\lambda,\mathbf{q}}(t+1) - \phi_{\lambda,\mathbf{q}}(t)}{\epsilon} + \Omega_{\lambda,\mathbf{q}} \phi_{\lambda,\mathbf{q}}(t) \right] + \frac{g_{\lambda,\mathbf{q}}}{\sqrt{N}} [\phi_{\lambda,-\mathbf{q}}^*(t+1) + \phi_{\lambda,\mathbf{q}}(t)] Y_{-\mathbf{q}}(t). \quad (3.16)$$

We can now perform formally [75, 4] the continuum limit $\lim_{\epsilon \rightarrow 0}$. The sum over the Trotter times t in the exponent then becomes an integral in the sense of Riemann's definition. The partition function then is given by

$$Z = Z_s \int [\mathcal{D}\phi] \left\langle T_\tau \exp \left\{ - \int_0^\beta d\tau \sum_{\lambda,\mathbf{q}} \mathcal{L}[\phi^* \phi Y] \right\} \right\rangle \quad (3.17)$$

with the Lagrangian

$$\mathcal{L}[\phi^* \phi Y] = \phi_{\lambda,\mathbf{q}}^*(\tau) [\hbar \Omega_{\lambda,\mathbf{q}} + \partial_\tau] \phi_{\lambda,\mathbf{q}}(\tau) + \frac{g_{\lambda,\mathbf{q}}}{\sqrt{N}} [\phi_{\lambda,-\mathbf{q}}^*(\tau) + \phi_{\lambda,\mathbf{q}}(\tau)] Y_{-\mathbf{q}}(\tau). \quad (3.18)$$

$Z_s = \mathbf{Tr}_s \exp\{-\beta H_s\}$ is the partition function of the unperturbed spin Hamiltonian (3.4), T_τ is the imaginary time τ ordering operator, β is the inverse temperature, and the brackets give the thermodynamic expectation value of an arbitrary operator \hat{A} as

$$\langle \hat{A} \rangle = Z_s^{-1} \mathbf{Tr}_s e^{-\beta H_s} \hat{A},$$

where \mathbf{Tr}_s is the trace over the spin degrees of freedom. The differential operator is defined as

$$\partial_\tau \phi_{\lambda,\mathbf{q}}(\tau) = \lim_{\epsilon \rightarrow 0} \frac{\phi_{\lambda,\mathbf{q}}(t+1) - \phi_{\lambda,\mathbf{q}}(t)}{\epsilon}. \quad (3.19)$$

Via the grand canonical potential $F = -\beta^{-1} \ln Z$ all relevant physical quantities can be derived.

3.2 Ordered phase

In the distorted spin-Peierls phase the Peierls active phonon modes condense. It will turn out to be advantageous to immediately introduce shifted Bose operators

$$\tilde{b}_{\lambda,\mathbf{q}} = b_{\lambda,\mathbf{q}} - \langle b_{\lambda,\mathbf{q}_0} \rangle \delta_{\mathbf{q}=\mathbf{q}_0} \quad (3.20)$$

imposing $\langle \tilde{b}_{\lambda,q} \rangle = 0$. The properties of the expectation value of $\langle b_{\lambda,q_0} \rangle$ can be derived in the static limit of the functional integral formulation derived here which is done in section 4.1.1.

Introducing the shift (3.20) the phonon Hamiltonian (3.3) becomes

$$H_p = \sum_{\lambda,q} \hbar\Omega_{\lambda,q} \tilde{b}_{\lambda,q}^\dagger \tilde{b}_{\lambda,q} + \sum_{\lambda} \hbar\Omega_{\lambda,q_0} \left(\langle b_{\lambda,q_0} \rangle \tilde{b}_{\lambda,q_0}^\dagger + \langle b_{\lambda,q_0} \rangle^* \tilde{b}_{\lambda,q_0} \right) + \sum_{\lambda} \hbar\Omega_{\lambda,q_0} \left| \langle b_{\lambda,q_0} \rangle \right|^2 \quad (3.21)$$

The lattice distortion induces via (3.5) a magnetic exchange alternation

$$\delta_J(\mathbf{l}) = \frac{1}{\sqrt{N}} \sum_{\lambda} e^{i\mathbf{q}_0 \mathbf{R}_l + i\pi l_y} g_{\lambda,q_0} \left(\langle b_{\lambda,-\mathbf{q}_0} \rangle^* + \langle b_{\lambda,q_0} \rangle \right). \quad (3.22)$$

leading to the Hamiltonian

$$H_\delta = J \sum_l (1 + \delta_J(\mathbf{l})) \left[\frac{1}{2} (S_l^+ S_{l+\hat{z}}^- + S_l^- S_{l+\hat{z}}^+) + \frac{J_z}{J} S_l^z S_{l+\hat{z}}^z \right] + J_2 \sum_l \left[\frac{1}{2} (S_l^+ S_{l+2\hat{z}}^- + S_l^- S_{l+2\hat{z}}^+) + \frac{J_{2,z}}{J_2} S_l^z S_{l+2\hat{z}}^z \right] + \sum_{\lambda} \hbar\Omega_{\lambda,q_0} \left| \langle b_{\lambda,q_0} \rangle \right|^2. \quad (3.23)$$

This Hamiltonian is one-dimensional since the spin chains are decoupled. As discussed on page 19, the distortion modulated with \mathbf{q}_0 does not effect the next nearest neighbor part. I have included in (3.23) the constant $\sim \langle b_{\lambda,q_0} \rangle^2$ initially introduced in equation (3.21). In this representation phonon part then is

$$\tilde{H}_p = \sum_{\lambda,q} \hbar\Omega_{\lambda,q} \tilde{b}_{\lambda,q}^\dagger \tilde{b}_{\lambda,q} + \sum_{\lambda} \hbar\Omega_{\lambda,q_0} \left(\langle b_{\lambda,q_0} \rangle \tilde{b}_{\lambda,q_0}^\dagger + \langle b_{\lambda,q_0} \rangle^* \tilde{b}_{\lambda,q_0} \right) \quad (3.24)$$

and describes displaced harmonic oscillators at \mathbf{q}_0 . The spin-phonon coupling term (3.5) then has to be rewritten $H_{sp} \rightarrow \tilde{H}_{sp}$ by replacing $b_{\lambda,q} \rightarrow \tilde{b}_{\lambda,q}$.

$$\tilde{H}_{sp} = \frac{1}{\sqrt{N}} \sum_{\mathbf{q}} Y_{-\mathbf{q}} \sum_{\lambda} g_{\lambda,q} \left(\tilde{b}_{\lambda,-\mathbf{q}}^\dagger + \tilde{b}_{\lambda,q} \right). \quad (3.25)$$

The partition function can be derived according to section 3.1 introducing displaced fields $\tilde{\phi}_{\lambda,q}$.

$$Z = Z_\delta \int [\mathcal{D}\tilde{\phi}] \left\langle T_\tau \exp \left\{ - \int_0^\beta d\tau \sum_{\lambda,q} \tilde{\mathcal{L}}[\tilde{\phi}^* \tilde{\phi} Y] \right\} \right\rangle_\delta \quad (3.26)$$

with the Lagrangian

$$\tilde{\mathcal{L}}[\tilde{\phi}^* \tilde{\phi} Y] = \tilde{\phi}_{\lambda, \mathbf{q}}^*(\tau) [\hbar \Omega_{\lambda, \mathbf{q}} + \partial_\tau] \tilde{\phi}_{\lambda, \mathbf{q}}(\tau) + \frac{g_{\lambda, \mathbf{q}}}{\sqrt{N}} \left[\tilde{\phi}_{\lambda, -\mathbf{q}}^*(\tau) + \tilde{\phi}_{\lambda, \mathbf{q}}(\tau) \right] Y_{-\mathbf{q}}(\tau) + \hbar \Omega_{\lambda, \mathbf{q}_0} \left[\langle b_{\lambda, \mathbf{q}_0} \rangle \tilde{\phi}_{\lambda, \mathbf{q}_0}^*(\tau) + \langle b_{\lambda, \mathbf{q}_0} \rangle^* \tilde{\phi}_{\lambda, \mathbf{q}_0}(\tau) \right] \delta_{\mathbf{q}=\mathbf{q}_0}. \quad (3.27)$$

Note that the integral measure is not effected by the constant displacement of the fields. I introduced the partition function of the alternating spin system $Z_\delta = \mathbf{Tr}_s \exp\{-\beta H_\delta\}$, the expectation values $\langle \rangle_\delta$ are taken with respect to $\exp\{-\beta H_\delta\}$, and the evolution operator for the spin operators is $\exp\{-\tau H_\delta\}$. The same result is obtained when introducing

$$\tilde{\phi}_{\lambda, \mathbf{q}}(t) = \phi_{\lambda, \mathbf{q}}(t) - \langle b_{\lambda, \mathbf{q}_0} \rangle \delta_{\mathbf{q}=\mathbf{q}_0} \quad (3.28)$$

into equation (3.12) and performing the transformation to interaction representation (3.14) with respect to H_δ given in equation (3.23).

The expectation value of the phonon condensation

$$\langle b_{\lambda, \mathbf{q}_0} \rangle = \mathbf{Tr} e^{-\beta H} b_{\lambda, \mathbf{q}_0} \quad (3.29)$$

can be expressed in terms of the phonon fields by proceeding equivalently to the derivation of the partition function (3.15):

$$\langle b_{\lambda, \mathbf{q}_0} \rangle = \lim_{\epsilon \rightarrow 0} \mathbf{Tr}_s e^{-\beta H_s} T_t \int [\mathcal{D}\phi] e^{-\epsilon \sum_{\lambda, \mathbf{q}, t} \mathcal{L}_\epsilon[\phi^* \phi Y]} \phi_{\lambda, \mathbf{q}_0}(M) = \langle \phi_{\lambda, \mathbf{q}_0}(\beta) \rangle. \quad (3.30)$$

Since the lattice distortion is static, i.e., $\langle \phi_{\lambda, \mathbf{q}_0}(t) \rangle \equiv \langle \phi_{\lambda, \mathbf{q}_0} \rangle$ is independent of the imaginary time, one can simply write

$$\langle b_{\lambda, \mathbf{q}_0} \rangle = \langle \phi_{\lambda, \mathbf{q}_0} \rangle \quad (3.31)$$

3.3 Fourier transform to Matsubara frequencies

The exponents in the expressions for the partition function in the ordered phase (3.17) or in the disordered phase (3.26) can be transformed to their Fourier representations introducing bosonic Matsubara frequencies $\omega_\nu = 2\pi\nu/\beta$ [76]. Because the functional integral definition in equation (3.10) is made on the discrete imaginary time lattice the Fourier transformation has to be done for discrete time Lagrangian (3.16) using finite Fourier sums. Afterwards the continuum limit $\lim_{\epsilon \rightarrow 0}$ can be formally performed again. Otherwise one encounters some ambiguity concerning the limit $\epsilon \rightarrow 0$. I give a discussion of the problems connected in section 3.3.3.

3.3.1 Discrete transformation

I define the discrete Fourier transform

$$\tilde{\phi}_{\lambda,q,\nu} = \frac{1}{\sqrt{M}} \sum_{t=0}^{M-1} e^{i\omega_\nu \epsilon t} \tilde{\phi}_{\mathbf{q}}(t) \quad (3.32)$$

and its inverse

$$\tilde{\phi}_{\mathbf{q}}(t) = \frac{1}{\sqrt{M}} \sum_{\nu=-M/2}^{M/2-1} e^{-i\omega_\nu \epsilon t} \tilde{\phi}_{\lambda,q,\nu}. \quad (3.33)$$

I recall that $\beta = \epsilon M$ and $\tau = \epsilon t$. Note that the number of fields in imaginary time space $\phi_{\lambda,q}(t)$ and in Fourier space $\phi_{\lambda,q,\nu}$ is equal. The number of degrees of freedom is conserved and the limits $\lim_{\epsilon \rightarrow 0} = \lim_{\beta/M \rightarrow 0}$ are not independent. Equivalently the transformations of the dimer operators are defined.

$$Y_{\mathbf{q},\nu} = \frac{1}{\sqrt{M}} \sum_{t=0}^{M-1} e^{i\omega_\nu \epsilon t} Y_{\mathbf{q}}(t) \quad (3.34)$$

$$Y_{\mathbf{q}}(t) = \frac{1}{\sqrt{M}} \sum_{\nu=-M/2}^{M/2-1} e^{-i\omega_\nu \epsilon t} Y_{\mathbf{q},\nu} \quad (3.35)$$

The Fourier coefficients have been chosen such that they are orthonormal

$$\frac{1}{M} \sum_t e^{i\omega_\nu t} e^{i\omega_{\nu'} t} = \delta_{\nu=\nu'} \quad (3.36)$$

and complete

$$\frac{1}{M} \sum_\nu e^{i\omega_\nu t} e^{i\omega_{\nu'} t'} = \delta_{t=t'}. \quad (3.37)$$

I present here the calculation for the more general ordered case. The disordered expressions are recovered by simply setting $\langle b_{\lambda,q_0}^\dagger \rangle = 0$. I alter the notation of the partition function (3.26)

$$Z = Z_\delta \lim_{\substack{M \rightarrow \infty \\ (\epsilon \rightarrow 0)}} \int [\mathcal{D}\tilde{\phi}] \left\langle T_\tau \exp \left\{ -\tilde{\mathcal{H}}_\epsilon \right\} \right\rangle_\delta \quad (3.38)$$

by introducing the operator in discrete time representation

$$\begin{aligned} \tilde{\mathcal{H}}_\epsilon &= \sum_{\lambda,q,t} \tilde{\phi}_{\lambda,q}^*(t+1) \left[\tilde{\phi}_{\lambda,q}(t+1) - \tilde{\phi}_{\lambda,q}(t) \right] + \frac{\beta}{M} \sum_{\lambda,q,t} \hbar \Omega_{\lambda,q} \tilde{\phi}_{\lambda,q}^*(t+1) \tilde{\phi}_{\lambda,q}(t) \\ &+ \frac{\beta}{M} \sum_{\lambda,q,t} \frac{g_{\lambda,q}}{\sqrt{N}} \left[\tilde{\phi}_{\lambda,-q}^*(t+1) + \tilde{\phi}_{\lambda,q}(t) \right] Y_{-q}(t) \\ &+ \frac{\beta}{M} \sum_{\lambda,t} \hbar \Omega_{\lambda,q_0} \left[\langle b_{\lambda,q_0} \rangle \tilde{\phi}_{\lambda,q_0}^*(t+1) + \langle b_{\lambda,q_0} \rangle^* \tilde{\phi}_{\lambda,q_0}(t) \right]. \end{aligned} \quad (3.39)$$

The latter is obtained by introducing the field shift (3.28) into the discrete time Lagrangian (3.16). (One must consider $\epsilon = \beta/M$ and $\sum_t [\tilde{\phi}_{\lambda, \mathbf{q}_0}(t+1) - \tilde{\phi}_{\lambda, \mathbf{q}_0}(t)] = 0$.) Applying the transformations (3.32) through (3.35) I find

$$\begin{aligned} \tilde{\mathcal{H}}_\nu &= \frac{\beta}{\sqrt{M}} \sum_\lambda \hbar\Omega_{\lambda, \mathbf{q}_0} \left[\langle b_{\lambda, \mathbf{q}_0} \rangle \tilde{\phi}_{\lambda, \mathbf{q}_0, 0}^* + \langle b_{\lambda, \mathbf{q}_0} \rangle^* \tilde{\phi}_{\lambda, \mathbf{q}_0, 0} \right] + \sum_{\lambda, \mathbf{q}, \nu} \tilde{\phi}_{\lambda, \mathbf{q}, \nu}^* [1 - e^{i\omega_\nu \epsilon}] \tilde{\phi}_{\lambda, \mathbf{q}, \nu} \\ &+ \frac{\beta}{M} \sum_{\lambda, \mathbf{q}, \nu} \left\{ \hbar\Omega_{\lambda, \mathbf{q}} \tilde{\phi}_{\lambda, \mathbf{q}, \nu}^* e^{i\omega_\nu \epsilon} \tilde{\phi}_{\lambda, \mathbf{q}, \nu} + \frac{g_{\lambda, \mathbf{q}}}{\sqrt{N}} \left[\tilde{\phi}_{\lambda, -\mathbf{q}, -\nu}^* e^{-i\omega_\nu \epsilon} + \tilde{\phi}_{\lambda, \mathbf{q}, \nu} \right] Y_{-\mathbf{q}, -\nu} \right\}. \end{aligned} \quad (3.40)$$

The factors $\exp\{i\omega_\nu \epsilon\} = \exp\{i\pi\nu/M\}$ describe the phase picked up by the fields $\tilde{\phi}_{\lambda, \mathbf{q}}(t)$ between two time slices t and $t+1$. It vanishes for all finite frequencies in the limit $\epsilon \rightarrow 0$. A common shorthand is

$$\lim_{\epsilon \rightarrow 0} e^{i\omega_\nu \epsilon} = e^{i\omega_\nu 0^+}. \quad (3.41)$$

Since the whole expression (3.38) has to be taken in the limit $\epsilon \rightarrow 0$ I may use

$$\lim_{\epsilon \rightarrow 0} [1 - e^{i\omega_\nu \epsilon}] = -\lim_{\epsilon \rightarrow 0} \epsilon \frac{\partial e^{i\omega_\nu \epsilon}}{\partial \epsilon} = \lim_{\substack{M \rightarrow \infty \\ (\epsilon \rightarrow 0)}} -\frac{\beta}{M} i\omega_\nu e^{i\omega_\nu \epsilon} \quad (3.42)$$

The resulting partition function then is

$$Z = Z_\delta \lim_{\substack{M \rightarrow \infty \\ (\epsilon \rightarrow 0)}} \int [\mathcal{D}\tilde{\phi}_\nu] \left\langle T_\tau \exp \left\{ -\frac{\beta}{M} \sum_{\lambda, \mathbf{q}, \nu} \tilde{\mathcal{L}}_\nu \right\} \right\rangle_\delta \quad (3.43)$$

while the transformed exponent holds the Matsubara frequency Lagrangian

$$\begin{aligned} \tilde{\mathcal{L}}_\nu &= \tilde{\phi}_{\lambda, \mathbf{q}, \nu}^* e^{i\omega_\nu \epsilon} [\hbar\Omega_{\lambda, \mathbf{q}} - i\omega_\nu] \tilde{\phi}_{\lambda, \mathbf{q}, \nu} + \frac{g_{\lambda, \mathbf{q}}}{\sqrt{N}} \left[\tilde{\phi}_{\lambda, -\mathbf{q}, -\nu}^* e^{-i\omega_\nu \epsilon} + \tilde{\phi}_{\lambda, \mathbf{q}, \nu} \right] Y_{-\mathbf{q}, -\nu} \\ &+ \sqrt{M} \sum_\lambda \hbar\Omega_{\lambda, \mathbf{q}_0} \left[\langle b_{\lambda, \mathbf{q}_0} \rangle \tilde{\phi}_{\lambda, \mathbf{q}_0, 0}^* + \langle b_{\lambda, \mathbf{q}_0} \rangle^* \tilde{\phi}_{\lambda, \mathbf{q}_0, 0} \right]. \end{aligned} \quad (3.44)$$

Note that in the static limit $\nu = 0$ with time independent fields $\tilde{\phi}_{\lambda, \mathbf{q}}(t) \equiv \tilde{\phi}_{\lambda, \mathbf{q}}$ or operators $Y_{\mathbf{q}}(t) \equiv Y_{\mathbf{q}}$ the static Fourier components attain the correct limiting values

$$\lim_{M \rightarrow \infty} \frac{\tilde{\phi}_{\lambda, \mathbf{q}, 0}}{\sqrt{M}} = \tilde{\phi}_{\lambda, \mathbf{q}}, \quad (3.45)$$

$$\lim_{M \rightarrow \infty} \frac{Y_{\mathbf{q},0}}{\sqrt{M}} = Y_{\mathbf{q}}. \quad (3.46)$$

It is important to notice that equation (3.45) and (3.46) define the static fields $\tilde{\phi}_{\lambda,\mathbf{q}}$ and operators $Y_{\mathbf{q}}$ as time-averaged values, compare equations (3.32) and (3.34).

The integral measure in the partition function (3.43) has been transformed accordingly. Since the Fourier coefficients in equations (3.32) through (3.35) have been normalized, the Jacobi determinant denoted \mathcal{J} is unity. This can be checked immediately by considering the Gaussian identity

$$1 = \int [\mathcal{D}\tilde{\phi}] \exp \left\{ - \sum_{\lambda,\mathbf{q},t} \tilde{\phi}_{\lambda,\mathbf{q}}^*(t) \tilde{\phi}_{\lambda,\mathbf{q}}(t) \right\}, \quad (3.47)$$

where $[\mathcal{D}\tilde{\phi}]$ is defined via $[\mathcal{D}\phi]$ in equation (3.11) replacing $\phi \rightarrow \tilde{\phi}$ since the constant shift from equation (3.28) leaves the integral measure unaltered. Applying the transformations (3.32) and (3.33), equation (3.47) is transformed into

$$1 = \lim_{\epsilon \rightarrow 0} \prod_{\lambda,\mathbf{q},t} \left[\int_{\mathcal{C}} \frac{d\tilde{\phi}_{\lambda,\mathbf{q},\nu}^* d\tilde{\phi}_{\lambda,\mathbf{q},\nu}}{2\pi i} \mathcal{J} \exp \left\{ - \tilde{\phi}_{\lambda,\mathbf{q},\nu}^* \tilde{\phi}_{\lambda,\mathbf{q},\nu} \right\} \right]. \quad (3.48)$$

Since the transformations (3.32) and (3.33) are linear the Jacobi determinant \mathcal{J} is independent of the fields. Rotating the fields to real and imaginary part representation

$$d\tilde{\phi}_{\lambda,\mathbf{q},\nu}^* d\tilde{\phi}_{\lambda,\mathbf{q},\nu} = 2i d\text{Re}\tilde{\phi}_{\lambda,\mathbf{q},\nu}^* d\text{Im}\tilde{\phi}_{\lambda,\mathbf{q},\nu} \quad (3.49)$$

the Gaussian integrals in equation (3.48) can be integrated out. I obtain for the Jacobi determinant

$$\mathcal{J} = \left| \frac{\partial \tilde{\phi}_{\lambda,\mathbf{q}}^*(t)}{\partial \tilde{\phi}_{\lambda,\mathbf{q},\nu}^*} \frac{\partial \tilde{\phi}_{\lambda,\mathbf{q}}(t)}{\partial \tilde{\phi}_{\lambda,\mathbf{q},\nu}} \right| = 1. \quad (3.50)$$

Consequently the integral measures are found to be equal, in other words $[D\tilde{\phi}_{\nu}] = [D(\tilde{\phi} \rightarrow \tilde{\phi}_{\nu})]$.

3.3.2 Partition function of the unperturbed phonon system

The partition function of the unperturbed phonon system is obtained from equation (3.43) with the Lagrangian (3.44) by setting $g_{\lambda,\mathbf{q}} \equiv 0$, $\langle b_{\lambda,\mathbf{q}} \rangle \equiv 0$, and disregarding the spin contribution Z_{δ} . Note that then $\tilde{\phi} \equiv \phi$.

$$Z_p = \lim_{M \rightarrow \infty} \int [\mathcal{D}\phi_{\nu}] \exp \left\{ - \frac{\beta}{M} \sum_{\lambda,\mathbf{q},\nu} \phi_{\lambda,\mathbf{q},\nu}^* e^{i\omega_{\nu}\epsilon} [\hbar\Omega_{\lambda,\mathbf{q}} - i\omega_{\nu}] \phi_{\lambda,\mathbf{q},\nu} \right\} \quad (3.51)$$

The functional integration can simply be performed via the intermediate step (see equation (3.49))

$$Z_p = \lim_{M \rightarrow \infty} \prod_{\lambda, q, \nu} \left[\int_{\mathcal{C}} \frac{d\text{Re } \phi_{\lambda, q, \nu} d\text{Im } \phi_{\lambda, q, \nu}}{\pi} \times \exp \left\{ -\frac{\beta}{M} \sum_{\lambda, q, \nu} e^{i\omega_\nu \epsilon} [\hbar\Omega_{\lambda, q} - i\omega_\nu] [(\text{Re } \phi_{\lambda, q, \nu})^2 + (\text{Im } \phi_{\lambda, q, \nu})^2] \right\} \right]. \quad (3.52)$$

One has

$$Z_p = \lim_{M \rightarrow \infty} \prod_{\lambda, q, \nu} \frac{M}{\beta} \frac{e^{-i\omega_\nu \epsilon}}{\hbar\Omega_{\lambda, q} - i\omega_\nu}. \quad (3.53)$$

The evaluation of this expression is rather tedious because the usual technical approach via functional analysis collides with the limit $\lim_{M \rightarrow \infty}$. For related problems with the limits see section 3.3.3. I will not go into the details here because the result is well known by other means [4].

$$Z_p = \prod_{\lambda, q} (1 - e^{-\beta\hbar\Omega_{\lambda, q}})^{-1} \quad (3.54)$$

The derivation of expression (3.53) will be useful later on.

3.3.3 Continuous transformation and problems involved

The phonon fields $\tilde{\phi}_q(\tau)$ and the dimer operators $Y_q(\tau)$ in the Lagrangian (3.27) can be interpreted as the interpolations of the fields $\hat{\phi}_q(t)$ and operators $Y_q(t)$ defined at the discrete Trotter times t . The continuous transforms then can be defined the usual way.

$$\tilde{\phi}_{\lambda, q, \nu} = \frac{1}{\sqrt{\beta}} \int_0^\beta d\tau e^{i\omega_\nu \tau} \tilde{\phi}_{\lambda, q}(\tau) \quad (3.55)$$

$$\tilde{\phi}_{\lambda, q}(\tau) = \frac{1}{\sqrt{\beta}} \sum_{\nu=-\infty}^{\infty} e^{-i\omega_\nu \tau} \tilde{\phi}_{\lambda, q, \nu} \quad (3.56)$$

The dimer operators transform equivalently as

$$\underline{Y}_{q, \nu} = \frac{1}{\sqrt{\beta}} \int_0^\beta d\tau e^{i\omega_\nu \tau} Y_q(\tau), \quad (3.57)$$

$$Y_q(\tau) = \frac{1}{\sqrt{\beta}} \sum_{\nu} e^{-i\omega_\nu \tau} \underline{Y}_{q, \nu}. \quad (3.58)$$

The integrals are defined in the sense of Riemann's definition.

The distinction of the Fourier transforms $\tilde{\underline{\phi}}_{\lambda,\mathbf{q},\nu}$ and $\underline{Y}_{\mathbf{q},\nu}$ is necessary because the normalization is different than for the discrete Fourier transforms defined in equations (3.32) and (3.34).

$$\tilde{\underline{\phi}}_{\lambda,\mathbf{q},\nu} = \lim_{\epsilon \rightarrow 0} \sqrt{\epsilon} \tilde{\phi}_{\lambda,\mathbf{q},\nu} \quad (3.59)$$

$$\underline{Y}_{\mathbf{q},\nu} = \lim_{\epsilon \rightarrow 0} \sqrt{\epsilon} Y_{\mathbf{q},\nu} \quad (3.60)$$

equations (3.55) through (3.58) are not normalized in contrast to the discrete transformations (3.32) through (3.35).

The direct application of the continuous transformations (3.55) through (3.58) to the continuous Lagrangian (3.27) in the partition function (3.26) has three unpleasant effects.

- Most importantly, the phase factors $\exp\{i\omega_\nu 0^+\}$ in the Lagrangian (3.44) are absent. This is erratic as is explained below. The phase factors serve as convergence factors when performing frequency sums [77].
- The prefactor $\beta/M = \epsilon$ is absent in contrast to the exponent of the partition function (3.43). The fields $\underline{\phi}$ and operators \underline{Y} carry the units of $\sqrt{\text{Energy}}$.
- The integral measure is not unity any more. The Jacobi determinant (3.50) becomes

$$\underline{\mathcal{J}} = \left| \frac{\partial \tilde{\phi}_{\lambda,\mathbf{q}}^*(\tau)}{\partial \tilde{\underline{\phi}}_{\lambda,\mathbf{q},\nu}^*} \frac{\partial \tilde{\phi}_{\lambda,\mathbf{q}}(\tau)}{\partial \tilde{\underline{\phi}}_{\lambda,\mathbf{q},\nu}} \right| = \lim_{M \rightarrow \infty} \prod_{\lambda,\mathbf{q}} \prod_{\nu=-M/2}^{M/2-1} \frac{\beta}{M} \quad (3.61)$$

and has the unit of an energy to the $4MN$ -th power. Recall that N is the number of unit cells, M is the number of time slices and the number of relevant phonon modes in CuGeO_3 is 4.

Neglecting phase factors \equiv neglecting discontinuous paths

Here I try to develop an understanding of the underlying error implied by the neglected phase factors when applying the continuous Fourier transformation. I recall that I used the definition of the differential operator (3.19) to obtain the continuous Lagrangians (3.18) and (3.27). Alternatively one may demand the fields $\tilde{\phi}_{\lambda,\mathbf{q}}(\tau)$ to *continuously* interpolate the fields $\tilde{\phi}_{\lambda,\mathbf{q}}(t)$. Then one can approximate

$$\lim_{\epsilon \rightarrow 0} \tilde{\phi}_{\lambda,\mathbf{q}}(t+1) = \lim_{\epsilon \rightarrow 0} \left(\tilde{\phi}_{\lambda,\mathbf{q}}(t) + \epsilon \dot{\tilde{\phi}}_{\lambda,\mathbf{q}}(\tau) \Big|_{\tau=ct} \right), \quad (3.62)$$

where $\dot{\tilde{\phi}}_{\mathbf{q}}(\tau)$ is the derivative of the continuous field with respect to τ . Inserting the expression (3.62) into the discrete representation of the exponent (3.39), neglecting terms $\sim \epsilon^2$, and applying *then* the discrete Fourier transformations (3.32) through (3.35) one also obtains the frequency space Lagrangian (3.44) *without* the phase factors.

Thus the omission of the phase factors $\exp\{i\omega_\nu 0^+\}$ in the frequency space Lagrangian is equivalent to only allowing continuous paths in imaginary time space. The definition of the functional integral (3.12) includes no restriction on fields $-\infty \leq \tilde{\phi}_{\lambda,q}(t) \leq \infty$. Thus, applying any restriction on the fields $\tilde{\phi}_{\lambda,q}(\tau)$ is an approximation.

Mathematically the origin of the inconsistencies lies in the violation of the uniqueness of the infinitesimal limit. To obtain the derivative $\tilde{\phi}_q(\tau)$ a limit has already been performed – even though, in the sense of the definition of ∂_τ in equation (3.19), it is *not independent* of the limit $\epsilon \rightarrow 0$. Performing the limits in equations (3.59) and (3.60) independently imposes just the same error.

Mean-field \equiv continuous paths

For any finite frequency the phase factors are irrelevant since then $\exp\{i\omega_\nu 0^+\} = 1$. Consequently the mean-field approaches, where only the static limit $\omega_\nu = 0$ is considered, only allow for continuous paths. This is what is expected since mean-field approaches describe classical saddle points.

Procedure for practical purposes

It is still convenient to work with the continuous representation of the partition function (3.26) and Lagrangian (3.27). I will use the representation in what follows, keeping in mind that the origin of the definition is discrete. In principle, it is always possible but tedious to go back to the discrete representation. I will permit myself to take the shortcut via the continuous Fourier transformations and renormalizations (3.55) through (3.60) and include the phase factors at the appropriate places. The latter is straight forward since regarding the transformation from expression (3.39) to expression (3.40) it is clear that all the complex conjugate fields $\tilde{\phi}^*(\tau) = \lim_{\epsilon \rightarrow 0} \tilde{\phi}^*(t+1)$ pick up the phase factor.

Chapter 4

Mappings and approximations

A rigorous determination of the partition function (3.43) derived in the last chapter is not possible. Mappings to other representations or limiting cases allow some insight into the physics and the interdependence of problems. I discuss some applicable approximations, their physical or mathematical justification, and their limits.

4.1 Integrating out phonon degrees of freedom: effective spin models

Integrating out the phonon degrees of freedom — either rigorously or by applying approximations — yields effective spin or electronic models that have been studied in the literature. Additionally it is possible to show the equivalence of different field-theoretical approaches as shown in section 4.1.6.

4.1.1 Static limit

Starting point is the partition function (3.43) on page 42. The static limit is obtained by retaining only the Fourier components with $\omega_\nu = 0$ in the Matsubara frequency Lagrangian (3.44). Using the notation for the renormalized static fields (3.45) and the renormalized operator (3.46) one has

$$\begin{aligned} \tilde{\mathcal{L}}_0 = & \hbar\Omega_{\lambda,q} \tilde{\phi}_{\lambda,q}^* \tilde{\phi}_{\lambda,q} + \frac{g_{\lambda,q}}{\sqrt{N}} \left[\tilde{\phi}_{\lambda,-q}^* + \tilde{\phi}_{\lambda,q} \right] Y_{-q} \\ & + \hbar\Omega_{\lambda,q_0} \left[\langle b_{\lambda,q_0}^\dagger \rangle \tilde{\phi}_{\lambda,q_0} + \langle b_{\lambda,q_0} \rangle \tilde{\phi}_{\lambda,q_0}^* \right] \delta_{q=q_0} \end{aligned} \quad (4.1)$$

in the static partition function

$$Z_{\text{stat}} = Z_{\delta} \int [\mathcal{D}\tilde{\phi}_0] \left\langle T_{\tau} \exp \left\{ -\beta \sum_{\lambda, \mathbf{q}} \tilde{\mathcal{L}}_0 \right\} \right\rangle_{\delta}. \quad (4.2)$$

The integral measure was adapted to the rescaled fields.

$$\int [\mathcal{D}\tilde{\phi}_0] = \lim_{M \rightarrow \infty} \prod_{\lambda, \mathbf{q}} \int_{\mathcal{C}} \frac{d\tilde{\phi}_{\lambda, \mathbf{q}}^* d\tilde{\phi}_{\lambda, \mathbf{q}}}{2\pi i} M \quad (4.3)$$

It is useful here to also regard the representation without the static lattice distortion $\langle b_{\lambda, \mathbf{q}_0} \rangle$ or, in other words, the representation with the unshifted fields ϕ . The Lagrangian is

$$\mathcal{L}_0 = \hbar \Omega_{\lambda, \mathbf{q}} \phi_{\lambda, \mathbf{q}}^* \phi_{\lambda, \mathbf{q}} + \frac{g_{\lambda, \mathbf{q}}}{\sqrt{N}} [\phi_{\lambda, -\mathbf{q}}^* + \phi_{\lambda, \mathbf{q}}] Y_{-\mathbf{q}} \quad (4.4)$$

in the partition function

$$Z_{\text{stat}} = Z_s \int [\mathcal{D}\phi_0] \left\langle T_{\tau} \exp \left\{ -\beta \sum_{\lambda, \mathbf{q}} \mathcal{L}_0 \right\} \right\rangle. \quad (4.5)$$

The Lagrangian (4.4) describes a displaced harmonic oscillator with a displacement proportional to the operator $Y_{-\mathbf{q}}$. As discussed in detail in chapter 2 [73], the spin-Peierls distortion in CuGeO_3 is modulated with $\mathbf{q}_0 = (\pi/a, 0, \pi/c)$, where a and c are the lattice constants in x and z direction respectively. Only the fields at \mathbf{q}_0 are actually shifted by the spin-phonon coupling. $2\mathbf{q}_0$ is a reciprocal lattice vector so that the ordering is commensurate with the lattice. Thus, one has $\phi_{\lambda, -\mathbf{q}_0} = \phi_{\lambda, \mathbf{q}_0}$. In other words, at \mathbf{q}_0 only the real part of the corresponding field couples to the spin system.

$$\frac{g_{\lambda, \mathbf{q}_0}}{\sqrt{N}} [\phi_{\lambda, -\mathbf{q}_0}^* + \phi_{\lambda, \mathbf{q}_0}] Y_{-\mathbf{q}_0} = \frac{g_{\lambda, \mathbf{q}_0}}{\sqrt{N}} 2\text{Re} \phi_{\lambda, \mathbf{q}_0} Y_{-\mathbf{q}_0} \quad (4.6)$$

The imaginary part is not shifted so that $\langle \phi_{\lambda, \mathbf{q}_0} \rangle$ is real and via equation (3.31) on page 40 one finds that $\langle b_{\lambda, \mathbf{q}_0} \rangle$ is real.

From equation (2.32) on page 23 then follows that for \mathbf{q}_0 the polarization vectors are real. Regarding equation (2.20) on page 19 shows that $g_{\lambda, \mathbf{q}_0}$ is real. The magnetic exchange alternation defined in equation (3.22) simplifies to

$$\delta_J(\mathbf{l}) = \frac{2}{\sqrt{N}} (-1)^{l_x + l_y + l_z} \sum_{\lambda} g_{\lambda, \mathbf{q}_0} \langle b_{\lambda, \mathbf{q}_0} \rangle \quad (4.7)$$

and is real. These reflections simplify the discussion of the static saddle point in section 4.1.2. For incommensurate ordering the situation changes as discussed in section 4.1.3.

4.1.2 Static saddle point

The saddle point is obtained by replacing the fields by their expectation value such that the static Lagrangian is minimized. Recalling that the shifted operators $\tilde{b}_{\mathbf{q}}$ in equation (3.20) on page 38 were defined such that $0 = \langle \tilde{b}_{\lambda, \mathbf{q}_0} \rangle = \langle \tilde{\phi}_{\lambda, \mathbf{q}_0} \rangle$, the static saddle point partition function is simply $Z_{\delta} = \mathbf{Tr}_s \exp\{-\beta H_{\delta}\}$. The Hamiltonian H_{δ} is given by equation (3.23) on page 39. Note that the relation $\langle \tilde{b}_{\lambda, \mathbf{q}_0} \rangle = \langle \tilde{\phi}_{\lambda, \mathbf{q}_0} \rangle$ can be obtained equivalently to $\langle b_{\lambda, \mathbf{q}_0} \rangle = \langle \phi_{\lambda, \mathbf{q}_0} \rangle$ in the unshifted case described in section 3.2.

Klümper *et al.* have used an equivalent isotropic model with $J_z = J$ and $J_{2,z} = J_2$ to describe thermodynamical properties of CuGeO_3 using finite temperature DMRG [57, 63]. Their notation is

$$H_{\text{MF}} = J \sum_{l_z} [1 + (-1)^{l_z} \delta_J] \mathbf{S}_{l_z} \cdot \mathbf{S}_{l_z+1} + J_2 \sum_{l_z} \mathbf{S}_{l_z} \cdot \mathbf{S}_{l_z+2} + \frac{1}{2} LK \delta_J^2. \quad (4.8)$$

I denote with L the number of ions of a Cu chain. The lattice alternation δ_J^2 has to be determined self consistently by minimizing the free energy $F = -k_B T \ln Z_{\delta}$.

A direct comparison of the elastic energy terms in (4.8) using the definition of δ_J in equation (4.7) and (3.23) yields:

$$K \sum_{\lambda, \lambda'} g_{\lambda, \mathbf{q}_0} g_{\lambda', \mathbf{q}_0} \langle b_{\lambda, \mathbf{q}_0} \rangle \langle b_{\lambda', \mathbf{q}_0} \rangle = \frac{1}{2} \sum_{\lambda} \hbar \Omega_{\lambda, \mathbf{q}_0} \langle b_{\lambda, \mathbf{q}_0} \rangle^2 \quad (4.9)$$

Note that in order to adapt the one-dimensional formulation one must replace $2N \rightarrow L$. I recall that there are two Cu ions per unit cell and that in this work the energies are usually defined per unit cell and not per Cu ion. This is responsible for the factor of 1/2 on the right hand side of equation (4.9).

In the applied harmonic approximation K must be independent of the distortion fields $\langle b_{\lambda, \mathbf{q}_0} \rangle$. Comparing coefficients in equation (4.9) yields a set of four linear equations which can be rewritten to decouple as

$$\frac{\hbar \Omega_{\lambda, \mathbf{q}_0}}{g_{\lambda, \mathbf{q}_0}} \langle b_{\lambda, \mathbf{q}_0} \rangle = K \sum_{\lambda'} \frac{2 g_{\lambda', \mathbf{q}_0}^2}{\hbar \Omega_{\lambda', \mathbf{q}_0}} \frac{\hbar \Omega_{\lambda', \mathbf{q}_0}}{g_{\lambda', \mathbf{q}_0}} \langle b_{\lambda', \mathbf{q}_0} \rangle. \quad (4.10)$$

The right hand side of equation (4.10) is the same for all λ and thus $\hbar \Omega_{\lambda, \mathbf{q}_0} \langle b_{\lambda, \mathbf{q}_0} \rangle / g_{\lambda, \mathbf{q}_0} = \text{const}$ in full agreement with equation (2.34) on page 23 derived in chapter 2. This result is generalized to all eigenmodes of the system at finite frequencies and arbitrary \mathbf{q} within the framework of the RPA approach in equation (4.56) discussed in section 4.2.1. Further one can identify

$$K = \left(\sum_{\lambda} \frac{2 g_{\lambda, \mathbf{q}_0}^2}{\hbar \Omega_{\lambda, \mathbf{q}_0}} \right)^{-1}. \quad (4.11)$$

This definition yields full consistency between the values of the coupling constants derived via equations (2.35) and (2.36) and the values of K given in reference [57]. Note that in reference [57] $J_2/J = 0.35$ and consequently $\chi_0 = (T_{\text{SP}}/J) \approx 1$ as discussed in section 2.7.

In the high temperature phase, where $\delta_J = 0$, the model (4.8) has been used to successfully describe the magnetic susceptibility in CuGeO_3 [24]. The same is true in the ordered phase and also the estimated magnetic entropy liberated up to the transition temperature can be matched [57]. On the other hand, the critical exponent of the order parameter is mean-field like $1/2$, whereas experiments give an exponent of ~ 0.35 [78, 79]. The value of K most consistent with the entropy and susceptibility measurements gives a transition temperature which is slightly too high [63]. Also, the temperature dependence of the magnetic exchange discussed in section 2.5.3 has not been included and will alter the results. The possible significance of the phonon fluctuations has been discussed at the end of section 2.6. The influence of dynamical phonons of the spin spectrum is already established [58, 59, 50]. Löw and Kühne [69] have shown in a recent work that one-dimensional phonons also have a significant effect on the magnetic susceptibility. An answer to the discrepancies may be accessible by including Gaussian fluctuations as proposed in section 4.2.3.

4.1.3 Short remark on incommensurate ordering

If $2\mathbf{q}_0$ is not a reciprocal lattice vector such that the ordering is incommensurate with the lattice the preceding argumentation about $\langle b_{\lambda, \mathbf{q}_0} \rangle$ to be real fails. The expectation values acquire complex phases. Indeed does CuGeO_3 show incommensurate ordering in an external magnetic field larger than about 12 Tesla [80, 81, 82, 5, 83, 84]. As was discussed in section (3.2), in the distorted spin-Peierls phase the Peierls-active phonon modes condense. For a domain-wall-like modulation higher harmonics condense, too, with the appropriate Fourier weight. equation (3.20) then must be generalized to

$$\tilde{b}_{\lambda, \mathbf{q}} = b_{\lambda, \mathbf{q}} - \sum_{s=1}^{N_s} \langle b_{\lambda, \mathbf{q}_s} \rangle \delta_{\mathbf{q}=\mathbf{q}_s} \quad (4.12)$$

imposing $\langle \tilde{b}_{\lambda, \mathbf{q}} \rangle = 0$. The index s labels the N_s modes that condense. The magnetic exchange alternation (3.22) is then also generalized.

$$\delta_J(\mathbf{l}) = \frac{1}{\sqrt{N}} \sum_{\lambda, s} e^{i\mathbf{q}_s \mathbf{R}_l + i\pi l_y} g_{\lambda, \mathbf{q}_s} \left(\langle b_{\lambda, -\mathbf{q}_s} \rangle^* + \langle b_{\lambda, \mathbf{q}_s} \rangle \right). \quad (4.13)$$

Such a generalized magnetic exchange alternation has been successfully used in a real-space model equivalent to equation (4.8) to describe the incommensurate phase in CuGeO_3 [83, 85]. An overview of the efforts made to describe the incommensurate phase can be obtained through reference [86] and the references therein. For a discussion of the theoretical background of the Goldstone modes connected to the incommensurate ordering, the so called phasons, and the general phase diagram referred to as Lifshitz critical behavior, see reference [87] and the references therein.

4.1.4 Effective spin model with long range interaction

The phonon fields in the partition function (3.17) can be integrated out. For that purpose the generating functional

$$P[j^*, j] = \exp \left\{ - \int_0^\beta d\tau \sum_{\lambda, \mathbf{q}} [j_{\lambda, \mathbf{q}}^*(\tau) \phi_{\lambda, \mathbf{q}}(\tau) + \phi_{\lambda, \mathbf{q}}^*(\tau) j_{\lambda, \mathbf{q}}(\tau)] \right\} \quad (4.14)$$

is introduced [75]. It satisfies $\lim_{j^*, j \rightarrow 0} P = 1$. The new fields have the same definitions of the continuum limit as the phonon field, as discussed at the end of section 3.3.3:

$$j(\tau) = \lim_{\epsilon \rightarrow 0} j(t), \quad j^*(\tau) = \lim_{\epsilon \rightarrow 0} j^*(t + 1). \quad (4.15)$$

The phonon fields in the spin-phonon coupling part in the action (3.17) can then be expressed as functional differential operators with respect to the fields j .

$$Z = Z_s \lim_{j^*, j \rightarrow 0} \left\langle T_\tau \exp \left\{ \int_0^\beta d\tau \sum_{\lambda, \mathbf{q}} \frac{g_{\lambda, \mathbf{q}}}{\sqrt{N}} \left[\frac{\delta}{\delta j_{\lambda, -\mathbf{q}}(\tau)} + \frac{\delta}{\delta j_{\lambda, \mathbf{q}}^*(\tau)} \right] Y_{-\mathbf{q}}(\tau) \right\} \right\rangle Z_p[j^*, j] \quad (4.16)$$

At this point it is useful to notice that the differentiation with respect to the fields j is derived from the discrete representation as

$$\left[\frac{\delta}{\delta j_{\lambda, -\mathbf{q}}(\tau)} + \frac{\delta}{\delta j_{\lambda, \mathbf{q}}^*(\tau)} \right] = \lim_{\epsilon \rightarrow 0} \left[\frac{\delta}{\delta j_{\lambda, -\mathbf{q}}(t)} + \frac{\delta}{\delta j_{\lambda, \mathbf{q}}^*(t + 1)} \right] \quad (4.17)$$

consistent with expressions (4.15). The phononic partition functional is given by

$$Z_p[j^*, j] = \int [\mathcal{D}\phi] \exp \left\{ - \int_0^\beta d\tau \sum_{\lambda, \mathbf{q}} \phi_{\lambda, \mathbf{q}}^*(\tau) [\hbar\Omega_{\lambda, \mathbf{q}} + \partial_\tau] \phi_{\lambda, \mathbf{q}}(\tau) \right\} P[j^*, j] \quad (4.18)$$

and can be brought into quadratic form by shifting the phonon fields as [75]

$$\phi_{\lambda, \mathbf{q}}(\tau) = \check{\phi}_{\lambda, \mathbf{q}}(\tau) - [\hbar\Omega_{\lambda, \mathbf{q}} + \partial_\tau]^{-1} j_{\lambda, \mathbf{q}}(\tau), \quad (4.19)$$

$$\phi_{\lambda, \mathbf{q}}^*(\tau) = \check{\phi}_{\lambda, \mathbf{q}}^*(\tau) - j_{\lambda, \mathbf{q}}^*(\tau) [\hbar\Omega_{\lambda, \mathbf{q}} + \partial_\tau]^{-1}. \quad (4.20)$$

The fields $\check{\phi}$ can then be integrated out [4]. I formally introduce a Dirac distribution and find

$$Z_p[j^*, j] = Z_p \exp \left\{ \int_0^\beta d\tau \int_0^\beta d\tau' \sum_{\lambda, \mathbf{q}} j_{\lambda, \mathbf{q}}^*(\tau) [\hbar\Omega_{\lambda, \mathbf{q}} + \partial_\tau]^{-1} \delta(\tau - \tau') j_{\lambda, \mathbf{q}}(\tau') \right\}, \quad (4.21)$$

where Z_p is the partition function of the bare harmonic phonon system given in equation (3.54). Introducing the unperturbed phonon Green's function

$$d_{\lambda,\mathbf{q}}^{(0)}(\tau) = e^{-\hbar\Omega_{\lambda,\mathbf{q}}\tau} \left(\theta(\tau) \frac{1}{1 - e^{-\beta\hbar\Omega_{\lambda,\mathbf{q}}}} + \theta(-\tau) \frac{1}{e^{\beta\hbar\Omega_{\lambda,\mathbf{q}}} - 1} \right), \quad (4.22)$$

satisfying

$$[\hbar\Omega_{\lambda,\mathbf{q}} + \partial_\tau]^{-1} \delta(\tau - \tau') = d_{\lambda,\mathbf{q}}^{(0)}(\tau - \tau'), \quad (4.23)$$

one can insert $Z_p[j^*, j]$ from equation (4.21) into equation (4.16), carry out the functional differentiation and the limit $j^*, j \rightarrow 0$ to find

$$Z = Z_s Z_p \left\langle T_\tau \exp \left\{ \int_0^\beta d\tau \int_0^\beta d\tau' \sum_{\lambda,\mathbf{q}} \frac{g_{\lambda,\mathbf{q}} g_{\lambda,-\mathbf{q}}}{N} Y_{\mathbf{q}}(\tau) d_{\lambda,\mathbf{q}}^{(0)}(\tau - \tau') Y_{-\mathbf{q}}(\tau') \right\} \right\rangle. \quad (4.24)$$

Transforming the exponent via equations (3.57), (3.58), and (3.60) introducing Matsubara frequencies $\omega_\nu = 2\pi\nu/\beta$ yields the effective spin representation of the partition function.

$$Z = Z_s Z_p \lim_{M \rightarrow \infty} \left\langle T_\tau \exp \left\{ \frac{\beta}{M} \sum_{\lambda,\mathbf{q},\nu} \frac{g_{\lambda,\mathbf{q}} g_{\lambda,-\mathbf{q}}}{N} Y_{\mathbf{q},\nu} (\hbar\Omega_{\lambda,\mathbf{q}} - i\omega_\nu)^{-1} Y_{\mathbf{q},\nu}^* \right\} \right\rangle \quad (4.25)$$

Note that $Y_{\mathbf{q},\nu}^\dagger = Y_{\mathbf{q},\nu}^* = Y_{-\mathbf{q},-\nu}$.

The induced dimer-dimer interaction is proportional to the Fourier transform of the unperturbed phonon propagator (4.22) [77].

$$d_{\lambda,\mathbf{q},\nu}^{(0)} = \int_0^\beta d\tau e^{i\omega_\nu\tau} d_{\lambda,\mathbf{q}}^{(0)}(\tau) = \frac{1}{\hbar\Omega_{\lambda,\mathbf{q}} - i\omega_\nu} \quad (4.26)$$

It is a dynamical potential and thus no effective Hamiltonian can be given corresponding to the representation (4.25) of the partition function.

The result (4.25), of course, can also be obtained by applying an equivalent approach directly to the Fourier transformed representation of the partition function given in equation (3.43) and (3.44) in the limit $\langle b_{\lambda,\mathbf{q}_0} \rangle = 0$, $\check{\phi} = \phi$. The imaginary time representation has the advantage that in integration over the phonon fields $\check{\phi}$ leading to the unperturbed phonon partition function Z_p in equation (4.21) is well defined and given in the literature [4]. It is free of the problems connected with the limit $\epsilon \rightarrow 0$ mentioned in section 3.3.2.

4.1.5 Limiting cases

Using $Y_{\mathbf{q},\nu}^* = Y_{-\mathbf{q},-\nu}$, the summation in the exponent in the partition function (4.25) can be transformed by setting $\sum_\nu = 1/2 \sum_\nu + 1/2 \sum_{\nu \rightarrow -\nu}$. The partition function then is rewritten to

$$Z = Z_s Z_p \lim_{M \rightarrow \infty} \left\langle T_\tau \exp \left\{ \frac{\beta}{M} \sum_{\mathbf{q},\nu} Y_{\mathbf{q},\nu} V_{\text{eff}}(\mathbf{q}, \omega_\nu) Y_{\mathbf{q},\nu}^* \right\} \right\rangle. \quad (4.27)$$

In this form the phonon induced effective electron-electron interaction is, after continuation to the real axis $i\omega_\nu \rightarrow \omega + i\epsilon$, written as

$$V_{\text{eff}}(\mathbf{q}, \omega) = - \sum_{\lambda} \frac{g_{\lambda, \mathbf{q}} g_{\lambda, -\mathbf{q}} \hbar \Omega_{\lambda, \mathbf{q}}}{N [\hbar^2 \Omega_{\lambda, \mathbf{q}}^2 - (\omega + i\epsilon)^2]} \quad (4.28)$$

Such phonon induced interactions are usually considered in electronic systems where one replaces

$$H_s \rightarrow H_e = \sum_{\mathbf{k}\sigma} E_{\mathbf{k}}^{(e)} c_{\mathbf{k}\sigma}^\dagger c_{\mathbf{k}\sigma}, \quad (4.29)$$

$$Y_{\mathbf{q}, \nu} \rightarrow \rho_{\mathbf{q}, \nu} = \frac{1}{\sqrt{\beta}} \int_0^\beta e^{i\omega_\nu \tau} \sum_{\mathbf{k}\sigma} c_{\mathbf{k}-\mathbf{q}\sigma}^\dagger(\tau) c_{\mathbf{k}\sigma}(\tau). \quad (4.30)$$

The operators $c_{\mathbf{k}\sigma}$ and $c_{\mathbf{k}\sigma}^\dagger$ are electronic annihilation and creation operators, σ is the spin index, $E_{\mathbf{k}}^{(e)}$ is the dispersion of the unperturbed electronic system and the phonons couple to the electronic density.

The possible attractiveness of such an induced interaction was first noticed by Fröhlich [88]. In the static limit the potential (4.28) is indeed attractive [77]. The above model with an electron gas ($E_{\mathbf{k}}^{(e)} \sim \hbar^2 \mathbf{k}^2$), where the electronic density couples to acoustic phonon modes with a cut-off of the order of the Debye temperature, is the basis for the description of conventional superconductivity [77]. The appearance of superconductivity is governed by the competition of the phonon mediated interaction and the repulsive coulomb interaction [76].

In the static limit the exponent in the partition function (4.27) is frequency independent and the problem can be written in terms of an effective Hamiltonian. Note that for $\mathbf{q} = 0$ the density operator $\rho_{0, \nu}$ commutes with H_e and is time independent, i.e., $\rho_{0, \nu} = \rho_0 \delta_{\nu=0}$. For small momentum transfer $\mathbf{q} \rightarrow 0$ the static approximation should thus be reliable. If the phonons are three dimensional, the problem is equivalent to that of three dimensional interacting electrons with spin degeneracy which is usually reduced to effective one-particle descriptions via mean-field theories, effective screening potentials, or Landau theories [76]. In the one-dimensional case the model can be treated by bosonization techniques [10]. Reviews are given by Voit [89] and by Schulz *et al.* in the form of lecture notes [90].

The Peierls instability, where $E_{\mathbf{k}}^{(e)} \sim \cos k_z c$ near half filling, has been treated in a mean-field approach by Rice and Strässler [91], starting from a generalized coulomb interaction using bosonization by Chui *et al.* [92] (see also references therein), and in RPA by Leung [93].

In the case of the nearest neighbor XY model, where $J_z = J_2 = J_{2,z} = 0$, the Jordan-Wigner transformation described in section 4.3.1 can be applied to obtain a model of interacting spinless fermions. The corresponding unperturbed Hamiltonian (3.4) and the

dimer operator (3.6) can be written as

$$H_s^{\text{XY}} = J \sum_{\mathbf{k}} \cos(k_z c) c_{\mathbf{k}}^\dagger c_{\mathbf{k}} \quad (4.31)$$

$$Y_{\mathbf{q},\nu}^{\text{XY}} = \sum_{\mathbf{k}} \left(e^{ik_z c} + e^{-i(k_z + q_z)c} \right) c_{\mathbf{k}+\mathbf{q}+2\pi\hat{y}/b,\nu}^\dagger c_{\mathbf{k},\nu} \quad (4.32)$$

The operators $c_{\mathbf{k}}$ and $c_{\mathbf{k}}^\dagger$ are spinless fermion annihilation and creation operators. Note that the momentum transfer $2\pi\hat{y}/b$ is just an artefact of the alternating ordering in the reduced unit cells derived in section 2.2. It is specific to the given configuration in CuGeO_3 and I drop it for the next two equations. The problem can be viewed as interacting spinless fermions

$$Z_{\text{XY}} = Z_s^{\text{XY}} Z_p \lim_{M \rightarrow \infty} \left\langle T_\tau \exp \left\{ \frac{\beta}{M} \sum_{\mathbf{k}, \mathbf{k}', \mathbf{q}, \nu} V_{\text{eff}}^{\text{XY}}(\mathbf{q}, \mathbf{k}, \mathbf{k}', \omega_\nu) c_{\mathbf{k}+\mathbf{q},\nu}^\dagger c_{\mathbf{k},\nu} c_{\mathbf{k}'-\mathbf{q},-\nu}^\dagger c_{\mathbf{k}',-\nu} \right\} \right\rangle \quad (4.33)$$

with the effective dynamical potential

$$V_{\text{eff}}^{\text{XY}}(\mathbf{q}, \mathbf{k}, \mathbf{k}', \omega_\nu) = -\cos(k_z + q_z/2) \cos(k'_z - q_z/2) \frac{g_{\lambda,\mathbf{q}} g_{\lambda,-\mathbf{q}} \hbar \Omega_{\lambda,\mathbf{q}}}{N [\hbar^2 \Omega_{\lambda,\mathbf{q}}^2 + \omega_\nu^2]}. \quad (4.34)$$

Neglecting the q_x and q_y dependence of the coupling constants $g_{\lambda,-\mathbf{q}}$ and of the phonon dispersions $\Omega_{\lambda,\mathbf{q}}$ the problem becomes one-dimensional.

For $J = 0$ one has Ising chains coupled to phonons. The spin operators commute with the spin Hamiltonian $[H_s^{\text{Ising}}, Y_{\mathbf{q}}^{\text{Ising}}] = 0 \forall \mathbf{q}$ and are time independent $Y_{\mathbf{q},\nu}^{\text{Ising}} = Y_{\mathbf{q}}^{\text{Ising}} \delta_{\nu=0}$. The interaction then is static and the above transformation yields a three-dimensional Ising model. This approach has been used for $J_2 = 0$ by Pytte [3] to describe the Jahn-Teller effect. In chapter 6 I apply a static approximation to the partition function (4.25) to motivate the phenomenological Ising model used for the description of the thermodynamics in the ordered phase of CuGeO_3 .

4.1.6 Equivalence of dimer and distortion fields

Macris and Piguet [94] have recently shown that from

$$[H, b_{\lambda,\mathbf{q}}^\dagger] = \hbar \Omega_{\lambda,\mathbf{q}} b_{\lambda,\mathbf{q}}^\dagger + \frac{g_{\lambda,\mathbf{q}}}{\sqrt{N}} Y_{-\mathbf{q}} \quad (4.35)$$

follows $\langle b_{\lambda,\mathbf{q}} \rangle \neq 0 \Leftrightarrow \langle Y_{\mathbf{q}} \rangle \neq 0$, i.e., long range elastic and dimer order must appear simultaneously.

This conjecture can be easily supported here. The Hubbard-Stratonovich transformation [95, 96, 97] makes use of the Gaussian identity

$$e^{C_{\lambda,\mathbf{q},\nu} \hat{A}_{\lambda,\mathbf{q},\nu} \hat{B}_{\lambda,\mathbf{q},\nu}} = \int_{\mathcal{C}} \frac{d\psi_{\lambda,\mathbf{q},\nu}^* d\psi_{\lambda,\mathbf{q},\nu}}{2\pi i C_{\lambda,\mathbf{q},\nu}} \exp \left\{ -\frac{|\psi_{\lambda,\mathbf{q},\nu}|^2}{C_{\lambda,\mathbf{q},\nu}} - \hat{A}_{\lambda,\mathbf{q},\nu} \psi_{\lambda,\mathbf{q},\nu} - \hat{B}_{\lambda,\mathbf{q},\nu} \psi_{\lambda,\mathbf{q},\nu}^* \right\} \quad (4.36)$$

to decouple two arbitrary operators \hat{A} and \hat{B} . The fields are integrated over the entire complex plane. The transformation can be used to introduce dimer fields in (4.25) by identifying the operators

$$\begin{aligned}\hat{A}_{\lambda,\mathbf{q},\nu} &= \frac{\beta}{M} \frac{g_{\lambda,\mathbf{q}}}{\sqrt{N}} Y_{\mathbf{q},\nu}^*, \\ \hat{B}_{\lambda,\mathbf{q},\nu} &= \frac{\beta}{M} e^{i\omega_\nu \epsilon} \frac{g_{\lambda,-\mathbf{q}}}{\sqrt{N}} Y_{\mathbf{q},\nu},\end{aligned}$$

and the prefactor

$$C_{\lambda,\mathbf{q},\nu} = \frac{M}{\beta} e^{-i\omega_\nu \epsilon} (\Omega_{\lambda,\mathbf{q}} - i\omega_\nu)^{-1}. \quad (4.37)$$

I find the partition function

$$\begin{aligned}Z &= Z_s Z_p \lim_{\substack{M \rightarrow \infty \\ (\epsilon \rightarrow 0)}} \left[\prod_{\lambda,\mathbf{q},\nu} \frac{M}{\beta} \frac{e^{-i\omega_\nu \epsilon}}{\Omega_{\lambda,\mathbf{q}} - i\omega_\nu} \right]^{-1} \\ &\quad \left\langle \prod_{\lambda,\mathbf{q},\nu} \int_{\mathcal{C}} \frac{d\psi_{\lambda,\mathbf{q},\nu}^* d\psi_{\lambda,\mathbf{q},\nu}}{2\pi i} \exp \left\{ -\frac{\beta}{M} \sum_{\lambda,\mathbf{q},\nu} \mathcal{L}_\psi[\psi^* \psi Y] \right\} \right\rangle.\end{aligned} \quad (4.38)$$

The action is

$$\begin{aligned}\mathcal{L}_\psi[\psi^* \psi Y] &= \psi_{\lambda,\mathbf{q},\nu}^* e^{i\omega_\nu \epsilon} (\Omega_{\lambda,\mathbf{q}} - i\omega_\nu) \psi_{\lambda,\mathbf{q},\nu} \\ &\quad + \frac{g_{\lambda,\mathbf{q}}}{\sqrt{N}} (\psi_{\lambda,-\mathbf{q},-\nu}^* e^{-i\omega_\nu \epsilon} + \psi_{\lambda,\mathbf{q},\nu}) Y_{-\mathbf{q},-\nu},\end{aligned} \quad (4.39)$$

where I have performed a resummation $\mathbf{q} \rightarrow -\mathbf{q}$ and $\nu \rightarrow -\nu$ in the last term. I recall that $Y_{-\mathbf{q},-\nu} = Y_{\mathbf{q},\nu}^*$.

Comparing equation (3.53) and (3.54) for the unperturbed phonon partition function on page 44 it is clear that

$$Z_p \lim_{\substack{M \rightarrow \infty \\ (\epsilon \rightarrow 0)}} \left[\prod_{\lambda,\mathbf{q},\nu} \frac{M}{\beta} \frac{e^{-i\omega_\nu \epsilon}}{\Omega_{\lambda,\mathbf{q}} - i\omega_\nu} \right]^{-1} = 1. \quad (4.40)$$

Comparing the Lagrangian (4.39) with the phonon field Lagrangian (3.44) on page 42 in the undistorted limit, i.e., $\langle b_{\lambda,\mathbf{q}_0} \rangle \equiv 0$ and $\tilde{\phi} = \phi$, one finds the phonon fields and the here introduced dimer fields to be identical.

$$\boxed{\psi_{\lambda,\mathbf{q},\nu} = \phi_{\lambda,\mathbf{q},\nu}} \quad (4.41)$$

In a sense I have just performed a calculation in a circle. But it proves that the problem is described by only one field-theoretical representation, as long as the spin degrees of freedom are represented by operators $Y_{\mathbf{q},\nu}$. Of course, an arbitrary scaling of the fields can be introduced via the definition of the operators $\hat{A}_{\lambda,\mathbf{q},\nu}$ and $\hat{B}_{\lambda,\mathbf{q},\nu}$ and the prefactor $C_{\lambda,-\mathbf{q},\nu}$. This cannot alter the underlying physics, though.

4.2 Spin degrees of freedom: cumulant expansion

The representations of the partition function (3.43) with the Lagrangian (3.44) on page 42 can be interpreted as moment generating functions for the operators $Y_{\mathbf{q}}(\tau)$ [98]. The partition function can then be rewritten with the trace over the spin degrees of freedom in the exponent [98]

$$Z = Z_{\delta} \lim_{M \rightarrow \infty} \int [\mathcal{D}\tilde{\phi}] \exp \left\{ -\mathcal{S}[\tilde{\phi}^* \tilde{\phi} Y] \right\}, \quad (4.42)$$

defining the action

$$\begin{aligned} \mathcal{S} = & - \sum_{n=1}^{\infty} \frac{1}{n!} \left\langle \left[-\frac{\beta}{M} \sum_{\lambda, \mathbf{q}, \nu} \frac{g_{\lambda, \mathbf{q}}}{\sqrt{N}} \left(\tilde{\phi}_{\lambda, -\mathbf{q}, -\nu}^* e^{-i\omega_{\nu}\epsilon} + \tilde{\phi}_{\lambda, \mathbf{q}, \nu} \right) Y_{\mathbf{q}, \nu}^* \right]^n \right\rangle_{\delta, \text{cum}} \\ & + \frac{\beta}{M} \sum_{\lambda, \mathbf{q}, \nu} \tilde{\phi}_{\lambda, \mathbf{q}, \nu}^* e^{i\omega_{\nu}\epsilon} [\hbar\Omega_{\lambda, \mathbf{q}} - i\omega_{\nu}] \tilde{\phi}_{\lambda, \mathbf{q}, \nu} + \hbar\Omega_{\lambda, \mathbf{q}_0} \langle b_{\lambda, \mathbf{q}_0} \rangle \left[\tilde{\phi}_{\lambda, \mathbf{q}_0}^* + \tilde{\phi}_{\lambda, \mathbf{q}_0} \right]. \end{aligned} \quad (4.43)$$

I refer to the modulation wave vector \mathbf{q}_0 in CuGeO₃ so $\langle b_{\lambda, \mathbf{q}_0} \rangle = \langle \phi_{\lambda, \mathbf{q}_0} \rangle$ is real as discussed in section 4.1.1, the static field $\tilde{\phi}_{\lambda, \mathbf{q}_0}$ and its complex conjugate is defined according to equation (3.45) on page 42. The index *cum* implies that the expectation values are calculated as cumulants [98].

4.2.1 Random Phase Approximation (RPA)

I first consider the disordered phase where $\langle Y_{\mathbf{q}, \nu} \rangle = \langle b_{\lambda, \mathbf{q}} \rangle = 0$ and thus $\tilde{\phi} = \phi$. Expanding the action (4.43) to second order in the phonon fields I find

$$\begin{aligned} \mathcal{S}_{\text{RPA}} = & \frac{\beta}{M} \sum_{\lambda, \mathbf{q}, \nu} \phi_{\lambda, \mathbf{q}, \nu}^* e^{i\omega_{\nu}\epsilon} [\hbar\Omega_{\lambda, \mathbf{q}} - i\omega_{\nu}] \phi_{\lambda, \mathbf{q}, \nu} \\ & - \frac{\beta^2}{2M^2} \sum_{\lambda, \mathbf{q}, \nu} \sum_{\lambda', \mathbf{q}', \nu'} \frac{g_{\lambda, \mathbf{q}} g_{\lambda', \mathbf{q}'}}{N} \left(\phi_{\lambda, -\mathbf{q}, -\nu}^* e^{-i\omega_{\nu}\epsilon} + \phi_{\lambda, \mathbf{q}, \nu} \right) \\ & \quad \times \left(\phi_{\lambda', -\mathbf{q}', -\nu'}^* e^{-i\omega_{\nu'}\epsilon} + \phi_{\lambda', \mathbf{q}', \nu'} \right) \langle Y_{\mathbf{q}, \nu}^* Y_{\mathbf{q}', \nu'}^* \rangle_{\text{cum}}. \end{aligned} \quad (4.44)$$

The partition function reads

$$Z_{\text{RPA}} = Z_s \lim_{M \rightarrow \infty} \int [\mathcal{D}\phi] \exp \left\{ -\mathcal{S}_{\text{RPA}}[\phi^* \phi Y] \right\}. \quad (4.45)$$

In the disordered phase the second order cumulant simplifies to the bare dimer-dimer correlation function:

$$\langle Y_{\mathbf{q}, \nu}^* Y_{\mathbf{q}', \nu'}^* \rangle_{\text{cum}} = \langle Y_{\mathbf{q}, \nu}^* Y_{\mathbf{q}', \nu'}^* \rangle - \langle Y_{\mathbf{q}, \nu}^* \rangle \langle Y_{\mathbf{q}', \nu'}^* \rangle = \langle Y_{\mathbf{q}, \nu}^* Y_{\mathbf{q}', \nu'}^* \rangle. \quad (4.46)$$

The dimer-dimer correlation function is determined by

$$\begin{aligned} \langle Y_{\mathbf{q},\nu}^* Y_{\mathbf{q}',\nu'}^* \rangle &= \frac{1}{M} \sum_{t,t'} e^{i(\omega_\nu \epsilon t + \omega_{\nu'} \epsilon t')} \langle Y_{\mathbf{q}}^*(t) Y_{\mathbf{q}'}^*(t') \rangle \\ &= \sum_{\Delta t} e^{i\omega_\nu \epsilon \Delta t} \langle Y_{\mathbf{q}}^*(\Delta t) Y_{\mathbf{q}'}^*(0) \rangle \delta_{\nu=-\nu'}. \end{aligned} \quad (4.47)$$

In the last step I used the definition of the imaginary time dependence (3.13) and the cyclic invariance under the trace to find that the correlation function depends on the time difference $\Delta t = t - t'$ only. Using the real-space definition for the dimer operators (3.6) and defining $\Delta \mathbf{l} = \mathbf{l} - \mathbf{l}'$ one has

$$\begin{aligned} \langle Y_{\mathbf{q}}^*(\Delta t) Y_{\mathbf{q}'}^*(0) \rangle &= \frac{1}{4} \sum_{\mathbf{l}, \Delta \mathbf{l}} e^{i(\mathbf{q} + \mathbf{q}') \cdot \mathbf{R}_{\mathbf{l}}} e^{-i\mathbf{q}' \cdot \mathbf{R}_{\Delta \mathbf{l}} - i\pi \Delta l_y} \\ &\times \left\langle \left[S_{\mathbf{l}}^+(\Delta t) S_{\mathbf{l}+\hat{z}}^-(\Delta t) + S_{\mathbf{l}}^-(\Delta t) S_{\mathbf{l}+\hat{z}}^+(\Delta t) + 2\gamma S_{\mathbf{l}}^z(\Delta t) S_{\mathbf{l}+\hat{z}}^z(\Delta t) \right] \right. \\ &\times \left. \left[S_{\mathbf{l}-\Delta \mathbf{l}}^+(0) S_{\mathbf{l}-\Delta \mathbf{l}+\hat{z}}^-(0) + S_{\mathbf{l}-\Delta \mathbf{l}}^-(0) S_{\mathbf{l}-\Delta \mathbf{l}+\hat{z}}^+(0) + 2\gamma S_{\mathbf{l}-\Delta \mathbf{l}}^z(0) S_{\mathbf{l}-\Delta \mathbf{l}+\hat{z}}^z(0) \right] \right\rangle. \end{aligned} \quad (4.48)$$

I recall that the position vector of the reduced unit cell (see figure 2.1 on page 14) may be defined as $\mathbf{R}_{\mathbf{l}} = (a l_x, b/2 l_y, c l_z)$. In the disordered phase translational invariance is given and thus the real-space correlation function in (4.48) is independent of \mathbf{l} so that

$$\langle Y_{\mathbf{q}}^*(\Delta t) Y_{\mathbf{q}'}^*(0) \rangle = \langle Y_{\mathbf{q}}^*(\Delta t) Y_{-\mathbf{q}}^*(0) \rangle N \delta_{\mathbf{q}' = -\mathbf{q}} = \langle Y_{-\mathbf{q}}(\Delta t) Y_{\mathbf{q}}(0) \rangle N \delta_{\mathbf{q}' = -\mathbf{q}}. \quad (4.49)$$

In short, I define the correlation function

$$\chi_Y(\mathbf{q}, \nu) = -\frac{\beta}{M} \sum_{\Delta t} e^{i\omega_\nu \epsilon \Delta t} \langle Y_{-\mathbf{q}}(\Delta t) Y_{\mathbf{q}}(0) \rangle \delta_{\nu=-\nu} \delta_{\mathbf{q}' = -\mathbf{q}} \quad (4.50)$$

This is just the spin-polarization bubble (see section 5.1 and reference [14]) which accounts for the title of the present section.

The action now can be written as

$$\begin{aligned} \mathcal{S}_{\text{RPA}} &= \frac{\beta}{M} \sum_{\lambda, \mathbf{q}, \nu} \left\{ \phi_{\lambda, \mathbf{q}, \nu}^* e^{i\omega_\nu \epsilon} [\hbar \Omega_{\lambda, \mathbf{q}} - i\omega_\nu] \phi_{\lambda, \mathbf{q}, \nu} \right. \\ &\quad \left. + \frac{\chi_Y(-\mathbf{q}, -\nu)}{2} (\phi_{\lambda, -\mathbf{q}, -\nu}^* e^{-i\omega_\nu \epsilon} + \phi_{\lambda, \mathbf{q}, \nu}) \sum_{\lambda'} g_{\lambda, \mathbf{q}} g_{\lambda', -\mathbf{q}} (\phi_{\lambda', \mathbf{q}, \nu}^* e^{i\omega_\nu \epsilon} + \phi_{\lambda', -\mathbf{q}, -\nu}) \right\}. \end{aligned} \quad (4.51)$$

The classical (mean-field) expectation values of the fields of such a dynamical system can be obtained by minimizing the action. I will here refer only to finite (or vanishing)

frequencies and I may thus drop the phase factors. By requesting $\partial \mathcal{S}_{\text{RPA}} / \partial \phi_{\lambda, \mathbf{q}, \nu} = 0$ and $\partial \mathcal{S}_{\text{RPA}} / \partial \phi_{\lambda, \mathbf{q}, \nu}^* = 0$ one finds

$$[\hbar\Omega_{\lambda, \mathbf{q}} + i\omega_\nu] \langle \phi_{\lambda, -\mathbf{q}, -\nu}^* \rangle = -\text{Re} \chi_Y(\mathbf{q}, \nu) \sum_{\lambda'} g_{\lambda, -\mathbf{q}} g_{\lambda', \mathbf{q}} (\langle \phi_{\lambda', -\mathbf{q}, -\nu}^* \rangle + \langle \phi_{\lambda', \mathbf{q}, \nu} \rangle), \quad (4.52)$$

$$[\hbar\Omega_{\lambda, \mathbf{q}} - i\omega_\nu] \langle \phi_{\lambda, \mathbf{q}, \nu} \rangle = -\text{Re} \chi_Y(\mathbf{q}, \nu) \sum_{\lambda'} g_{\lambda', \mathbf{q}} g_{\lambda, -\mathbf{q}} (\langle \phi_{\lambda', -\mathbf{q}, -\nu}^* \rangle + \langle \phi_{\lambda', \mathbf{q}, \nu} \rangle). \quad (4.53)$$

Note that to obtain equation (4.52) I have performed a transformation $\mathbf{q} \rightarrow -\mathbf{q}$ and $\nu \rightarrow -\nu$ after the differentiation. I have also used the fact that, since the spin operators in equation (4.48) are self adjoint,

$$[\chi_Y(\mathbf{q}, \nu) + \chi_Y(-\mathbf{q}, -\nu)] = 2 \text{Re} \chi_Y(\mathbf{q}, \nu). \quad (4.54)$$

The same results are obtained by setting $\partial \mathcal{S}_{\text{RPA}} / \partial \text{Re} \phi_{\lambda, \mathbf{q}, \nu} = 0$ and $\partial \mathcal{S}_{\text{RPA}} / \partial \text{Im} \phi_{\lambda, \mathbf{q}, \nu} = 0$.

equations (4.52) and (4.53) are trivially fulfilled for $\langle \phi_{\lambda, \mathbf{q}, \nu} \rangle = \langle \phi_{\lambda, \mathbf{q}, \nu}^* \rangle = 0$ consistent with the Gaussian integral formulation. The nontrivial solutions allow for the macroscopic (thermodynamic) occupation of the states identified by the corresponding quantum numbers λ, \mathbf{q}, ν . They thus characterise eigenstates of the spin-phonon coupled system.

Multiplying equation (4.52) by $(\hbar\Omega_{\lambda, \mathbf{q}} - i\omega_\nu) / (2g_{\lambda, -\mathbf{q}} \hbar\Omega_{\lambda, \mathbf{q}})$, then multiplying equation (4.53) by $(\hbar\Omega_{\lambda, \mathbf{q}} + i\omega_\nu) / (2g_{\lambda, -\mathbf{q}} \hbar\Omega_{\lambda, \mathbf{q}})$, and adding them up I obtain

$$\frac{\hbar^2 \Omega_{\lambda, \mathbf{q}}^2 + \omega_\nu^2}{2g_{\lambda, -\mathbf{q}} \hbar\Omega_{\lambda, \mathbf{q}}} (\langle \phi_{\lambda, -\mathbf{q}, -\nu}^* \rangle + \langle \phi_{\lambda, \mathbf{q}, \nu} \rangle) = -\text{Re} \chi_Y(\mathbf{q}, \nu) \sum_{\lambda'} g_{\lambda', \mathbf{q}} (\langle \phi_{\lambda', -\mathbf{q}, -\nu}^* \rangle + \langle \phi_{\lambda', \mathbf{q}, \nu} \rangle). \quad (4.55)$$

This equation is equivalent to equation (4.10) in the limit $\mathbf{q} \rightarrow \mathbf{q}_0$ and $\nu \rightarrow 0$ found in section 4.1.2. Since the right hand side is independent of the phonon mode index λ so must be the left hand side.

$$\boxed{\frac{\hbar^2 \Omega_{\lambda, \mathbf{q}}^2 + \omega_\nu^2}{2g_{\lambda, -\mathbf{q}} \hbar\Omega_{\lambda, \mathbf{q}}} (\langle \phi_{\lambda, -\mathbf{q}, -\nu}^* \rangle + \langle \phi_{\lambda, \mathbf{q}, \nu} \rangle) = \zeta_{\mathbf{q}, \nu}} \quad (4.56)$$

equation (4.55) can then be rewritten as to reproduce the relation defining the poles of the normal coordinate propagator in RPA used for the description of the phonon dynamics in chapter 5.

$$\boxed{0 = 1 - \text{Re} \chi_Y(\mathbf{q}, \nu) \sum_{\lambda} g_{\lambda, \mathbf{q}} g_{\lambda, -\mathbf{q}} D_{\lambda, \mathbf{q}, \nu}^{(0)}} \quad (4.57)$$

Here I have introduced the definition of the renormalized, unperturbed normal-coordinate propagator as it is given in the literature [76].

$$D_{\lambda,\mathbf{q},\nu}^{(0)} = -\frac{2\hbar\Omega_{\lambda,\mathbf{q}}}{\hbar^2\Omega_{\lambda,\mathbf{q}}^2 + \omega_\nu^2} \quad (4.58)$$

It is derived from

$$\begin{aligned} D_{\lambda,\mathbf{q},\nu}^{(0)} &= -\frac{2\Omega_{\lambda,\mathbf{q}}}{\hbar} \int_0^\beta d\tau e^{i\omega_\nu\tau} \langle Q_{\lambda,\mathbf{q}}(\tau) Q_{\lambda,-\mathbf{q}}(0) \rangle_p \\ &= -\int_0^\beta d\tau \left\langle \left(b_{\lambda,-\mathbf{q}}^\dagger(\tau) + b_{\lambda,\mathbf{q}}(\tau) \right) \left(b_{\lambda,\mathbf{q}}^\dagger(0) + b_{\lambda,-\mathbf{q}}(0) \right) \right\rangle_p, \end{aligned} \quad (4.59)$$

where the trace is taken with respect to the unperturbed phonon Hamiltonian (3.3). For the relation between normal coordinates and Bose operators see the definition (2.7) on page 14.

Transition temperature

The criticality is characterized by diverging thermodynamic quantities such as correlation lengths or specific heat [99, 55]. The divergencies are driven by critical fluctuations due to low energy excitations. The transition temperature T_{SP} is thus characterized by the existence of zero a frequency eigenmode at the appropriate wave vector:

$$0 = 1 + \chi_Y(\mathbf{q}_0, 0, T_{\text{SP}}) \sum_{\lambda} \frac{2g_{\lambda,\mathbf{q}_0}^2}{\hbar\Omega_{\lambda,\mathbf{q}_0}}. \quad (4.60)$$

For the isotropic Heisenberg chain, where $\chi_Y(\mathbf{q}_0, 0, T_{\text{SP}})$ has been shown to reduce to $\chi_0/k_{\text{B}}T_{\text{SP}}$, equation (4.60) becomes equation (2.25) used for the determination of the coupling constants in section 2.3.

4.2.2 Ordered phase

In the ordered phase the expansion of equation (4.43) up to second order also contains terms linear in the phonon fields.

$$\begin{aligned}
\mathcal{S}_{(2)} = & \frac{\beta}{M} \sum_{\lambda, \mathbf{q}, \nu} \frac{g_{\lambda, \mathbf{q}}}{\sqrt{N}} \left[\tilde{\phi}_{\lambda, -\mathbf{q}, -\nu}^* e^{-i\omega_\nu \epsilon} + \tilde{\phi}_{\lambda, \mathbf{q}, \nu} \right] \langle Y_{\mathbf{q}, \nu}^* \rangle_\delta + \beta \sum_{\lambda} \hbar \Omega_{\lambda, \mathbf{q}_0} \langle b_{\lambda, \mathbf{q}_0} \rangle \left[\tilde{\phi}_{\lambda, \mathbf{q}_0}^* + \tilde{\phi}_{\lambda, \mathbf{q}_0} \right] \\
& + \frac{\beta}{M} \sum_{\lambda, \mathbf{q}, \nu} \tilde{\phi}_{\lambda, \mathbf{q}, \nu}^* e^{i\omega_\nu \epsilon} [\hbar \Omega_{\lambda, \mathbf{q}} - i\omega_\nu] \tilde{\phi}_{\lambda, \mathbf{q}, \nu} \\
& - \frac{\beta^2}{2M^2} \sum_{\lambda, \mathbf{q}, \nu} \sum_{\mathbf{q}', \lambda', \nu'} \frac{g_{\lambda, \mathbf{q}} g_{\lambda', \mathbf{q}'}}{N} \left(\tilde{\phi}_{\lambda, -\mathbf{q}, -\nu}^* e^{-i\omega_\nu \epsilon} + \tilde{\phi}_{\lambda, \mathbf{q}, \nu} \right) \\
& \quad \times \left(\tilde{\phi}_{\lambda', -\mathbf{q}', -\nu'}^* e^{-i\omega_{\nu'} \epsilon} + \tilde{\phi}_{\lambda', \mathbf{q}', \nu'} \right) \langle Y_{\mathbf{q}, \nu}^* Y_{\mathbf{q}', \nu'}^* \rangle_{\delta, \text{cum}}. \quad (4.61)
\end{aligned}$$

Note that this is not an expansion in the order parameters $\langle b_{\lambda, \mathbf{q}_0} \rangle$ but in the fluctuation fields $\tilde{\phi}$ around the static distortion and in the dimer operators. The order parameter $\langle b_{\lambda, \mathbf{q}_0} \rangle$ is included in the spin-system expectation values $\langle \rangle_\delta$ to arbitrary order. The dimer expectation value and the dimer-dimer correlation function may not even be analytic in $\langle b_{\lambda, \mathbf{q}_0} \rangle$. This raises the issue of stability of the expansion which I address in section 4.2.3.

In the first order term the notion of the cumulant loses its sense. Using the Fourier representation (3.34), the definition of the imaginary time dependence (3.13), and cyclic invariance under the trace the expectation value of the dimer operator

$$\frac{\langle Y_{\mathbf{q}, \nu}^* \rangle_\delta}{\sqrt{M}} = \frac{1}{M} \sum_{t=1}^M e^{i\omega_\nu \epsilon t} \langle Y_{\mathbf{q}}^*(t) \rangle_\delta = \langle Y_{\mathbf{q}_0}^* \rangle_\delta \delta_{\nu=0} \delta_{\mathbf{q}=\mathbf{q}_0} \quad (4.62)$$

is found to be static. It is only nonzero in the ordered phase and only for the wave vector of the modulation of the distortion. Note that I used the renormalized static operator according to equation (3.46).

The second order cumulant is defined as [98]

$$\langle Y_{\mathbf{q}, \nu}^* Y_{\mathbf{q}', \nu'}^* \rangle_{\delta, \text{cum}} = \langle Y_{\mathbf{q}, \nu}^* Y_{\mathbf{q}', \nu'}^* \rangle_\delta - \langle Y_{\mathbf{q}, \nu}^* \rangle_\delta \langle Y_{\mathbf{q}', \nu'}^* \rangle_\delta. \quad (4.63)$$

The dimer-dimer correlation function is determined analogously to that in section 4.2.1 by simply replacing the expectation value $\langle \rangle$ by $\langle \rangle_\delta$ in equations (4.47) and (4.48). In the ordered phase the translational invariance is broken so that the expectation values for \mathbf{l} and $\mathbf{l} + \hat{x}$, $\mathbf{l} + \hat{y}$, and $\mathbf{l} + \hat{z}$ are different. In reciprocal space this corresponds to the loss of the conservation of momentum due to new Bragg reflections inherent of the superlattice structure and the resulting reduced Brillouin zone. The correlation function

has four contributions.

$$\begin{aligned}
\langle Y_{\mathbf{q}}^*(\Delta t) Y_{\mathbf{q}'}^*(0) \rangle_{\delta} &= \langle Y_{\mathbf{q}}^*(\Delta t) Y_{-\mathbf{q}}^*(0) \rangle_{\delta} N \delta_{\mathbf{q}'=-\mathbf{q}} \\
&+ \langle Y_{\mathbf{q}+\mathbf{q}_0}^*(\Delta t) Y_{-\mathbf{q}+\mathbf{q}_0}^*(0) \rangle_{\delta} N \delta_{\mathbf{q}'=-\mathbf{q}} \\
&+ \langle Y_{\mathbf{q}}^*(\Delta t) Y_{-\mathbf{q}+\mathbf{q}_0}^*(0) \rangle_{\delta} N \delta_{\mathbf{q}'=-\mathbf{q}+\mathbf{q}_0} \\
&+ \langle Y_{\mathbf{q}}^*(\Delta t) Y_{-\mathbf{q}-\mathbf{q}_0}^*(0) \rangle_{\delta} N \delta_{\mathbf{q}'=-\mathbf{q}-\mathbf{q}_0}
\end{aligned} \tag{4.64}$$

I recall that $2\mathbf{q}_0 = 2(\pi/a, 0, \pi/c)$ is reciprocal lattice vector. For simplicity I introduce the shorthand

$$\chi_{\delta}(\mathbf{q}_1, \mathbf{q}_2, \nu) = -\frac{\beta}{MN} \sum_{\Delta t} e^{i\omega_{\nu}\epsilon\Delta t} \langle Y_{\mathbf{q}_1}(\Delta t) Y_{\mathbf{q}_2}(0) \rangle_{\delta} - \beta \langle Y_{\mathbf{q}_0}^* \rangle_{\delta}^2 \delta_{\nu=0} \delta_{\mathbf{q}_1=\mathbf{q}_0} \delta_{\mathbf{q}_2=\mathbf{q}_0}, \tag{4.65}$$

where thus $\mathbf{q}_1 \in \{\mathbf{q}, \mathbf{q} + \mathbf{q}_0\}$ and $\mathbf{q}_2 \in \{\mathbf{q}, \mathbf{q} \pm \mathbf{q}_0\}$. Using equations (4.63), (4.62), and (4.47) with $\langle \rangle_{\delta}$ one finds the connection to the initial cumulant:

$$-\frac{\beta}{MN} \langle Y_{-\mathbf{q},-\nu} Y_{-\mathbf{q}',-\nu'} \rangle_{\delta, \text{cum}} = \chi_{\delta}(-\mathbf{q}_1, -\mathbf{q}_2, -\nu) \delta_{\nu=-\nu'} \delta_{\mathbf{q}=\mathbf{q}_1} \delta_{\mathbf{q}'=\mathbf{q}_2}. \tag{4.66}$$

The action (4.61) is now rewritten using the above results for the expectation values.

$$\begin{aligned}
\mathcal{S}_{(2)} &= \beta \sum_{\lambda} \left[\frac{g_{\lambda, \mathbf{q}_0}}{\sqrt{N}} \langle Y_{\mathbf{q}_0}^* \rangle_{\delta} + \hbar \Omega_{\lambda, \mathbf{q}_0} \langle b_{\lambda, \mathbf{q}_0} \rangle \right] \left[\tilde{\phi}_{\lambda, \mathbf{q}_0}^* + \tilde{\phi}_{\lambda, \mathbf{q}_0} \right] \\
&+ \frac{\beta}{M} \sum_{\lambda, \mathbf{q}, \nu} \tilde{\phi}_{\lambda, \mathbf{q}, \nu}^* e^{i\omega_{\nu}\epsilon} [\hbar \Omega_{\lambda, \mathbf{q}} - i\omega_{\nu}] \tilde{\phi}_{\lambda, \mathbf{q}, \nu} + \mathcal{S}_{(2)}^{\text{corr}}
\end{aligned} \tag{4.67}$$

Here I have defined the correlation part $\mathcal{S}_{(2)}^{\text{corr}}$ where the coupling to the spin system correlates different phonon modes at different wave vectors. For clarity it will be useful here to define the shorthand

$$\tilde{\Phi}_{\lambda, \mathbf{q}, \nu} = \left[\tilde{\phi}_{\lambda, -\mathbf{q}, -\nu}^* e^{-i\omega_{\nu}\epsilon} + \tilde{\phi}_{\lambda, \mathbf{q}, \nu} \right]. \tag{4.68}$$

The correlation term then reads

$$\begin{aligned}
\mathcal{S}_{(2)}^{\text{corr}} &= \frac{\beta}{M} \sum_{\lambda, \lambda', \mathbf{q}, \nu} \left\{ \frac{g_{\lambda, \mathbf{q}} g_{\lambda', -\mathbf{q}}}{2} \tilde{\Phi}_{\lambda, \mathbf{q}, \nu} \tilde{\Phi}_{\lambda', -\mathbf{q}, -\nu} \chi_{\delta}(-\mathbf{q}, \mathbf{q}, -\nu) \right. \\
&+ \frac{g_{\lambda, \mathbf{q}} g_{\lambda', \mathbf{q}}}{2} \tilde{\Phi}_{\lambda, \mathbf{q}, \nu} \tilde{\Phi}_{\lambda', -\mathbf{q}, -\nu} \chi_{\delta}(-\mathbf{q} - \mathbf{q}_0, \mathbf{q} - \mathbf{q}_0, -\nu) \\
&+ \frac{g_{\lambda, \mathbf{q}} g_{-\mathbf{q}-\mathbf{q}_0, \lambda'}}{2} \tilde{\Phi}_{\lambda, \mathbf{q}, \nu} \tilde{\Phi}_{-\mathbf{q}+\mathbf{q}_0, \lambda', -\nu} \chi_{\delta}(-\mathbf{q}, \mathbf{q} - \mathbf{q}_0, -\nu) \\
&\left. + \frac{g_{\lambda, \mathbf{q}} g_{\lambda', -\mathbf{q}-\mathbf{q}_0}}{2} \tilde{\Phi}_{\lambda, \mathbf{q}, \nu} \tilde{\Phi}_{\lambda', -\mathbf{q}-\mathbf{q}_0, -\nu} \chi_{\delta}(-\mathbf{q}, \mathbf{q} + \mathbf{q}_0, -\nu) \right\}. \tag{4.69}
\end{aligned}$$

As can be seen by considering $\mathbf{q} \sim \mathbf{q}_0$ or $\mathbf{q} \sim 0$ the last three terms of equation (4.69) couple acoustic phonon modes to zone boundary phonons and dimer excitations at $\mathbf{q} = \mathbf{q}_0$ as well as at $\mathbf{q} = 0$. In the static limit these terms give a contribution to the spontaneous strain observed in the ordered phase as discussed in section 2.5.3. Dynamically the terms are responsible for the ultrasonic sound velocity anomalies observed at and below the phase transition [66]. They thus describe anharmonic effects induced by the coupling of the phonons to the spin system [1].

The energy involved in the spin-Peierls distortion has been determined in section 2.5 to be $\langle H_p \rangle / (N k_B) = 5$ K. The size of the static effect has been determined in section 2.5.3 to involve energies four orders of magnitude smaller than those of the spin-Peierls distortion. The energy scale of the ultrasonic sound measurements with frequencies of 200 MHz $\approx 10^{-5} k_B / h$ K is even smaller. The anomalies are only of the order of 0.1% of the sound wave velocities. The coupling is thus weak and — as has been stated in section 2.5.3 — it can be concluded that the $\mathbf{q} \rightarrow 0$ effects will not have a notable influence on the spin-Peierls transition.

The small coupling might result from the fact that the weight of the spin excitation spectrum vanishes for $\mathbf{q} \rightarrow 0$. This has been calculated for alternating Heisenberg chains [37] in good agreement with experiments on CuGeO_3 [26]. A closer analysis would require the investigation of the dimer-dimer correlation function $\chi_\delta(-\mathbf{q}, \mathbf{q}, 0, T)$. This has to my knowledge not yet been done for the reasons described in section 4.3.

4.2.3 Static limit, mean-field results, and stability

As has just been shown, the last three terms of equation (4.69) have a negligible influence on the spin-Peierls distortion. Including only the first term of equation (4.69), the static action thus is reduced to

$$\begin{aligned}
\mathcal{S}_{(2)}^{\text{stat}} &= \beta \sum_{\lambda} \left[\frac{g_{\lambda, \mathbf{q}_0}}{\sqrt{N}} \langle Y_{\mathbf{q}_0}^* \rangle_{\delta} + \hbar \Omega_{\lambda, \mathbf{q}_0} \langle b_{\lambda, \mathbf{q}_0} \rangle \right] 2 \text{Re} \tilde{\phi}_{\lambda, \mathbf{q}_0} \\
&+ \beta \sum_{\lambda, \lambda'} \left\{ \hbar \Omega_{\lambda, \mathbf{q}_0} \left[(\text{Re} \tilde{\phi}_{\lambda, \mathbf{q}_0})^2 + (\text{Im} \tilde{\phi}_{\lambda, \mathbf{q}_0})^2 \right] + 2 \chi_{\delta}(\mathbf{q}_0, \mathbf{q}_0, 0) g_{\lambda, \mathbf{q}_0} g_{\lambda', \mathbf{q}_0} \text{Re} \tilde{\phi}_{\lambda, \mathbf{q}_0} \text{Re} \tilde{\phi}_{\lambda', \mathbf{q}_0} \right\} \\
&+ \beta \sum_{\substack{\mathbf{q} \neq \mathbf{q}_0 \\ \lambda, \lambda'}} \left\{ \hbar \Omega_{\lambda, \mathbf{q}} \tilde{\phi}_{\lambda, \mathbf{q}}^* \tilde{\phi}_{\lambda, \mathbf{q}} + \chi_{\delta}(-\mathbf{q}, \mathbf{q}, 0) \frac{g_{\lambda, \mathbf{q}} g_{\lambda', -\mathbf{q}}}{2} \left[\tilde{\phi}_{\lambda, -\mathbf{q}}^* + \tilde{\phi}_{\lambda, \mathbf{q}} \right] \left[\tilde{\phi}_{\lambda', \mathbf{q}}^* + \tilde{\phi}_{\lambda', -\mathbf{q}} \right] \right\}.
\end{aligned} \tag{4.70}$$

Again, I have used the renormalization of the static fields $\lim_{M \rightarrow \infty} \tilde{\phi}_{\lambda, \mathbf{q}, 0} / \sqrt{M} = \tilde{\phi}_{\lambda, \mathbf{q}}$ defined in equation (3.45) on page 42. I have written the contribution at the wave vector of the instability \mathbf{q}_0 separately and I made use of the fact that twice the modulation wave vector $2\mathbf{q}_0$ is a reciprocal lattice vector. This way it becomes immediately clear that the first two lines of equation (4.70) represent an displaced harmonic oscillator with respect to the fields $\text{Re} \tilde{\phi}_{\lambda, \mathbf{q}_0}$.

The static saddle point is defined such as to minimize the action, i.e., the first derivatives of the action with respect to the fields have to vanish. As discussed in section 4.2.1 this procedure defines the mean-field expectation values of the fields. For the \mathbf{q}_0 part of equation (4.70) the condition $\partial \mathcal{S}_{(2)}^{\text{stat}} / \partial \text{Im} \tilde{\phi}_{\lambda, \mathbf{q}_0} = 0$ gives trivially $\langle \text{Im} \tilde{\phi}_{\lambda, \mathbf{q}_0} \rangle = 0$, whereas for $\partial \mathcal{S}_{(2)}^{\text{stat}} / \partial \text{Re} \tilde{\phi}_{\lambda, \mathbf{q}_0} = 0$ one has the set of equations

$$\frac{g_{\lambda, \mathbf{q}_0}}{\sqrt{N}} \langle Y_{\mathbf{q}_0}^* \rangle_{\delta} + \hbar \Omega_{\lambda, \mathbf{q}_0} \langle b_{\lambda, \mathbf{q}_0} \rangle = -\hbar \Omega_{\lambda, \mathbf{q}_0} \langle \text{Re} \tilde{\phi}_{\lambda, \mathbf{q}_0} \rangle - 2\chi_{\delta}(\mathbf{q}_0, \mathbf{q}_0, 0) \sum_{\lambda'} g_{\lambda, \mathbf{q}_0} g_{\lambda', \mathbf{q}_0} \langle \text{Re} \tilde{\phi}_{\lambda', \mathbf{q}_0} \rangle. \quad (4.71)$$

I recall that $\langle b_{\lambda, \mathbf{q}_0} \rangle$ was defined such that $\langle \tilde{b}_{\lambda, \mathbf{q}_0} \rangle = \langle \tilde{\phi}_{\lambda, \mathbf{q}_0} \rangle = 0$ and thus

$$\boxed{\frac{g_{\lambda, \mathbf{q}_0}}{\sqrt{N}} \langle Y_{\mathbf{q}_0}^* \rangle_{\delta} + \hbar \Omega_{\lambda, \mathbf{q}_0} \langle b_{\lambda, \mathbf{q}_0} \rangle = 0.} \quad (4.72)$$

Note the consistency with the equivalence of dimer and distortional ordering discussed in section 4.1.6. In the isotropic limit, where $J = J_z$, this is the equation (2.34) used in section 2.3 to determine the normal mode coupling constants $g_{\lambda, \mathbf{q}_0}$.

Applying equation (4.72), the action (4.70) is equivalent to the static limit of the undistorted case discussed in section 4.2.1 with $\phi \rightarrow \tilde{\phi}$ and $\chi_Y \rightarrow \chi_{\delta}$. The trivial solutions minimizing the static action (4.70) are $\langle \tilde{\phi}_{\lambda, \mathbf{q}} = 0 \rangle$. The nontrivial solutions are for arbitrary \mathbf{q} [compare equation (4.60)]

$$0 = 1 + \text{Re} \chi_{\delta}(-\mathbf{q}, \mathbf{q}, 0, T) \sum_{\lambda} \frac{2 g_{\lambda, \mathbf{q}} g_{\lambda, -\mathbf{q}}}{\hbar \Omega_{\lambda, \mathbf{q}}}. \quad (4.73)$$

I added the temperature dependence T to the argument of the dimer-dimer correlation function $\chi_{\delta}(-\mathbf{q}, \mathbf{q}, 0, T)$ for clarity. This equation is closely related to the issue of stability to be addressed next.

As discussed in section 4.2.1 a phase transition occurs when equation (4.73) has a solution. A stable phase for $T < T_{\text{SP}}$ requires thus equation (4.73) to have no solution. Moreover, for the Gaussian integrals in the static partition function with the action (4.70)

$$Z_{(2)}^{\text{stat}} = Z_{\delta} \int [\mathcal{D}\tilde{\phi}] \exp \left\{ -\mathcal{S}_{(2)}^{\text{stat}}[\tilde{\phi}^* \tilde{\phi}] \right\} \quad (4.74)$$

to converge it is necessary for the action $\mathcal{S}_{(2)}^{\text{stat}}$ to be a convex function (from below) of the static fields $\tilde{\phi}_{\lambda, \mathbf{q}}$ and $\tilde{\phi}_{\lambda, \mathbf{q}}^*$. One must thus request that the quadratic form

$$\sum_{\lambda, \lambda'} \tilde{\phi}_{\lambda, \mathbf{q}}^* \frac{\partial^2 \mathcal{S}_{(2)}^{\text{stat}}}{\partial \tilde{\phi}_{\lambda, \mathbf{q}}^* \partial \tilde{\phi}_{\lambda', \mathbf{q}}} \tilde{\phi}_{\lambda', \mathbf{q}} > 0 \quad (4.75)$$

is positive definite. This yields the condition

$$0 < 1 + \text{Re}\chi_\delta(-\mathbf{q}, \mathbf{q}, 0, T) \sum_\lambda \frac{2 g_{\lambda, \mathbf{q}} g_{\lambda, -\mathbf{q}}}{\hbar \Omega_{\lambda, \mathbf{q}}}. \quad (4.76)$$

For one phonon mode this result is straight forward. For many modes it is obtained easiest by considering that in the vicinity of the extremum of the action one can deduct equivalently to equation (4.56) in the static limit

$$\tilde{\zeta}_{\mathbf{q}, 0} = \frac{\hbar \Omega_{\lambda, \mathbf{q}}}{g_{\lambda, -\mathbf{q}}} \tilde{\phi}_{\lambda, \mathbf{q}}, \quad (4.77)$$

where $\tilde{\zeta}_{\mathbf{q}, 0}$ is a number independent of the phonon index λ . I have also used that at the extremum of the action subtracting equation (4.52) from equation (4.53) yields in the static limit $\tilde{\phi}_{\lambda, \mathbf{q}} = \tilde{\phi}_{\lambda, -\mathbf{q}}^*$. Note that the action in the herein discussed Gaussian approximation has but one extremum for every field. Stability in the vicinity of the extremum implies global stability.

Within the phonon-mean-field picture identical to the saddle point discussed here there is no doubt about the stability of the ordered phase. For the isotropic, frustrated Heisenberg chain this has been shown by Klümper *et al.* [57], in the XY case it has been proven by Beni and Pincus [100]. The physical reason was discussed in the introduction in section 1.2. Thus the inequality (4.76) must be fulfilled.

Gaussian fluctuations

The larger the right hand side of equation (4.76) the less important will be corrections of Gaussian fluctuations to the mean-field results. A closer analysis would require the investigation of $\chi_\delta(-\mathbf{q}, \mathbf{q}, 0, T)$. This has to my knowledge not yet been done for the reasons described in section 4.3. Since the spin system is gaped in the distorted phase and from analogy to the spin-spin correlation function studied by Uhrig and Schulz [37] in RPA, it is expected that $\lim_{T \rightarrow 0} \text{Im}\chi_\delta(-\mathbf{q}, \mathbf{q}, 0, T)$ is exponentially suppressed. Via the Kramers-Kronig relation this will lead also to a suppression of $\lim_{T \rightarrow 0} \text{Re}\chi_\delta(-\mathbf{q}, \mathbf{q}, 0, T)$. This would be consistent with the small size of the critical region obtained from the Ginzburg criterion in section 2.3.1.

Another approach, which I only mention here for completeness, would be to perform a self-consistency check on equation (4.72). The expectation values $\langle Y_{\mathbf{q}_0}^* \rangle_\delta$ and $\langle b_{\lambda, \mathbf{q}_0} \rangle$ can be calculated in the presence of Gaussian fluctuations by using the corresponding partition function (4.74) and performing the integration over the fields $\tilde{\phi}$. The good agreement of the coupling constants determined in chapter 2 with various experiments is a strong indication of the applicability of equation (4.72). This result then has to be contrasted to the expectation values obtained when considering Z_δ based on the Hamiltonian discussed in section 4.1.2.

Technically the expectation values can be obtained by considering the definition of the partition function Z in equation (3.1). It follows that

$$-\beta \frac{\partial \ln Z}{\partial g_{\lambda, \mathbf{q}_0}} = \frac{2}{\sqrt{N}} \langle Y_{\mathbf{q}_0}^* \rangle_{\delta} \langle b_{\lambda, \mathbf{q}_0} \rangle. \quad (4.78)$$

One can then approximate Z with $Z_{(2)}^{\text{stat}}$ or Z_{δ} , respectively. A second set of equations is obtained by minimizing the free energy $-\beta \ln Z_{(2)}^{\text{stat}}$ or $-\beta \ln Z_{\delta}$ with respect to $\langle b_{\lambda, \mathbf{q}_0} \rangle$.

4.3 Approaches to the spin system

The most difficult task in the partition function in representation (3.17) and (3.26) is the determination of the trace over the spin degrees of freedom, even in perturbative approaches. This becomes obvious from the discussion of the value on χ_0 in section 2.7 on page 33.

In the isotropic case ($J_z = J$) the relevant Hamiltonian for the expectation values $\langle \rangle_{\delta}$ is given in equation (4.8) on page 49. The ground state properties of the model are described by Chitra *et al.* [35]. The spectrum has a gap for all finite values of δ_J . Only for $\delta_J = 0$ and $J_2/J < 0.241$ is the spectrum gapless. At $\delta_J = 0$ and $J_2/J = 0.5$ the model is solved exactly [101, 102].

At present the only quantitatively reliable results appear to be obtained numerically by exact diagonalization [15, 34, 23, 24, 103, 16] and the density matrix renormalization group (DMRG) [35, 57, 63]. Quantum Monte Carlo methods are reliable for models without next nearest neighbor interaction, i.e., $J_2 = 0$ [65, 68]. Only recent developments also allow for finite J_2 [104]. Since the dynamical dimer-dimer correlation function used in chapter 5 has not yet been determined by any of these methods I review here briefly an analytical standard approach.

4.3.1 Spinless Fermions

One of the standard approaches for the Heisenberg model is the mapping to a fermionic description (see for example Fradkin [10]). The transformation of the next nearest neighbor terms incorporates the so called *sign problem* which I explain towards the end of the section. For now I set $J_2 = 0$ and consider the nearest neighbor part H_{δ}^{NN} of the dimerized Hamiltonian (3.23) on page 39.

Nearest neighbor terms

The spin operators are transformed on each chain to interacting spinless fermions via a Jordan-Wigner transformation [10].

$$S_{l_z}^+ = c_{l_z}^{\dagger} e^{i\pi \sum_{l'_z=1}^{l_z-1} c_{l'_z}^{\dagger} c_{l'_z}} \quad S_{l_z}^- = (S_{l_z}^+)^{\dagger} \quad (4.79)$$

$$S_{l_z}^z = \frac{1}{2} - \hat{n}_{l_z} \quad \hat{n}_{l_z} = c_{l_z}^{\dagger} c_{l_z} \quad (4.80)$$

Fourier transformation

$$c_l = \frac{1}{\sqrt{N}} \sum_{\mathbf{k}} e^{i\mathbf{R}_l \mathbf{k}} c_{\mathbf{k}}, \quad c_l^\dagger = \frac{1}{\sqrt{N}} \sum_{\mathbf{k}} e^{-i\mathbf{R}_l \mathbf{k}} c_{\mathbf{k}}^\dagger \quad (4.81)$$

then yields the spin Hamiltonian $H_\delta^{\text{NN}} = H_0 + H_{\text{int}}$ in reciprocal space.

$$H_0 = \sum_{\mathbf{k}} \left[(E_{\mathbf{k}} - J_z) c_{\mathbf{k}}^\dagger c_{\mathbf{k}} + \Delta_{\mathbf{k}} c_{\mathbf{k}+\mathbf{Q}}^\dagger c_{\mathbf{k}} \right] \quad (4.82)$$

$$H_{\text{int}} = J_z/J \sum_{\mathbf{q}} [E_{\mathbf{q}} \hat{n}_{\mathbf{q}} \hat{n}_{-\mathbf{q}} + \Delta_{\mathbf{q}} \hat{n}_{\mathbf{q}} \hat{n}_{-\mathbf{q}+\mathbf{Q}}] \quad (4.83)$$

The density operators are in Fourier space

$$\hat{n}_{\mathbf{q}} = \sum_{\mathbf{k}} c_{\mathbf{k}-\mathbf{q}}^\dagger c_{\mathbf{k}}. \quad (4.84)$$

I have introduced the dispersion and gap parameter as

$$E_{\mathbf{k}} = J \cos(k_z c), \quad \Delta_{\mathbf{k}} = iJ\delta_J \sin(k_z c), \quad (4.85)$$

respectively. c is the lattice constant in chain direction and $\mathbf{Q} = (0, 0, \pi/c)$.

H_{int} as given in (4.83) is the interaction term. Here it stems from the z part of the spin Hamiltonian. Coulomb interaction or phonon induced interaction, as discussed in section 4.1.5, give equivalent terms. The system $H_0 + H_{\text{int}}$ is thus a standard problem in many particle physics [2, 76, 77]. In the absence of a gap, for small T , and for small excitation energies the Hamiltonian $H_0 + H_{\text{int}}$ can be diagonalized by linearizing the spectrum of $E_{\mathbf{k}}$ around the Fermi surface and subsequent bosonization [10, 90, 89]. Of course the spectrum of the diagonalized system may exhibit a gap induced by the interaction H_{int} .

For small gaps $\sim \delta_J$ the system $H_0 + H_{\text{int}}$ can still be treated by continuum field theory [105, 37], for larger δ_J , treating H_{int} perturbatively, RPA yields results in agreement with numerical studies [37]. In the limit of the XY model, where $J_z = 0$, the interaction is absent and the model can be solved exactly [100].

Next nearest neighbor frustration

Transforming the next nearest neighbor term in the Hamiltonian (3.23) using equations (4.79) and (4.80) yields in real space

$$H_2 = \frac{J_2}{2} \sum_l \left(e^{i\pi \hat{n}_{l+\hat{z}}} c_l^\dagger c_{l+2\hat{z}} + e^{-i\pi \hat{n}_{l+\hat{z}}} c_{l+2\hat{z}}^\dagger c_l \right) + J_{2,z} \sum_l \left(\hat{n}_l - \frac{1}{2} \right) \left(\hat{n}_{l+2\hat{z}} - \frac{1}{2} \right). \quad (4.86)$$

The phase factors $e^{\pm i\pi \hat{n}_{l+\hat{z}}} = 1 - 2\hat{n}_{l+\hat{z}}$ are strongly sensitive to local fluctuations and are difficult to handle by Quantum Monte Carlo methods because of the varying sign [104]. Field-theoretical treatments yield qualitatively correct phase diagrams but are numerically

far from accurate [106, 107]. Bond operator techniques do not include solitonic elementary excitations and are only reliable for large J_2 or δ_J [106, 38].

For a discussion of the solitonic elementary excitations in one-dimensional dimerized systems see chapter 6 and references [102, 108, 109, 110]. An extensive revue is given by Mikeska and Steiner [111].

4.3.2 Dimer-dimer correlation function

For the quantitative analysis of the phonon dynamics of the spin-phonon coupled system in the undistorted phase performed in chapter 5 the determination of the dimer-dimer correlation function

$$\chi_Y(\mathbf{q}, \nu) = -\frac{1}{N} \int_0^\beta d\tau e^{i\omega\nu\tau} \langle Y_{\mathbf{q}}(\tau) Y_{-\mathbf{q}}(0) \rangle \quad (4.87)$$

is essential. I have here applied the continuum limit $\lim_{M \rightarrow \infty}$ to equation (4.50) in the sense of section 3.1. Because of the difficulties described above I limit myself to the unfrustrated case, where $J_2 = J_{2,z} = 0$.

Conduction electrons

When considering the case of the density of conduction electrons with spin degeneracy coupling to phonons, where

$$H_s \rightarrow H_e = \sum_{\mathbf{k}\sigma} E_{\mathbf{k}}^{(e)} c_{\mathbf{k}\sigma}^\dagger c_{\mathbf{k}\sigma}, \quad (4.88)$$

$$Y_{\mathbf{q}}(\tau) \rightarrow \rho_{\mathbf{q}}(\tau) = \sum_{\mathbf{k}\sigma} c_{\mathbf{k}-\mathbf{q}\sigma}^\dagger(\tau) c_{\mathbf{k}\sigma}(\tau). \quad (4.89)$$

The operators $c_{\mathbf{k}\sigma}$ and $c_{\mathbf{k}\sigma}^\dagger$ are electronic annihilation and creation operators, σ is the spin index. The correlation function is simply given by the Lindhard formula [76].

$$\chi_\rho(\mathbf{q}, \nu) = -\frac{1}{2N} \int_0^\beta d\tau e^{i\omega\nu\tau} \langle \rho_{\mathbf{q}}(\tau) \rho_{-\mathbf{q}}(0) \rangle = \frac{1}{N} \sum_{\mathbf{k}, \sigma} \frac{f_{\mathbf{k}} - f_{\mathbf{k}+\mathbf{q}}}{i\omega\nu + E_{\mathbf{k}} - E_{\mathbf{k}+\mathbf{q}}} \quad (4.90)$$

This implies that the dispersion $E_{\mathbf{k}}^{(e)}$ is bilinear in Fermion creation and annihilation operators so that Wick's theorem is applicable [4]. The Fermi distribution function is given by

$$f_{\mathbf{k}} = \frac{1}{1 + \exp\{\beta E_{\mathbf{k}}^{(e)}\}}. \quad (4.91)$$

For a short discussion of various applications of such a model see section 4.1.5.

XY case

In for $J_z = 0$ and $J_2 = J_{2,z} = 0$ the dimer operators in terms of the Jordan-Wigner spinless Fermi operators introduced in section 4.3.1 are given by

$$Y_{\mathbf{q}-\mathbf{q}'_y}^{\text{XY}}(\tau) = \sum_{\mathbf{k}} (e^{ik_z c} + e^{-i(k_z+q_z)c}) c_{\mathbf{k}+\mathbf{q}}^\dagger(\tau) c_{\mathbf{k}}(\tau). \quad (4.92)$$

I have introduced the shorthand $\mathbf{q}'_y = 2\pi\hat{y}/b$. It stems from the introduction of the reduced unit cells in section 2.2 together with the polarization of the Peierls-active phonon modes. It is specific to CuGeO₃ and accounts for the alternation of the ordering in adjacent Cu chains in unit cell (see figure 2.1 on page 14). It can usually be neglected especially since the correlation function (4.87) will only depend on q_z in chain direction.

The trace is taken with respect to $H_0 = J \sum_{\mathbf{k}} \cos k_z c_{\mathbf{k}}^\dagger c_{\mathbf{k}}$ as given by equation (4.82) and (4.85) with $\delta_J = 0$. The correlation function (4.87) then is a generalized Lindhard formula.

$$\chi_Y^{\text{XY}}(\mathbf{q}, \nu) = \frac{1}{2L} \sum_{k_z} [1 + \cos(2k_z + q_z)c] \frac{f_{k_z} - f_{k_z+q_z}}{i\omega_\nu + E_{k_z} - E_{k_z+q_z}} \quad (4.93)$$

cL is the length of a Cu chain in z direction. The problem is one-dimensional since the dispersion E_{k_z} in equation (4.85) only depends on k_z .

Isotropic case

In the isotropic case, where $J_z = J$, Cross and Fisher have determined the correlation function (4.87) using bosonization techniques and implying spin rotational invariance [14]. They find

$$\chi_Y^{\text{CF}}(\mathbf{q}, \omega_\nu) = -\frac{\chi_0}{0.35 k_B T} I_1 \left[\frac{\omega_\nu - v_s |q_z - \pi/c|}{2\pi k_B T} \right] I_1 \left[\frac{\omega_\nu + v_s |q_z - \pi/c|}{2\pi k_B T} \right]. \quad (4.94)$$

The prefactor has been chosen such that $\chi_Y^{\text{CF}}(\pi/c, 0) = \chi_0$ since $[I_1(0)]^2 = 0.35$. The spin-wave velocity is

$$v_s = J \frac{\pi}{2}. \quad (4.95)$$

The generalized Bessel functions I_1 can be given in integral representation or transformed to Gamma functions via Euler's Beta function [112]:

$$I_1(k) = \frac{1}{2\pi} \int_0^\infty dx e^{ikx} (\sinh(x))^{-1/2} = \frac{1}{\sqrt{8\pi}} \frac{\Gamma(\frac{1}{4} - \frac{1}{2}ik)}{\Gamma(\frac{3}{4} - \frac{1}{2}ik)}. \quad (4.96)$$

For $q_z = \pi/c$, i.e., at the wave vector of the Peierls instability, this correlation function is independent of the magnetic energy scale J . This reflects the scale invariant, quantum

critical behavior of the spin 1/2 Heisenberg chain at $T = 0$ [12]. $T\chi_Y^{\text{CF}}(\mathbf{q}, \omega_\nu)$ is a function of ω_ν/T only. This behavior is characteristic of quantum critical systems [113].

Cross and Fisher give an estimate value of $\chi_0 \approx 0.26$. Recent DMRG results of Klümper *et al.* are in contradiction to that result [57, 63]. They find $\chi_0(J/k_B T)$ to be significantly temperature dependent and not scale invariant. The quantum criticality thus breaks down at finite temperatures probably because the continuum limit underestimates local correlations.

For the determination of the coupling constants I have used the numerical values by Klümper *et al.* [63] as discussed in section 2.7. In chapter 5 I use the correlation function after analytical continuation $i\omega_\nu \rightarrow \omega + i\epsilon$ for a qualitative understanding of the phonon dynamics, lacking any better approximation. I contrast the result with those for the XY model and conduction electrons and show that the behavior is generic.

4.3.3 Quantum criticality in CuGeO_3

Schulz has determined the spin-spin correlation function also using bosonization techniques for anisotropic Heisenberg chains with arbitrary spin [72]. In the limit of the isotropic spin 1/2 chain he obtains just the same functional dependence. In the imaginary time formalism and implying spin rotational invariance one has

$$\tilde{\chi}_{\mathbf{S}}(q_z, \omega_\nu) = - \int_0^\beta d\tau e^{i\omega_\nu \tau} \langle \mathbf{S}_{q_z}(\tau) \mathbf{S}_{-q_z}(0) \rangle \sim \chi_Y^{\text{CF}}(\mathbf{q}, \omega_\nu). \quad (4.97)$$

Schulz has not attempted to specify the prefactor.

An estimate of how good the spin dynamics in CuGeO_3 is described by a one-dimensional Heisenberg chain is obtained by plotting the scaled magnetic structure factor after analytical continuation $i\omega_\nu \rightarrow \omega + i\epsilon$

$$T S_{\mathbf{S}}(\pi/c, \omega) \sim \lim_{\epsilon \rightarrow 0} \frac{1}{\pi k_B} \frac{\text{Im} \left[I_1 \left(\frac{\hbar\omega}{2\pi k_B T} \right) \right]^2}{1 - \exp\{-\beta\hbar\omega\}} \quad (4.98)$$

together with the scaled magnetic spectrum obtained by Hirota *et al.* [27]. Quantum criticality implies $T S_{\mathbf{S}}(\pi/c, \omega)$ to be an universal function of $\omega/(2\pi T)$, at least for small ω . The result is shown in figure 4.1 and the experimental data are observed to approximately obey the scaling, though there is substantial scattering of the data for small $\omega/(2\pi T)$. This is possibly due to the influence of non-critical contributions from the Peierls-fluctuations or by a crossover of the character of the magnetic excitations from one- to two-dimensional near the Peierls transition [26, 36].

It is also interesting to note that the prediction for $T S_{\mathbf{S}}(\pi/c, \omega)$ is independent of J and that the data for other one-dimensional Heisenberg antiferromagnets with very different values of the coupling J , like KCuF_3 [114], should fall onto the same universal curve presented in figure 4.1.

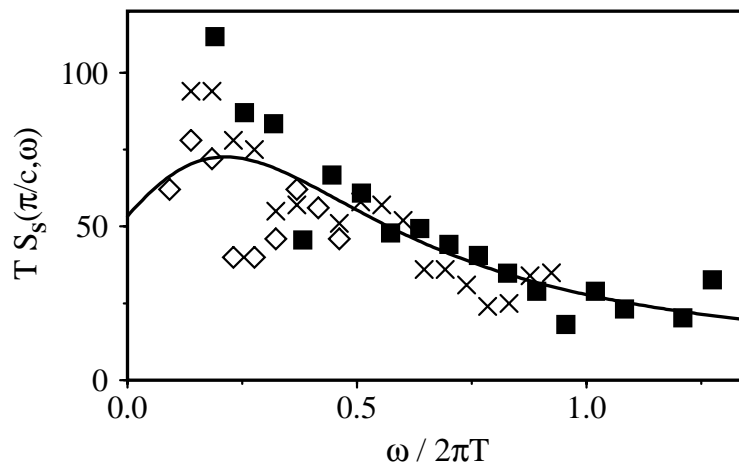


Figure 4.1: $T S_S(\pi/c, \omega)$, as a function of $\omega/(2\pi T)$, as predicted by bosonization (solid line, equation (4.98)), and the neutron-scattering results [27], for $T = 14.5$ K (filled squares), $T = 20$ K (crosses) and $T = 50$ K (diamonds).

Chapter 5

Phonon dynamics

In principle the here discussed phonon dynamics in the disordered phase of a spin-phonon coupled system is given within the random phase approximation (RPA) by the saddle point found in section 4.2.1. For a comparison with experiment the propagator of the spin-phonon coupled system is also needed. In the framework of RPA this can also be obtained via the partition function Z_{RPA} given in equation (4.45) by integrating out the fields ϕ and considering $\partial^2 Z_{\text{RPA}}/\partial g_{\lambda,q}$. I prefer though to introduce here the more straight forward standard perturbative method to obtain the correlation function.

5.1 Normal-coordinate propagator in RPA

The definition of the renormalized, unperturbed normal-coordinate propagator was given in section 4.2.1 in equation (4.58) and (4.59). I recall the resulting

$$D_{\lambda,q,\nu}^{(0)} = -\frac{2\hbar\Omega_{\lambda,q}}{\hbar^2\Omega_{\lambda,q}^2 + \omega_\nu^2}. \quad (5.1)$$

To study the dynamics in the spin-phonon coupled system the interaction has to be included. This done by the standard perturbative approach of the S-Matrix [76].

$$D_{\lambda,q,\nu} = -\frac{2\Omega_{\lambda,q}}{\hbar} \int_0^\beta d\tau e^{i\omega_\nu\tau} \frac{\left\langle T_\tau e^{-\int_0^\beta H_{sp}(\tau')d\tau'} Q_{\lambda,q}(\tau) Q_{\lambda,-q}(0) \right\rangle}{\left\langle T_\tau e^{-\int_0^\beta H_{sp}(\tau')d\tau'} \right\rangle} \quad (5.2)$$

For the relation between normal coordinates and Bose operators see the definition (2.7) on page 14. The spin-phonon coupling term H_{sp} was derived in section 2.2 for CuGeO₃ and generalized to anisotropic chains in equation (3.5). The imaginary time dependence in interaction representation is given for any operator \hat{A} by

$$\hat{A}(\tau) = e^{-(H_p+H_s)\tau} \hat{A} e^{(H_p+H_s)\tau}, \quad (5.3)$$

where H_p and H_s are given by equation (3.3) and (3.4), respectively. Here the trace has to be taken with respect to both the unperturbed spin and phonon system.

$$\langle \hat{A} \rangle = \frac{\mathbf{Tr}_s \mathbf{Tr}_p e^{-\beta(H_s+H_p)} \hat{A}}{\mathbf{Tr}_s \mathbf{Tr}_p e^{-\beta(H_s+H_p)}} \quad (5.4)$$

H_p is bilinear in Bose operators so that Wick's theorem is applicable in the phonon channel. For H_s this is generally not true. Instead I introduce the notion of cumulants, allowing for an equivalent decomposition of the expectation values. The second order dimer-dimer term was already discussed in section 4.2.1:

$$\langle Y_{\mathbf{q}}(\tau) Y_{\mathbf{q}'}(\tau') \rangle_{\text{cum}} = \langle Y_{\mathbf{q}}(\tau) Y_{\mathbf{q}'}(\tau') \rangle - \langle Y_{\mathbf{q}}(\tau) \rangle \langle Y_{\mathbf{q}'}(\tau') \rangle. \quad (5.5)$$

This can be generalized to higher orders [98]. As discussed in section 4.3, in the limit of the unfrustrated XY model, where $J_z = J_2 = J_{2,z} = 0$, H_s and $Y_{\mathbf{q}}^*(\tau)$ are bilinear in spinless Fermi operators. Then Wick's theorem is applicable and the cumulant is described by a connected graph. The expectation values of the dimer operators are time independent $\langle Y_{\mathbf{q}}(\tau) \rangle = \langle Y_{\mathbf{q}} \rangle$ which becomes clear from the definition of the time dependence (5.3) and cyclic invariance under the trace. Additionally, in the disordered phase which I consider here, the translational invariance of the system implies $\langle Y_{\mathbf{q}} \rangle = 0$ so that the lowest order contribution in the spin channel is the dimer-dimer correlation function $\langle Y_{\mathbf{q}}(\tau) Y_{\mathbf{q}'}(\tau') \rangle$.

By introducing a generating functional

$$Q_{\lambda,\mathbf{q}}(\tau) Q_{\lambda,-\mathbf{q}}(0) = \lim_{h \rightarrow 0} \frac{\partial}{\partial h} \exp\{h Q_{\lambda,\mathbf{q}}(\tau) Q_{\lambda,-\mathbf{q}}(0)\} \quad (5.6)$$

numerator and denominator of equation (5.2) can be rewritten to cumulant expansions [98].

$$D_{\lambda,\mathbf{q},\nu} = -\frac{2\Omega_{\lambda,\mathbf{q}}}{\hbar} \int_0^\beta d\tau e^{i\omega_\nu \tau} \lim_{h \rightarrow 0} \frac{\partial}{\partial h} \frac{e^{\sum_{n=1}^{\infty} \frac{1}{n!} \langle T_\tau [-\int_0^\beta d\tau' H_{sp}(\tau') + h Q_{\lambda,\mathbf{q}}(\tau) Q_{\lambda,-\mathbf{q}}(0)]^n \rangle_{\text{cum}}}}{e^{\sum_{n=1}^{\infty} \frac{1}{n!} \langle T_\tau [-\int_0^\beta d\tau' H_{sp}(\tau')]^n \rangle_{\text{cum}}}} \quad (5.7)$$

The limit implies that only terms linear in h will contribute. After differentiation the exponential functions in the numerator and denominator cancel.

$$D_{\lambda,\mathbf{q},\nu} = -\frac{2\Omega_{\lambda,\mathbf{q}}}{\hbar} \int_0^\beta d\tau e^{i\omega_\nu \tau} \left\langle T_\tau \sum_{n=1}^{\infty} \frac{1}{(n-1)!} \left[-\int_0^\beta H_{sp}(\tau') d\tau' \right]^{n-1} Q_{\lambda,\mathbf{q}}(\tau) Q_{\lambda,-\mathbf{q}}(0) \right\rangle_{\text{cum}} \quad (5.8)$$

In the XY limit, where $J_z = J_2 = J_{2,z} = 0$, or for the model describing conduction electrons discussed in section 4.3.2 Wick's theorem is applicable and equation (5.8) is just a linked cluster expansion [76, 4]. In that case $D_{\lambda,\mathbf{q},\nu}$ can be represented diagrammatically as shown in figure 5.1. In the general case equation (5.8) still is an expansion in connected terms

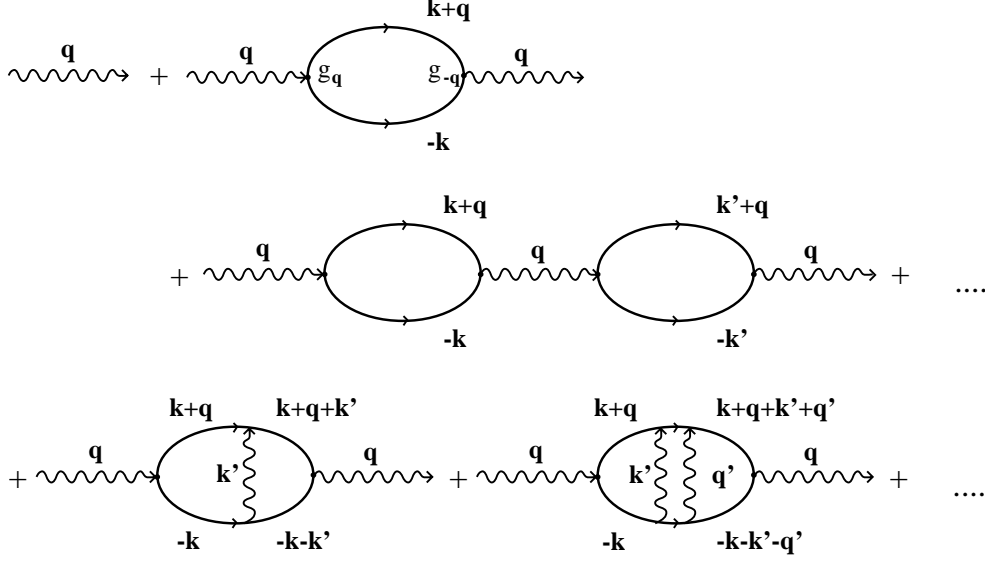


Figure 5.1: Lowest order terms of the series representation of the normal coordinate propagator given in equation (5.8). Wiggled lines are unperturbed normal coordinate propagators (5.1), straight lines are electronic propagators. Away from the limit of the XY model or conduction electrons (see section 4.3.2) the electronic loops have to be viewed as generalized to cumulant contributions. In RPA only electronic loops with two vertices are retained.

since Kubo [98] has shown that a cumulant is zero if one of the variables is statistically independent of the others. Every phonon propagator is connected to a spin vertex as shown in figure 5.1.

In RPA only spin loops with two vertices are retained. Using the definition of the spin-phonon coupling term (3.5), writing the normal-mode operators $Q_{\lambda,q}(\tau)$ as a function of Bose operators as shown in equation (2.7), and recalling the definition of the dimer-dimer correlation function

$$\chi_Y(\mathbf{q}, \nu) = -\frac{1}{N} \int_0^\beta d\tau e^{i\omega_\nu \tau} \langle Y_{\mathbf{q}}(\tau) Y_{-\mathbf{q}}(0) \rangle,$$

which was given in equation (4.87), one has

$$D_{\lambda,\mathbf{q},\nu} = D_{\lambda,\mathbf{q},\nu}^{(0)} + D_{\lambda,\mathbf{q},\nu}^{(0)} g_{\lambda,\mathbf{q}} \sum_{n=0}^{\infty} \left[\chi_Y(\mathbf{q}, \nu) \sum_{\lambda'} g_{\lambda',\mathbf{q}} g_{\lambda',-\mathbf{q}} D_{\lambda',\mathbf{q},\nu}^{(0)} \right]^n \chi_Y(\mathbf{q}, \nu) g_{\lambda,-\mathbf{q}} D_{\lambda,\mathbf{q},\nu}^{(0)} \quad (5.9)$$

Note that all terms odd in the Bose operators $b_{\lambda,q}$ vanish since H_p is diagonal.

After rewriting the geometric series in equation (5.9) I obtain Dyson's equation in RPA

[76].

$$D_{\lambda,\mathbf{q},\nu} = \frac{D_{\lambda,\mathbf{q},\nu}^{(0)} \left(1 - \chi_Y(\mathbf{q}, \nu) \sum_{\lambda' \neq \lambda} g_{\lambda',\mathbf{q}} g_{\lambda',-\mathbf{q}} D_{\lambda',\mathbf{q},\nu}^{(0)} \right)}{1 - \chi_Y(\mathbf{q}, \nu) \sum_{\lambda'} g_{\lambda',\mathbf{q}} g_{\lambda',-\mathbf{q}} D_{\lambda',\mathbf{q},\nu}^{(0)}} \quad (5.10)$$

The physically relevant retarded normal-coordinate propagator is obtained through analytical continuation $i\omega_\nu \rightarrow \hbar\omega + i\epsilon$.

$$D_\lambda(\mathbf{q}, \omega) = \frac{D_\lambda^{(0)}(\mathbf{q}, \omega) \left(1 - \chi_Y(\mathbf{q}, \omega) \sum_{\lambda' \neq \lambda} g_{\lambda',\mathbf{q}} g_{\lambda',-\mathbf{q}} D_{\lambda'}^{(0)}(\mathbf{q}, \omega) \right)}{1 - \chi_Y(\mathbf{q}, \omega) \sum_{\lambda'} g_{\lambda',\mathbf{q}} g_{\lambda',-\mathbf{q}} D_{\lambda'}^{(0)}(\mathbf{q}, \omega)} \quad (5.11)$$

The unperturbed propagator then is

$$D_{\lambda,\mathbf{q},\nu}^{(0)} = \frac{2 \hbar \Omega_{\lambda,\mathbf{q}}}{(\hbar\omega + i\epsilon)^2 - \hbar^2 \Omega_{\lambda,\mathbf{q}}^2}. \quad (5.12)$$

5.2 Phonon softening versus central peak

In this section I show that generically there are two scenarios included in the RPA approach to spin-phonon coupling. For clarity I limit the discussion to a single mode coupling to the electronic system. For the application to CuGeO₃ in section 5.3 the results can be generalized to four modes without a problem.

$$D(\mathbf{q}, \omega) = \frac{D^{(0)}(\mathbf{q}, \omega)}{1 - \chi_Y(\mathbf{q}, \omega) g_{\mathbf{q}} g_{-\mathbf{q}} D^{(0)}(\mathbf{q}, \omega)} \quad (5.13)$$

The eigenmodes of the perturbed phonon system are given by the poles of the normal-coordinate propagator (5.11). Consistent with the saddle point evaluation equation (4.57) in section 4.2.1 the poles are given by the zeros of the real part of the denominator of equation (5.13). For one phonon mode this simplifies to

$$0 = 1 - \text{Re} \chi_Y(\mathbf{q}, \omega) g_{\mathbf{q}} g_{-\mathbf{q}} D^{(0)}(\mathbf{q}, \omega) \quad (5.14)$$

As discussed in section 4.2.1 the transition occurs when equation (5.14) has a solution for $\omega = 0$.

$$0 = 1 + \chi_Y(\mathbf{q}_0, 0, T_{\text{SP}}) \frac{2 g_{\mathbf{q}_0}^2}{\hbar \Omega_{\mathbf{q}_0}}. \quad (5.15)$$

The coupling of the phonon to the spin system is strongest at the wave vector of the instability \mathbf{q}_0 . I will specify here

$$q_0^z = \pi/c \quad (5.16)$$

as the usual spin-Peierls or Peierls modulation particularly true for CuGeO_3 , see chapter 2. The exception of incommensurate ordering is briefly discussed in section 4.1.3.

A graphical solution of equation (5.14) can be obtained by writing out the bare propagator (5.12) with $\epsilon \rightarrow 0$.

$$\frac{\hbar(\omega_\pi^2 - \Omega_{\mathbf{q}_0}^2)}{2\Omega_{\mathbf{q}_0}g_{\mathbf{q}_0}^2} = \text{Re}\chi_Y(\mathbf{q}_0, \omega_\pi) \quad (5.17)$$

I now discuss the results for different approaches to the electronic system. The corresponding correlation functions χ_Y have been discussed already in section 4.3.2.

5.2.1 Isotropic case

In the isotropic case the dimer-dimer correlation function is given approximatively in equation (4.94). After analytical continuation I have

$$\chi_Y^{\text{CF}}(\mathbf{q}_0, \omega) = -\frac{\chi_0}{0.35 k_B T} \left(I_1 \left[\frac{\hbar\omega}{2\pi k_B T} \right] \right)^2. \quad (5.18)$$

The imaginary part of the frequency $i\epsilon$ is unimportant here. As discussed in section 4.3.2 the prefactor $\chi_0(k_B T/J)$ is temperature dependent and not scale invariant. It is very likely that it also has a frequency dependence, which yet has not been determined. To study qualitatively the phonon dynamics I will approximate χ_0 as a constant. The transition temperature is then given as [14]

$$k_B T_{\text{SP}} = \frac{2g_{\mathbf{q}_0}^2}{\hbar\Omega_{\mathbf{q}_0}} \chi_0. \quad (5.19)$$

Typical plots of the left hand side (broken lines) and right hand side (full lines) of equation (5.17) with $\chi_Y(\mathbf{q}_0, \omega) = \chi_Y^{\text{CF}}(\mathbf{q}_0, \omega)$ are presented in figure 5.2. For a small frequencies of the unperturbed phonon system $\Omega_{\mathbf{q}_0}$ equation (5.17) has a single solution for $T = T_{\text{SP}}$ and inspection of the temperature dependence of this solution for $T > T_{\text{SP}}$ (compare figure (5.2)) shows that this root continuously connects to the $T = \infty$ solution, $\lim_{T \rightarrow \infty} \omega_\pi = \Omega_{\mathbf{q}_0}$. For large frequencies $\Omega_{\mathbf{q}_0}$ equation (5.17) has two solutions at $T = T_{\text{SP}}$. The solution at $\omega = 0$ vanishes for $T > T_{\text{SP}}$. This is referred to as the central peak and is attributed to a mixed magneto-acoustic excitation in section 5.3.2. The temperature dependence of the solution at finite frequencies is illustrated in figure 5.3.

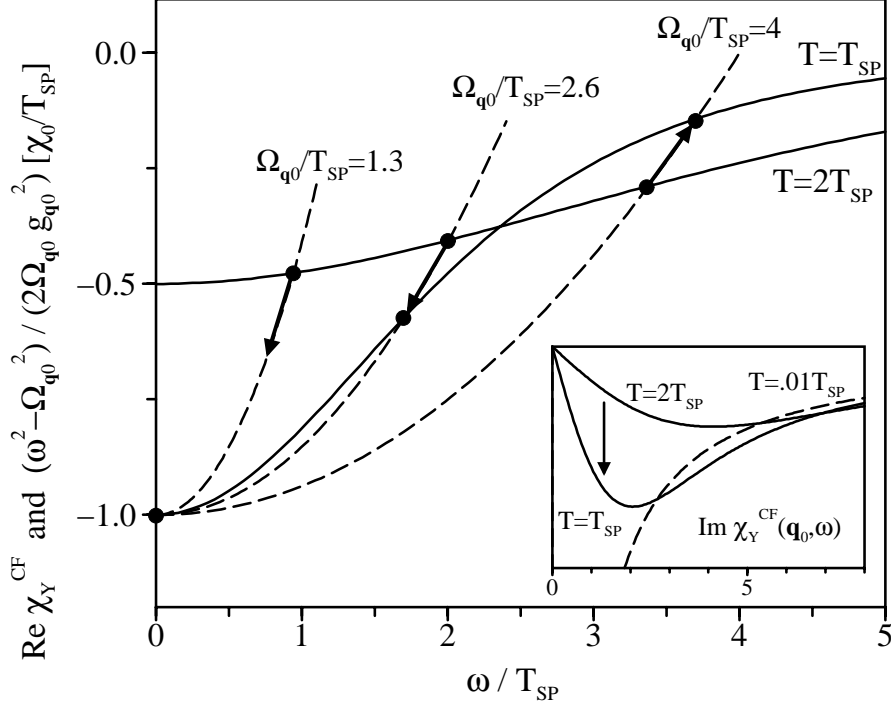


Figure 5.2: Plots of $\text{Re}\chi_Y^{\text{CF}}(\mathbf{q}_0, \omega)$ (solid lines) for $T = T_{\text{SP}}$ and $T = 2T_{\text{SP}}$, as a function of ω/T_{SP} . In the graph I have set $\hbar = k_B = 1$. The temperature independent left hand side of equation (5.17), $(\omega^2 - \Omega_{\mathbf{q}_0}^2)/(2\Omega_{\mathbf{q}_0}g_{\mathbf{q}_0}^2)$, is plotted for $\Omega_{\mathbf{q}_0}/T_{\text{SP}} = 1.3, 2.6, 4$ (dashed lines), with $g_{\mathbf{q}_0}$ given by equation (5.19). The filled circles denote the position of the phonon frequencies, ω_π . The arrows indicate the shift of ω_π with decreasing temperature. Inset: $\text{Im}\chi_Y^{\text{CF}}(\mathbf{q}_0, \omega)$.

The appearance of the regime with two solutions and a central peak can be quantified from the parabolic width of $\chi_Y^{\text{CF}}(\mathbf{q}_0, \omega, T_{\text{SP}})$ for small ω . For any finite temperature I can expand $\chi_Y^{\text{CF}}(\mathbf{q}_0, \omega)$ in $\omega/(2\pi T)$ as

$$\chi_Y^{\text{CF}}(\mathbf{q}_0, \omega) = -\frac{\chi_0}{k_B T} \left[1 + i\chi_1 \left(\frac{\hbar\omega}{2\pi k_B T} \right) - \chi_2 \left(\frac{\hbar\omega}{2\pi k_B T} \right)^2 + \dots \right], \quad (5.20)$$

with $\chi_1 \approx 3.14$ and $\chi_2 \approx 8.5$. The position of the poles ω_π of $D(\mathbf{q}_0, \omega)$ are then determined by the roots of

$$\frac{\hbar\omega_\pi^2}{2\Omega_{\mathbf{q}_0}g_{\mathbf{q}_0}^2} - \frac{\hbar\Omega_{\mathbf{q}_0}^2}{2\Omega_{\mathbf{q}_0}g_{\mathbf{q}_0}^2} \approx -\frac{\chi_0}{k_B T} + \frac{\chi_0\chi_2}{k_B T} \left(\frac{\hbar\omega_\pi}{2\pi k_B T} \right)^2, \quad (5.21)$$

Comparing the prefactor of the terms $\sim \omega_\pi^2$ of the right hand and left hand side of equation

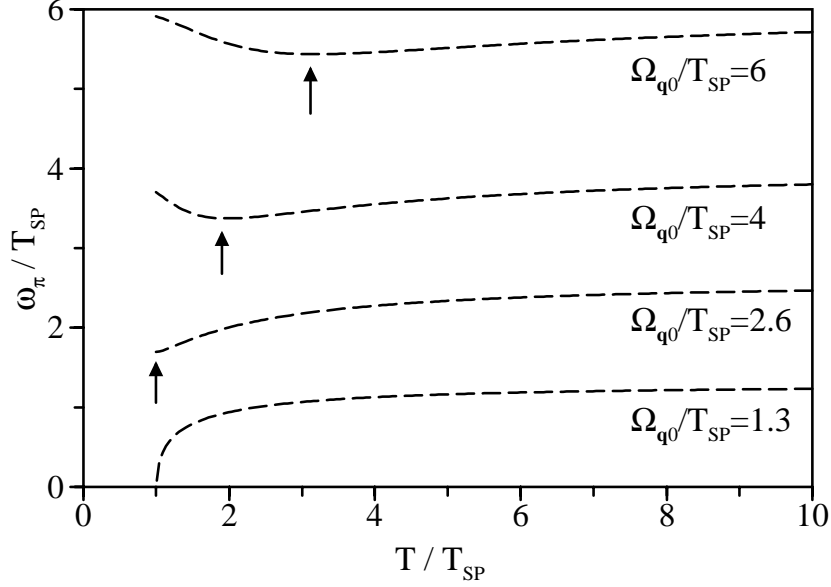


Figure 5.3: Temperature dependence of the phonon frequencies ω_π for various values of $\Omega_{q_0}/T_{\text{SP}}$ in the isotropic Heisenberg case. In the graph I have set $\hbar = k_B = 1$. Ω_{q_0} is the bare phonon frequency. The arrows indicate the respective minimal phonon frequency.

(5.21) one finds that for

$$\frac{1}{2g_{q_0}^2 \Omega_{q_0}} > \frac{\chi_0 \chi_2}{4\pi^2 (k_B T_{\text{SP}})^3}, \quad (5.22)$$

equation (5.17) has a single solution at $T = T_{\text{SP}}$ and the phonon softens completely as shown by the lowest curve in figure 5.3. I can use equation (5.19) to eliminate g_{q_0} from equation (5.22) and obtain

$$k_B T_{\text{SP}} > \frac{\hbar \Omega_{q_0}}{2\pi} \sqrt{\chi_2} \approx 0.46 \hbar \Omega_{q_0}, \quad \hbar \Omega_{q_0} < 2.2 k_B T_{\text{SP}}, \quad (5.23)$$

for the soft-phonon regime. For $\hbar \Omega_{q_0} > 2.2 k_B T_{\text{SP}}$ the Peierls-active phonon does not soften completely and an additional central peak shows up.

5.2.2 Conduction electrons

To show that the two regimes of phonon softening and the central peak are not an artefact of the approximations applied to the dimer-dimer correlation function in the isotropic Heisenberg case I consider here the model of the density of one-dimensional conduction electrons coupling to phonons. The Hamiltonian was given in equation (4.88) on page 67 and the operator $Y_q \rightarrow \rho_q$ is a density operator given in equation (4.89). This model is

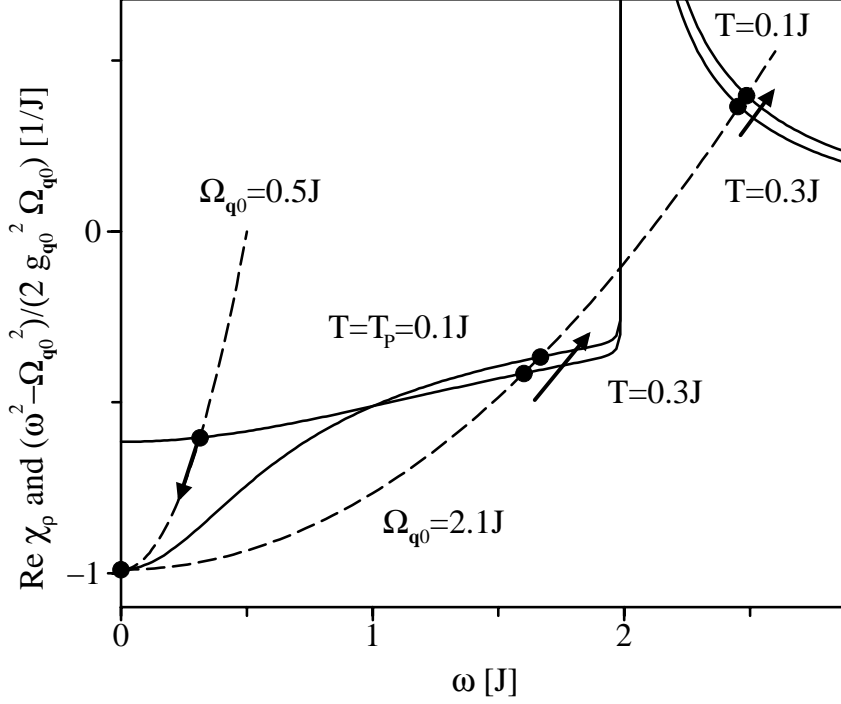


Figure 5.4: Plots of $\text{Re}\chi_\rho$ for neglecting the spin degree of freedom of the electron (solid lines) for $T = T_p = 0.1J$ and $T = 3T_p$ as a function of ω . In the graph I have set $\hbar = k_B = 1$. The temperature independent left hand side of equation (5.24), $(\omega^2 - \Omega_{q_0}^2)/(2g_{q_0}^2 \Omega_{q_0})$, is plotted for $\Omega_{q_0} = 0.5J$ and $2.1J$ (dashed lines), with g_{q_0} given self-consistently by equation (5.25). The filled circles denote the position of the phonon frequencies, ω_π . The arrows indicate the shift of ω_π with decreasing temperature. Note that for phonon frequencies near the band edge there are two poles showing the mixed electro-elastic nature of the electron-phonon coupled modes.

used to describe the Peierls instability [91, 92, 93]. The electronic correlation function χ_ρ then is the Lindhard formula (4.90), which can easily be determined numerically. The spin degree of freedom of the electrons is degenerate, so I can neglect it here.

The poles of the normal-coordinate propagator (5.13) are determined by the roots of the self-consistency equation

$$\frac{\hbar(\omega_\pi^2 - \Omega_{q_0}^2)}{2\Omega_{q_0}g_{q_0}^2} = \text{Re} \frac{1}{N} \sum_{\mathbf{k}} \frac{f_{\mathbf{k}} - f_{\mathbf{k}+q_0}}{\omega_\pi + E_{\mathbf{k}} - E_{\mathbf{k}+q_0} + i\epsilon}. \quad (5.24)$$

The dispersion is one dimensional $E_{\mathbf{k}} = J \cos k_z$ and there is no chemical potential corresponding to half filling. Plots of the left hand and right hand side of equation (5.24) are shown in figure 5.4. There is no scale invariance, the critical temperature has been set to

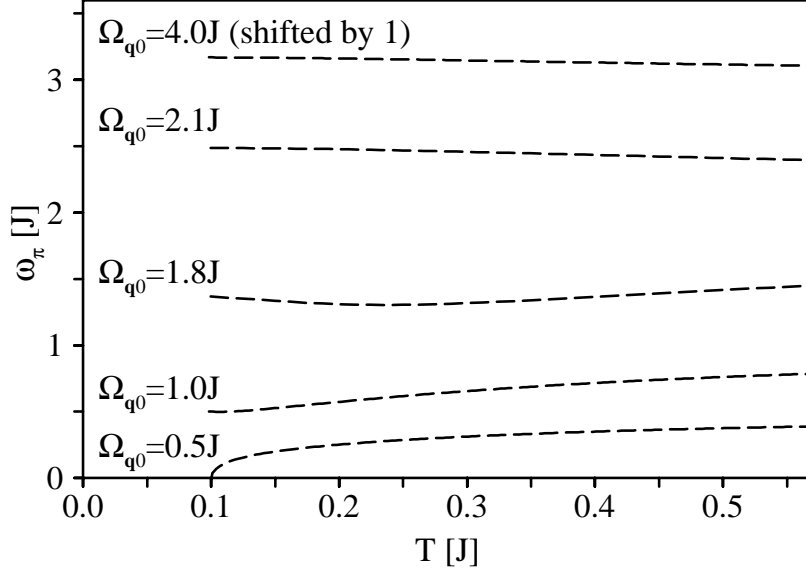


Figure 5.5: Temperature dependence of the phonon frequencies ω_π for various values of $\Omega_{q_0}/T_{\text{SP}}$ in the case of conduction electrons in a half filled cosine band, as obtained by iterating equation (5.24). In the graph I have set $\hbar = k_B = 1$. Ω_{q_0} is the bare phonon frequency. Phonons above the band width of $2J$ are always hardened.

$\hbar\Omega_{q_0}$	0.5J	1.0J	1.8J	4.0J
g_{q_0}	0.5J	0.71J	0.95J	1.4J

Table 5.1: Coupling constants for the conduction electron model with $T_P = 0.1J$ for different unperturbed phonon frequencies, as obtained by iterating equation (5.25). If the electronic spin degree of freedom is not neglected, the values have to be divided by two since the contribution from χ_ρ is doubled.

$T_P = 0.1J$. The coupling constant is then determined self-consistently by

$$0 = 1 + \frac{2g_{q_0}^2}{\hbar\Omega_{q_0}} \frac{1}{N} \sum_{\mathbf{k}} \frac{f_{\mathbf{k}}(T_P) - f_{\mathbf{k}+q_0}(T_P)}{E_{\mathbf{k}} - E_{\mathbf{k}+q_0}}. \quad (5.25)$$

The values are given in table 5.2.2.

Clearly, the two regimes of the soft phonon and the central peak are present. Numerical analysis yields that for $T_P = 0.1J$ only for $\hbar\Omega_{q_0} < 0.8J$ the phonon softens completely. For $\hbar\Omega_{q_0} > 0.8J$ the Peierls-active phonon does not become soft and a central peak arises at T_{SP} . Note that for phonon frequencies near the band edge there are two poles showing the electro-elastic nature of the electron-phonon coupled modes.

The corresponding temperature dependence of the eigenmodes are shown for various

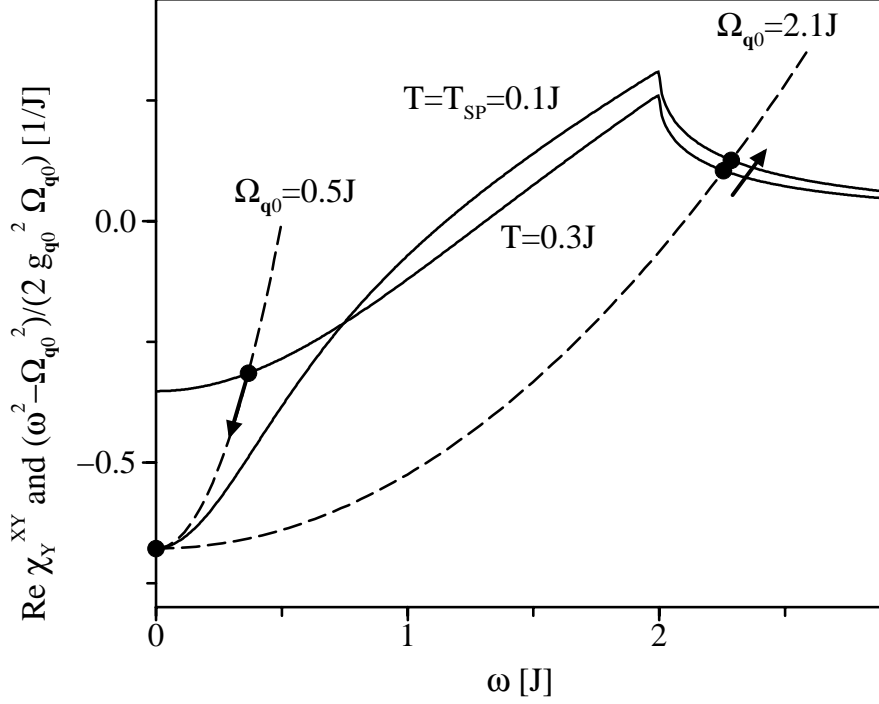


Figure 5.6: Plots of $\text{Re}\chi_Y^{XY}(\mathbf{q}_0, \omega)$ (solid lines) for $T = T_{\text{SP}} = 0.1J$ and $T = 3T_{\text{SP}}$. In the graph I have set $\hbar = k_B = 1$. The temperature independent left hand side of equation (5.26), $(\omega^2 - \Omega_{\mathbf{q}_0}^2)/(2g_{\mathbf{q}_0}^2 \Omega_{\mathbf{q}_0})$, is plotted for $\Omega_{\mathbf{q}_0} = 0.5J$ and $2.1J$ (dashed lines), with $g_{\mathbf{q}_0}$ given self-consistently by equation (5.27). The filled circles denote the position of the phonon frequencies, ω_{π} . The arrows indicate the shift of ω_{π} with decreasing temperature.

bare phonon frequencies in figure 5.5. Note that the second pole shown for $\hbar\Omega_{\mathbf{q}_0} = 2.1J$, which is clearly present in figure 5.4, is not an attractive fixed point of the self-consistency equation (5.24). Yet, the second mode is clearly present in the structure factor as shown and discussed further in section 5.3.2. The same is true for the $\hbar\Omega_{\mathbf{q}_0} = 1.8J$ mode not shown explicitly. The solutions obtained by the via equation (5.24) are those connecting continuously to the $T \rightarrow \infty$ solutions where the effects of the interaction are absent.

5.2.3 Ising and XY limit

The case of an Ising chain coupled to phonons, where $J = J_2 = J_{2,z} = 0$, has been treated by Pytte [3] to study the Jahn-Teller effect. He also performed an RPA approximation introducing a phenomenological damping. Although not having been worked out by him, there is also a parameter regime in his model where the phonon is not softened and a central peak is present.

The XY case can be determined equivalently to the case of conduction electrons dis-

cussed above, as can be seen by comparing the corresponding correlation functions (4.90) and $\chi_Y^{XY}(\mathbf{q}, \omega)$ in equation (4.93). After analytical continuation the eigenstates are given by the roots of

$$\frac{\hbar(\omega_\pi^2 - \Omega_{\mathbf{q}_0}^2)}{2\Omega_{\mathbf{q}_0}g_{\mathbf{q}_0}^2} = \text{Re} \frac{1}{2L} \sum_{k_z} [1 + \cos(2k_z + q_0^z)c] \frac{f_{k_z} - f_{k_z+q_0^z}}{\omega + E_{k_z} - E_{k_z+q_0^z} + i\epsilon}. \quad (5.26)$$

The plot of the left and right hand side of equation (5.26) is shown in figure 5.6. The coupling constant is determined self-consistently by

$$0 = 1 + \frac{2g_{\mathbf{q}_0}^2}{\hbar\Omega_{\mathbf{q}_0}} \frac{1}{2L} \sum_{k_z} [1 + \cos(2k_z + q_0^z)c] \frac{f_{k_z}(T_{\text{SP}}) - f_{k_z+q_0^z}(T_{\text{SP}})}{E_{k_z} - E_{k_z+q_0^z}}. \quad (5.27)$$

Qualitatively the same two regimes are given as in the other cases.

5.3 Application to CuGeO₃

For a long time the absence of a soft phonon mode in CuGeO₃ [27, 20] has been puzzling, since the behavior was believed not to be consistent with the standard approach to spin-Peierls transitions by Cross and Fisher [14]. The frequencies of the Peierls-active phonon modes being of the order of the magnetic exchange (section 2.1 and reference [44]), it has been argued that the Cross and Fisher approach is not applicable because of the non-adiabaticity of the phonons [67]. In the previous sections I have shown that the absence of phonon-softening is generically described within the RPA approach. Here I apply this result to reproduce the experimental results on CuGeO₃ and give arguments for the applicability of RPA.

The coupling constants in CuGeO₃ have been derived and tested for coherence with experiment in chapter 2. The magnetic system in CuGeO₃ has been shown to be well described by an isotropic Heisenberg chain so the appropriate correlation function is the dimer-dimer correlation function $\chi_Y^{\text{CF}}(\mathbf{q}_0, \omega)$ given in equation (4.94) in section 4.3.2. The condition for the soft phonon regime (5.23) has to be generalized. One obtains

$$k_{\text{B}}T_{\text{SP}} < \frac{\chi_2}{4\pi^2\chi_0} \left(\sum_{\lambda} \frac{2g_{\lambda, \mathbf{q}_0}^2}{\Omega_{\lambda, \mathbf{q}_0}^3} \right)^{-1} \quad (5.28)$$

for the soft-phonon regime. CuGeO₃ is found to be in the central peak regime.

In figure 5.7 I have plotted the results for the dynamical structure factor,

$$S(\mathbf{q}_0, \omega) = -\frac{1}{\pi} \frac{\sum_{\lambda} \text{Im}D_{\lambda}(\mathbf{q}_0, \omega + i\epsilon)}{1 - \exp(-\beta\hbar\omega)}, \quad (5.29)$$

where I have used the experimental resolution function

$$\epsilon \approx 0.023 + 0.028 \omega / (2\pi) \quad (5.30)$$

in units of THz [115]. Including the experimental resolution by a convolution with a Gaussian distribution while setting $\epsilon \rightarrow 0$ gives identical results for all practical purposes. The normal-coordinate propagator $D_\lambda(\mathbf{q}_0, \omega + i\epsilon)$ was defined in equation (5.11) with the dimer-dimer correlation function $\chi_Y^{\text{CF}}(\mathbf{q}_0, \omega)$.

The intensity of the experimental spectra [44], also shown in figure 5.7, have been scaled. The (constant) background has been adjusted. A rough comparison indicates, that the experimental intensity ratio of the lower T_2^+ mode at $T=295\text{K}$ and $T=16\text{K}$ is about 3:1 in agreement with theory, see figure 5.7. The overall agreement between experiment and theory is satisfactory, although the hardening of the lower phonon mode is somewhat more pronounced in the experiment (6% vs. 1%). This discrepancy is not surprising considering the numerical uncertainties in the dimer-dimer correlation function discussed in section 4.3.2 and 2.7. A reliable approach to the dynamical dimer-dimer correlation function in the presence of next nearest neighbor frustration would be quite desirable. No experimental data for the upper mode were available for $T = 16$ K.

In the inset a blowup of the central peak is given. It should be possible to resolve the predicted central peak below ~ 20 K. It has a width of ≈ 0.05 THz = 0.2 meV. From the neutron scattering data from Regnault *et al.* [30] no central peak was observed, but the analysis involved the subtraction of the incoherent beam which I do not consider too reliable. Brillouin scattering would be an appropriate technique, but it is only sensitive to the zone boundary at \mathbf{q}_0 after folding back the dispersion in the ordered phase below T_{SP} . In the ordered phase the dimer-dimer correlation function has not been determined yet. Additionally, the central peak only develops substantial spectral weight in the critical region determined by the Ginzburg criterion in section 2.3.1 so that fluctuations may suppress the peak.

5.3.1 Applicability of RPA

From the Ginzburg criterion discussed in section 2.3.1 the RPA approach should be reliable above ~ 16 K. The coupling constants determined in chapter 2 are rather large so that the small critical region is counter-intuitive at first sight. This result can be made plausible though by considering that RPA becomes exact for models with a finite number of phonons [116]. The \mathbf{q} dependence of the coupling constants is given in equation (2.20) on page 19. The phase factors are only weakly \mathbf{q} dependent. But away from the high symmetry point \mathbf{q}_0 in the Brillouin zone the the 30 phonon modes will be decomposed into less irreducible subgroups. Along the $[x, 0, x]$ direction 13 modes will all couple to the spin system [44]. A strong dephazation of the different contributions to the coupling constant is very likely suppressing the coupling away from \mathbf{q}_0 . The phase space of the phonons coupling the spin system is thus expected to be small.

In order to estimate the (quantitative) magnitude of the corrections to RPA for CuGeO_3 one may compare the RPA prediction for the inverse lattice correlation length $1/\xi_c$ with the experimental pre-transitional Peierls fluctuations. The lattice correlation length is

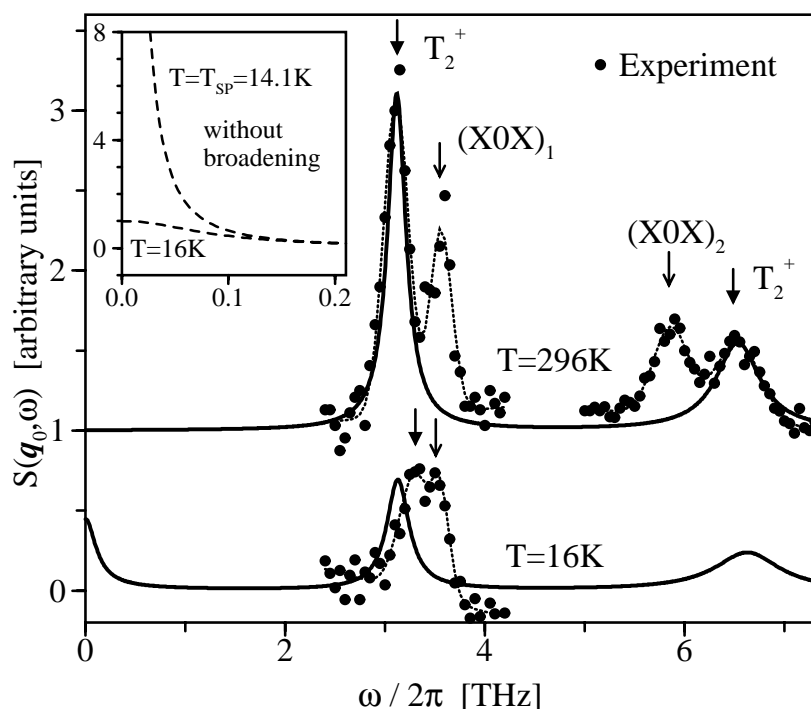


Figure 5.7: Theoretical (thick solid lines) and experimental (solid circles, [44]) results for the dynamical structure factor. The theoretical curve includes broadening due to the experimental resolution given in equation (5.30). The T_2^+ phonons are Peierls active and included in the theory, $(XOX)_1$ and $(XOX)_2$ are other nearby phonons. The data for $T = 296$ K has been shifted. Inset: Blowup of the central peak at $T = T_{\text{SP}} = 14.1$ K and $T = 16$ K (not broadened).

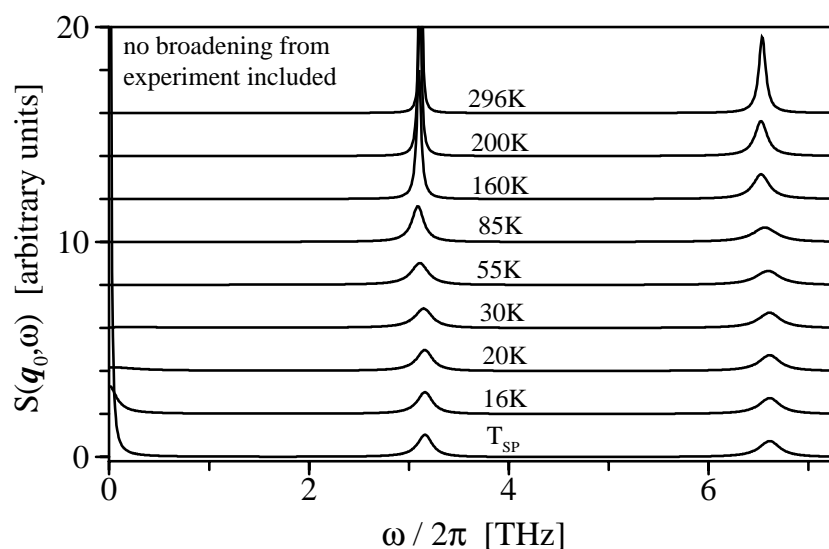


Figure 5.8: Temperature evolution of the theoretical dynamical structure factor. The resonances are the Peierls-active T_2^+ phonons. The data have been shifted.

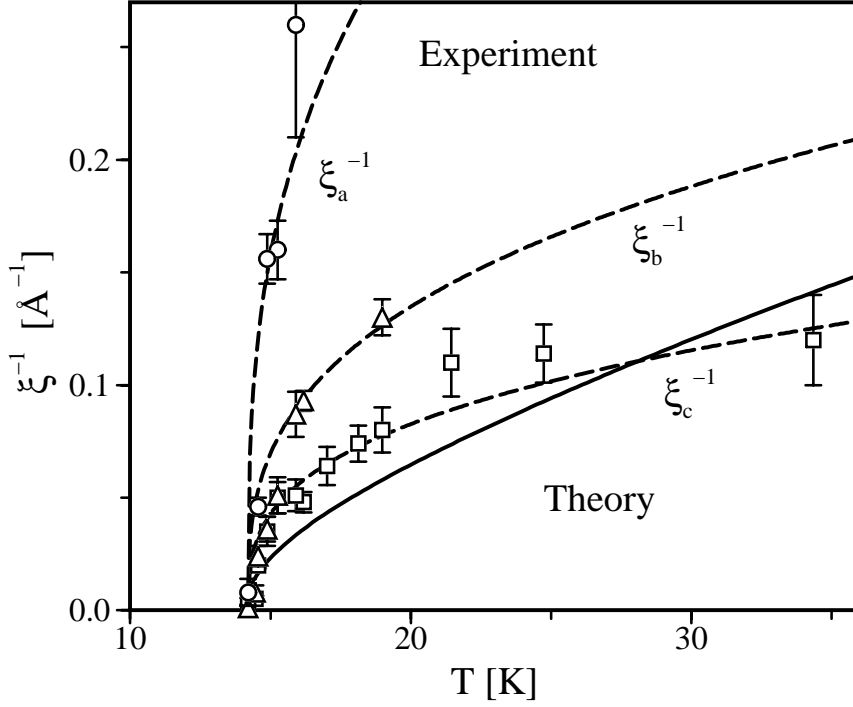


Figure 5.9: Inverse lattice correlation length $1/\xi_\alpha$. Experimental results [26] are given for the different crystallographic axes compared to the RPA result for $1/\xi_c$ along the chains. The broken lines are fits as given by equation (2.27) through (2.29) on page 22. The theoretical result is given by the full line and does not contain any free parameter.

determined by the long-distance falloff,

$$\lim_{z \rightarrow \infty} \int \frac{dq_z}{2\pi} e^{iq_z R_z} \text{Re}D(\mathbf{q}, 0) \sim e^{i\pi R_z/c} e^{-R_z/\xi_c}, \quad (5.31)$$

where $c = 2.94 \text{ \AA}$ is the c axis lattice constant of CuGeO_3 and $D(\mathbf{q}, \omega)$ is given by equation (5.11) with the dimer-dimer correlation function of the isotropic Heisenberg chain (4.94) given in section 4.3.2. I have calculated $1/\xi_c$ from equation (5.31) using $v_s = (\pi/2)J(1 - 1.12\alpha)$ [117] (which enters via the dimer-dimer correlation function (4.94)), $J = 150 \text{ K}$ for the exchange integral, and $\alpha = 0.24$ for the frustration parameter as discussed in section 2.7. I have neglected the \mathbf{q} dependence of the phonon frequencies and the coupling constants. The results for $1/\xi_c$ are presented in figure 5.9, together with results for CuGeO_3 obtained by diffusive X-ray scattering [26], which are consistent with neutron-scattering data and the absence of a soft phonon [27].

Close to the transition the theory shows mean-field behaviour, $1/\xi_c \sim \sqrt{T - T_{\text{SP}}}$ deviating from the fit to experiment given by equation (2.29) on page 22. For higher temperatures, when the correlation length is small, Fourier components further away from $q_z = \pi/c$ are

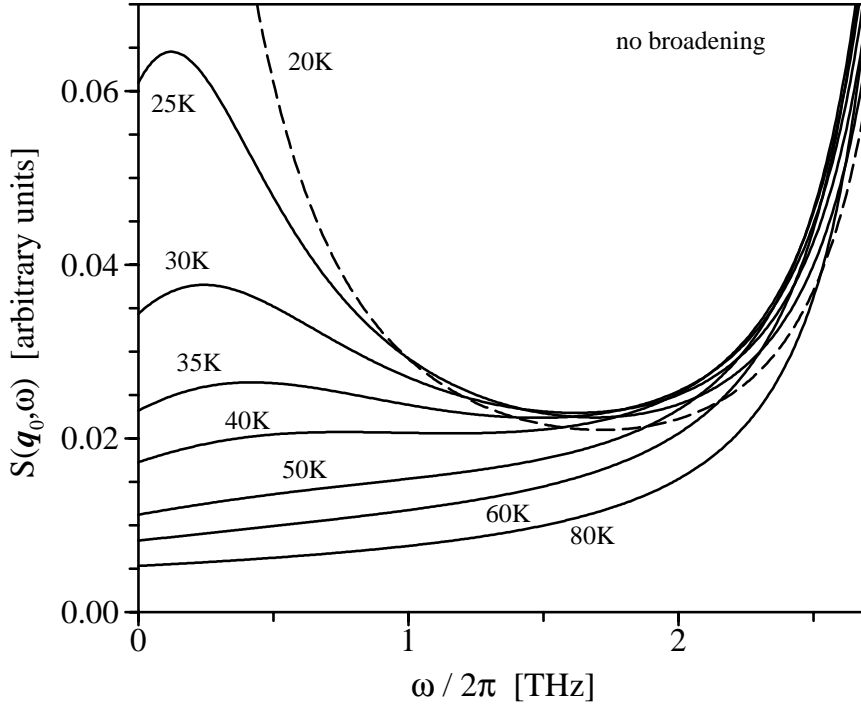


Figure 5.10: *Temperature dependence of the magneto-elastic mode leading to the central peak in the theoretical dynamical structure factor. The peak at higher frequencies is the lowest Peierls-active T_2^+ mode. No experimental broadening has been included.*

important and the approximation of the dimer-dimer correlation function (4.94) fails. One can conclude that there is no substantial quantitative deviation of the RPA result from experiments.

5.3.2 Magneto-elastic modes

The eigenstates of the spin-phonon system evolve adiabatically as a function of the spin-phonon coupling strength in the soft-phonon regime. In the central-peak regime a new magneto phonon appears at low frequencies and condenses at T_{SP} , leading to the structural transition and the formation of spin singlets. A blow-up of the central peak region of the structure factor (5.29) with the dimer-dimer correlation function χ_Y^{CF} in equation (4.94) is shown in figure 5.10. The appearance of a new maximum at about 40K is clearly visible. This mode is then turning soft developing the central peak.

This new mode is neither found in the roots of the real part of the denominator of the retarded normal-coordinate propagator (5.11) nor in the equivalent nontrivial saddle point solutions of the action (4.51). Only at the transition temperature T_{SP} the solution appears which then can be interpreted as the new Bragg peak related to the onset of the lattice

distortion. For a better understanding of the mathematical nature of the maximum an analysis of all the complex roots in the denominator of the normal-coordinate propagator (5.10)

$$0 = 1 - \chi_Y(\mathbf{q}, z) \sum_{\lambda} g_{\lambda, \mathbf{q}} g_{\lambda, -\mathbf{q}} D_{\lambda}^{(0)}(\mathbf{q}, z) \quad (5.32)$$

with the continuation $i\omega_{\nu} \rightarrow z$ is desirable. I recall that the new mode is not found within the dynamical saddle point approach in section 4.2.1. This might indicate that it has no classical analogue.

A physical interpretation of the new collective excitation can be given as a superposition of a phonon with two magnons in a (valence-bond) singlet state. Condensation of this magneto phonon at T_{SP} leads to the simultaneous formation of the valence-bond singlets and the dimerization of the lattice. The magneto phonon couples to the phonon propagator and therefore shows up as a low-energy resonance in $D(\mathbf{q}, \omega)$. The other resonances in $D(\mathbf{q}, \omega)$ at ω_{λ} have the limit $\lim_{g_{\lambda, \mathbf{q}_0} \rightarrow 0} \omega_{\lambda} = \Omega_{\lambda, \mathbf{q}_0}$. Therefore, one usually regards ω_{λ} to be “true” phonons. In terms of the eigenstates of the coupled spin-phonon system such a distinction does not make sense. In the central-peak regime the spectral weight of $D(\mathbf{q}, \omega)$ is divided between the “phonon resonances” at ω_{λ} and the soft magneto phonon.

A related scenario is found in the case of conduction electrons coupling to phonons. The additional root of the denominator of the retarded normal-coordinate propagator (5.11) with the Lindhard formula describing the electronic density-density correlation function has already been discussed in section 5.2.2 and was shown in figure (5.4). The resulting structure factor

$$S_{\rho}(\mathbf{q}_0, \omega) = -\frac{1}{\pi} \frac{\text{Im} D_{\rho}(\mathbf{q}_0, \omega + i\epsilon)}{1 - \exp(-\beta\hbar\omega)} = -\frac{1}{\pi} \frac{\text{Im} \frac{D^{(0)}(\mathbf{q}_0, \omega)}{1 - \chi_{\rho}(\mathbf{q}_0, \omega) g_{\mathbf{q}_0}^2 D^{(0)}(\mathbf{q}_0, \omega)}}{1 - \exp(-\beta\hbar\omega)} \quad (5.33)$$

is shown in figure 5.11. I have used a small regularization parameter $\epsilon = 0.0005J$ to assure numerical stability. The peak above the upper band edge of $\omega = 2J$ is broadened only by the finite ϵ since $\text{Im} \chi_{\rho}(\mathbf{q}_0, \omega > 2J) = 0$.

Even though the second peak just below the electronic band edge is not an attractive fixed point of the self-consistency equation (5.24) and is thus not shown in figure 5.5, it clearly is present in the structure factor. It vanishes for $T \rightarrow \infty$ so that the higher peak can be referred to the “true phonon”. At lower temperatures the spectral weight of the structure factor is split into the “renormalized phonon” and a new electro-acoustic mode. This new electro-acoustic mode can be interpreted as growing soft and diverges at the transition. Again, a detailed analysis of the roots of the denominator of $D_{\rho}(\mathbf{q}_0, z)$ with complex argument $\omega + i\epsilon \rightarrow z$ is desirable for a closer understanding of the nature of the coupled mode.

I do not show here results for the XY model. They are in qualitative agreement with the isotropic Heisenberg case.

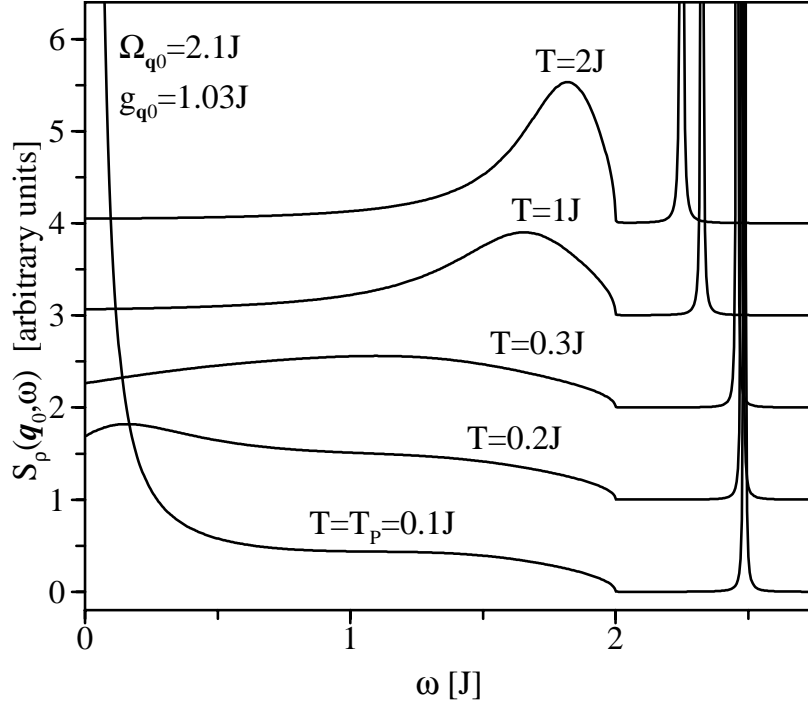


Figure 5.11: *Temperature dependence of the electro-elastic mode leading to the central peak in the theoretical dynamical structure factor where the electronic degrees of freedom are described by the Lindhard formula. A small regularization parameter leads to the slight broadening of the peak above the electronic band edge of $\omega = 2J$. Curves are shifted. In the graph I have set $\hbar = k_B = 1$.*

5.3.3 Conclusions

In this chapter I have shown that the puzzle of the absence of a soft phonon is naturally explained within RPA, regardless of the specific form of the electronic correlation function. New mixed magneto-elastic or electro-elastic excitations are observed, the further study of which is suggested. The calculated temperature-dependence of the phonon modes and that of the pre-transitional Peierls fluctuations are in satisfactory agreement with experiments on CuGeO_3 . A central peak of width 0.2 meV is predicted to appear at T_{SP} .

Chapter 6

Effective Ising model

In this chapter I discuss a model describing the driving physics of the spin-Peierls transition as the coherent ordering of preformed dimers. The resulting model is applied successfully to describe the thermodynamics in the ordered phase of CuGeO_3 . Mostovoy and Khomskii have used a similar approach to study doping effects in CuGeO_3 [108].

Ising models are a standard approach to order-disorder transitions [1]. Ising-like Landau-Ginzburg functionals have been used to estimate fluctuation effects in quasi-one-dimensional components [118, 119] and the resulting pseudo gap [120] as well as the Lifshitz criticality and the incommensurate transition in the presence of a magnetic field [87] can be described within this approach. For completeness I show the derivation of such models from the microscopic approach in section 6.4.3.

6.1 Effective real-space mean-field dimer partition function

Starting point is the representation of the partition function (4.25), where the phonon fields have been integrated out. I apply a static approximation by only keeping the component where $\nu = 0$.

$$Z_{\text{stat}} = Z_s Z_p \left\langle \exp \left\{ \beta \sum_{\lambda, q} \frac{g_{\lambda, q} g_{\lambda, -q}}{N \hbar \Omega_{\lambda, q}} Y_q Y_{-q} \right\} \right\rangle \quad (6.1)$$

I have used the definition $\lim_{M \rightarrow \infty} Y_{q,0} / \sqrt{M} = Y_q$ for the static dimer operator given in equation (3.46). I recall that $Z_s = \mathbf{Tr}_s \exp\{-\beta H_s\}$ and $Z_p = \mathbf{Tr}_p \exp\{-\beta H_p\}$, where H_s and H_p are given in equation (3.4) and (3.3), respectively.

I consider now the isotropic limit $J_z = J$ and $J_{2,z} = J_2$ and transform to real space using the definition of Y_{-q} in equation (3.6).

$$Z_{\text{stat}} = Z_s Z_p \left\langle T_\tau \exp \left\{ -\beta \sum_{l, l'} J_{l, l'} (\mathbf{S}_l \cdot \mathbf{S}_{l+\hat{z}}) (\mathbf{S}_{l'} \cdot \mathbf{S}_{l'+\hat{z}}) \right\} \right\rangle \quad (6.2)$$

I have defined the interaction

$$J_{\mathbf{l},\mathbf{l}'} = \frac{1}{N} \sum_{\lambda,\mathbf{q}} e^{-i\mathbf{q}(\mathbf{R}_{\mathbf{l}}-\mathbf{R}_{\mathbf{l}'})} e^{-i\pi(l_y-l'_y)} \frac{g_{\lambda,\mathbf{q}}g_{\lambda,-\mathbf{q}}}{\hbar\Omega_{\lambda,\mathbf{q}}}. \quad (6.3)$$

The \mathbf{q} dependence of the coupling constants is dominated by the polarization vectors as can be seen from their definition in equation (2.20). As discussed in section 5.3.1, the dephazation of the polarization vectors away from the wave vector of the spin-Peierls instability \mathbf{q}_0 will suppress the coupling constants. $J_{\mathbf{l},\mathbf{l}'}$ is then of long range justifying a mean-field decoupling of the exponent in equation (6.2).

$$(\mathbf{S}_{\mathbf{l}} \cdot \mathbf{S}_{\mathbf{l}+\hat{z}} - \langle \mathbf{S}_{\mathbf{l}} \cdot \mathbf{S}_{\mathbf{l}+\hat{z}} \rangle) (\mathbf{S}_{\mathbf{l}'} \cdot \mathbf{S}_{\mathbf{l}'+\hat{z}} - \langle \mathbf{S}_{\mathbf{l}'} \cdot \mathbf{S}_{\mathbf{l}'+\hat{z}} \rangle) \approx 0 \quad (6.4)$$

This decoupling should not be applied to the nearest neighbor terms $\mathbf{l} = \mathbf{l}' \pm \hat{z}$, since the overlap of the local dimer operators $\mathbf{S}_{\mathbf{l}} \cdot \mathbf{S}_{\mathbf{l}+\hat{z}}$ describes the one-dimensional character of the correlations. Denoting

$$J_{\text{NN}} = J_{\mathbf{l},\mathbf{l}+\hat{z}} = \frac{1}{N} \sum_{\lambda,\mathbf{q}} \cos(q_z c) \frac{g_{\lambda,\mathbf{q}}g_{\lambda,-\mathbf{q}}}{\hbar\Omega_{\lambda,\mathbf{q}}} \quad (6.5)$$

I thus obtain the partition function

$$Z_{\text{stat}} \approx Z_p Z_s Z_{\text{MF}} \quad (6.6)$$

where I introduced the mean-field dimer contribution

$$Z_{\text{MF}} = \left\langle T_\tau \exp \left\{ \beta J_{\text{NN}} \sum_{\mathbf{l}} (\mathbf{S}_{\mathbf{l}} \cdot \mathbf{S}_{\mathbf{l}+\hat{z}}) (\mathbf{S}_{\mathbf{l}+\hat{z}} \cdot \mathbf{S}_{\mathbf{l}+2\hat{z}}) + \beta \sum_{\mathbf{l},\mathbf{l}' \neq \mathbf{l}+\hat{z}} J_{\mathbf{l},\mathbf{l}'} [2(\mathbf{S}_{\mathbf{l}} \cdot \mathbf{S}_{\mathbf{l}+\hat{z}}) \langle \mathbf{S}_{\mathbf{l}'} \cdot \mathbf{S}_{\mathbf{l}'+\hat{z}} \rangle + 2\langle \mathbf{S}_{\mathbf{l}} \cdot \mathbf{S}_{\mathbf{l}+\hat{z}} \rangle \langle \mathbf{S}_{\mathbf{l}'} \cdot \mathbf{S}_{\mathbf{l}'+\hat{z}} \rangle] \right\} \right\rangle. \quad (6.7)$$

Z_{MF} is the underlying model for the mapping discussed in the next section. The model is one-dimensional. The net field of the second term can be described as

$$\bar{J}_{\mathbf{l}} = \sum_{\mathbf{l}' \neq \mathbf{l}+\hat{z}} J_{\mathbf{l},\mathbf{l}'} \langle \mathbf{S}_{\mathbf{l}'} \cdot \mathbf{S}_{\mathbf{l}'+\hat{z}} \rangle. \quad (6.8)$$

Its spatial dependence will be given in the ordered phase by an alternating contribution $\sim (-1)^{l_x+l_y+l_z}$.

6.2 Mapping on an effective Ising model

A strictly one-dimensional system, as described by Z_s and the contribution proportional to J_{NN} in the partition function (6.6) and the dimer part (6.7), shows no long-range order at finite temperatures due to the solitonic excitations. The appropriate solitons in a spin-Peierls state are domain-walls in between two different dimer coverings, see figure 6.1. In this picture a dimer consists of a NN pair of spins in a singlet state. A single soliton in an otherwise (dimer-) ordered chain is in reality a complicated object [102, 111]. It is spatially extended [80, 81, 84, 86] and has a spin degree of freedom together with a dispersion. In the purely magnetic and isotropic Majumdar-Gosh model [101], given by equation (3.4) with $J_z = J$, $J_{z,2} = J_2$, and $J_2 = J/2$, the dispersion has the form $J(5/4 - \cos 2k_z c)$. k_z is the wave number in units of inverse lattice spacings $1/c$ in chain direction. It has been shown [102], that the solitons yield an accurate description of the magnetic susceptibility and hence of the Hilbert space.

The dispersion of the solitons might be approximated, in general, by

$$E(k_z) = \sqrt{(E_s)^2 + (u J_{\text{NN}} \sin k_z c)^2}, \quad (6.9)$$

where E_s is the gap to solitonic excitations, J_{NN} is an effective exchange as introduced in section 6.1, u is a constant of order of unity. Only the low-energy solitons are effective in destroying the long-range dimer order, and I approximate here (6.9) by a constant $E(k_z) \equiv E_s$. I will include the spatial extent of the solitons later phenomenologically and include their spin-degree of freedom only when determining the susceptibility.

The finite temperature transition to long range order is introduced by the phonon induced interchain coupling derived in section 4.1.4. A direct coupling of the chains via magnetic exchange is also conceivable and discussed in section 6.4.1. The two configurations of coupling of dimers on neighboring chains are represented in figure 6.1 (b) and (c).

I take one of the two possible dimer configurations of the linear chain as the reference state and label every “good” dimer by +1 and every bond between two “wrong” dimers by -1; A bond between a soliton and a wrong dimer is also labeled -1 as shown in figure 6.1. Every possible soliton configuration is therefore mapped to a Ising-spin configuration living on every second bond. A similar mapping has been used recently by Mostovoy and Khomskii [108]. To obtain a mathematical description of the model I define by $\sigma_i = \pm 1$ the Ising variable on the $(2i-1)$ -th bond of a chain of length L . For this mapping I introduce a new coupling constant Δ_g . Translational invariance yields $\langle \sigma_i \rangle = \langle \sigma \rangle$ and the Hamiltonian for a single chain (the number of Ising variables is $L/2$) becomes in this approximation

$$H_{\text{Ising}} = -\frac{1}{2}E_s \sum_{i=1}^{L/2} \sigma_i \sigma_{i+1} - B \sum_{i=1}^{L/2} \sigma_i + \frac{L}{4}E_s + \frac{L}{4}\Delta_g \langle \sigma \rangle^2, \quad (6.10)$$

where I have set $B = \Delta_g \langle \sigma \rangle$. This is just the Ising Hamiltonian for a ferromagnetic spin chain in an external magnetic field B . Alternatively I can interpret equation (6.10) as an effective model for domain walls in a spin-Peierls state with a linear binding potential

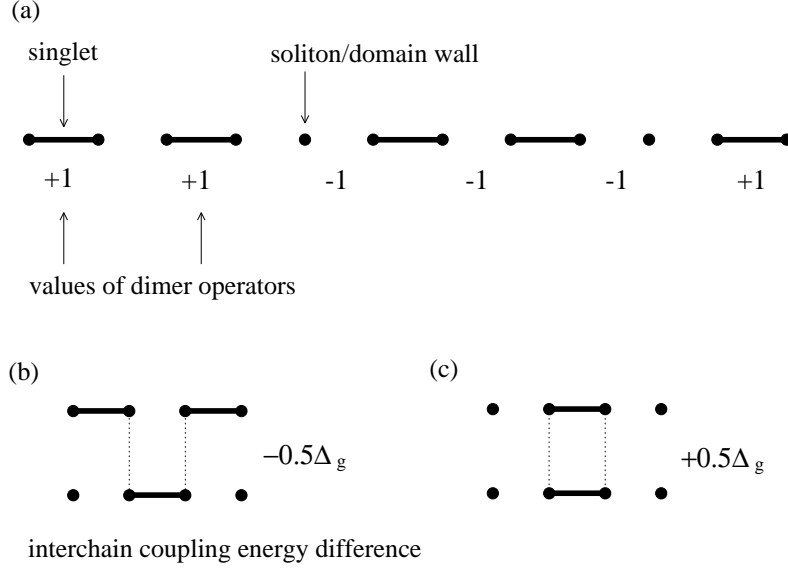


Figure 6.1: *Phenomenological picture of copper chains in CuGeO₃. (a): A soliton and an anti-soliton in a dimerized chain with the corresponding values of the dimer operators $\sigma_{i,l}$. There is one dimer operator for every pair of sites. (b) and (c): Illustration of two different dimer configurations which lead to an inter-chain coupling contribution to the energy of $\pm 0.5\Delta_g$. The origin of the coupling may be attributed to the inter-chain exchange as well as to phononic effects.*

$V(x) = B \cdot (x + 1)$ (with $x \geq 1$ being the distance in sites, not bonds) between a soliton and an anti-soliton [110].

The analogy with the mean-field model derived in section 6.1 is given by

$$\mathbf{S}_{2l_z-1} \cdot \mathbf{S}_{2l_z} \leftrightarrow \sigma_i \quad (6.11)$$

$$\langle \mathbf{S}_{2l_z-1} \cdot \mathbf{S}_{2l_z} \rangle \leftrightarrow \langle \sigma \rangle. \quad (6.12)$$

The constraint that the dimer operators only are defined on every second site is necessary to assure that no dimers can be located on adjacent bonds. The analogy for the partition function then is

$$Z_{\text{MF}} \leftrightarrow Z_{\text{Ising}} = \sum_{\{\sigma_i\}} \exp \{ -\beta H_{\text{Ising}} \}, \quad (6.13)$$

where $\sum_{\{\sigma_i\}}$ denotes the sum over all configurations of the Ising variables σ_i . For the external field the analogy is

$$B \leftrightarrow \bar{J}_{2l_z}. \quad (6.14)$$

The partition function Z_{Ising} can be obtained from equation (6.10) by the transfer matrix method. The free energy $F_{\text{Ising}} = -k_B T \ln Z_{\text{Ising}}$ is given in the thermodynamic

limit ($L \rightarrow \infty$)

$$F_{\text{Ising}} = -\frac{L}{2} k_B T \ln \lambda_0 + \frac{L}{4} \Delta_g \langle \sigma \rangle^2 \quad (6.15)$$

where

$$\lambda_0 = \cosh(\beta \Delta_g \langle \sigma \rangle) + \sqrt{\sinh^2(\beta \Delta_g \langle \sigma \rangle) + e^{-2\beta E_s}}, \quad (6.16)$$

with $\beta = 1/(k_B T)$ being the inverse temperature. From the free energy all physical quantities can be derived.

Note that Z_{Ising} is not the only contribution to the partition function Z . Clearly, the harmonic phononic part Z_p is also present as well as the part from the spin chain Z_s as can be seen from equation (6.2). The total partition function is given by the product

$$Z \approx Z_p Z_s Z_{\text{Ising}}. \quad (6.17)$$

Only the Ising part is order parameter dependent, though. Consequently Z_p and Z_s contribute a temperature dependent background to the free energy but have no influence on the transition.

6.2.1 Inclusion of the finite soliton width

The soliton width in CuGeO_3 has been determined experimentally in the incommensurate phase, where an external field induces a soliton lattice [80, 81, 84]. The width is of the order of $\xi_s \sim 10$ lattice spacings. Field theoretical approaches are compatible [121, 122] as well as DMRG studies [83, 85]. Although the soliton width has not been determined in zero magnetic field, the order of magnitude should be reliable since the field dependence of the width is not too strong [84].

In the effective Ising model the soliton width is only two lattice spacings, compare figure 6.1 and the prefactor of $L/2$ in equation (6.15). The true width may be included by imposing the additional restriction of introducing a dimer operator σ_i only on every tenth site. Depending on the external field the distance between solitons is experimentally of the order of 30 to 100 lattice sites which is also consistent with a model of dimer operators only on sites spaced by the soliton width. The free energy in such a renormalized system is given via equation (6.15), but the energy per site has to be rescaled via

$$f_{\text{site}} = \frac{F_{\text{Ising}}}{L} \approx -\frac{1}{\xi_s} k_B T \ln \lambda_0 + \frac{1}{2\xi_s} \Delta_g \langle \sigma \rangle^2. \quad (6.18)$$

I will use this equation to determine the soliton width necessary to reproduce the experimental results for CuGeO_3 and compare with the order of magnitude of $\xi_s \sim 10/c$ discussed above.

6.2.2 Excitation energies

There are two relevant excitation energies, the gap to single soliton excitations, given by E_s in equation (6.10), and the gap to triplet excitations, Δ_N , as measured in a neutron scattering experiment [28]. I now discuss the relation of Δ_N to E_s .

A triplet excitation can dissolve into a soliton/anti-soliton pair. The linear binding energy $V(x) = B \cdot (x + 1)$ in between a soliton and an anti-soliton in equation (6.10) leads to a confinement of soliton/anti-soliton pairs [123, 110]. In the model (6.10) I have neglected the kinetic energy of the single solitons, which is of order $v_s = (u J_{\text{NN}})^2/E_s$ as can be seen by expanding the dispersion (6.9) for $u J k_c \ll E_s$. (For $E_s \ll u J_{\text{NN}}$ one has $v_s = u J_{\text{NN}}$.) The energy levels of a particle in a linear confining potential are well known [124, 125, 110]. The lowest eigenstate has, in the limit $v_s \gg B$, the energy

$$\Delta_N = 2E_s + c' v_s \left(\frac{B}{v_s} \right)^{2/3}, \quad (6.19)$$

with $c' \approx 2.33$. Equation (6.19) gives then the gap to triplet excitations as a function of soliton energy E_s and the strength of the confining potential B . The mean extension of a soliton/anti-soliton pair scales like $(B/v_s)^{-1/3}$.

The order parameter $\langle \sigma \rangle$ measures the lattice distortion as becomes obvious in section 6.3.1. From the derivation of the dimerized spin model in section 2.5.1 it is then obvious that $\langle \sigma \rangle \sim \delta_J$. For a dimerized spin chain with exchange alternation δ_J it is known [14, 35] that the gap scales for $J_2/J < 0.241$ like $\sim \delta_J^{2/3}$ implying that $E_s \delta_J^{-2/3} \rightarrow 0$ for $\delta_J \rightarrow 0$. Comparison with numerical results for $J_2/J = 0.241$ give $\Delta_N \approx 2.1 J \delta_J^{2/3}$ [35]. This indicates a vanishing contribution from $2E_s$. Away from $J_2/J = 0.241$ corrections to the scaling with $\delta_J^{2/3}$ are observed [35].

The functional form of the dependence of the solitonic excitation energy E_s on δ_J , or alternatively on the dimerization order parameter $\langle \sigma \rangle$ is not known at present. It might be extracted for $J_2/J < 0.241$, in principle, from a sub-leading scaling analysis of the excitation energy

$$\Delta_N = \tilde{c} J (\delta_J)^{2/3} + 2E_s(\delta_J), \quad (6.20)$$

but this has not yet been done.

I have therefore decided to assume the functional form

$$E_s(\langle \sigma \rangle) = E_\infty + (E_0 - E_\infty) \langle \sigma \rangle^2, \quad (6.21)$$

where E_0 is the zero-temperature value of E_s and where E_∞ is the soliton energy in the disordered phase, i.e., for $T > T_{\text{SP}}$. Equation (6.21) is, in the spirit of a Landau functional (6.22), the simplest form consistent with the symmetry of $\langle \sigma \rangle$.

6.2.3 Landau expansion

I may expand the free energy (6.15) in powers of $\langle\sigma\rangle$,

$$F_{\text{Ising}} = F_0 + a(T)\langle\sigma\rangle^2 + b(T)\langle\sigma\rangle^4 + O(\langle\sigma\rangle^6). \quad (6.22)$$

Depending on the parameters I may have either a second-order phase transition with $b(T) > 0$ or a first-order phase transition with $b(T) < 0$. In the first case the transition temperature T_{SP} is given by $a(T_{\text{SP}}) = 0$ as

$$k_{\text{B}}T_{\text{SP}} = \frac{\Delta_g^2(1 + e^{-\beta E_\infty})}{2(E_0 - E_\infty)e^{-2\beta E_\infty} + \Delta_g(1 + e^{-\beta E_\infty})e^{-\beta E_\infty}}, \quad (6.23)$$

with $\beta \rightarrow 1/(k_{\text{B}}T_{\text{SP}})$. This transcendental equation takes a simple form in some limiting cases:

$$\begin{aligned} E_\infty = 0 : & \quad T_{\text{SP}} = \Delta_g^2/(\Delta_g + E_0) \\ E_\infty = E_0 : & \quad T_{\text{SP}} = \Delta_g e^{E_0/(k_{\text{B}}T_{\text{SP}})} \\ \Delta_g \rightarrow \infty : & \quad T_{\text{SP}} \rightarrow \Delta_g - E_0 + 2E_\infty \end{aligned} \quad (6.24)$$

For illustration I present in figure 6.2 (a) T_{SP} as a function of the inter-chain coupling constant Δ_g for $E_0 = 0.2$ meV. I obtain a first-order phase transition for $b(T_{\text{SP}}) < 0$, which is the case for values of E_0 larger than a certain critical value of the soliton energy E_c , which is determined from $b(T_{\text{SP}}) = 0$ as

$$E_c = E_\infty + \frac{\Delta_g^2}{T_{\text{SP}}} (1 + e^{E_\infty/T_{\text{SP}}})^2 \left(\sqrt{\frac{1 + 3e^{E_\infty/T_{\text{SP}}} + 3e^{2E_\infty/T_{\text{SP}}}}{6(1 + e^{E_\infty/T_{\text{SP}}})^2}} - \frac{1}{2} \right). \quad (6.25)$$

For a fixed transition temperature $T_{\text{SP}} = 14.15$ K and using equation (6.23), E_c and the corresponding inter-chain coupling energy Δ_g can be calculated as a function of E_∞ . The resulting phase diagram is given in figure 6.2 (b). The numerical results presented throughout this chapter are obtained within the second-order regime, indicated by the crosses in figure 6.2 (b).

6.3 Application to CuGeO_3

The effective Hamiltonian (6.10) contains three free parameters, namely E_∞ , E_0 and Δ_g . I examine two scenarios. The first is the case of $J_2/J < 0.241$ with $E_\infty = 0$. The second is the case of $0.241 < J_2/J \approx 0.35$. Then the spin system H_s has a gap even without dimerization which is included setting $E_\infty = 0.15$ meV. This corresponds to a gap in the

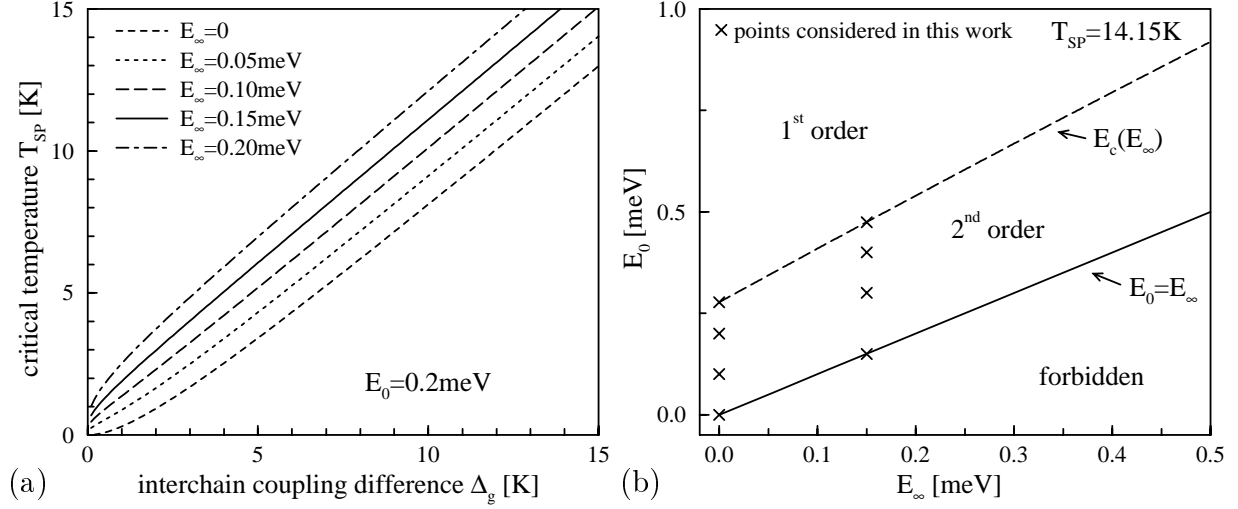


Figure 6.2: (a): Illustration of the spin-Peierls transition temperature T_{SP} for $E_0 = 0.2 \text{ meV}$ as a function of Δ_g . (b): Phase diagram as a function of E_∞ and E_0 for fixed $T_{SP} = 14.15 \text{ K}$. Only the region $E_0 > E_\infty$ is allowed (above the solid line). Above the dashed line the phase transition is of first-order, below it is of second-order. The crosses indicate the parameter values considered for comparison with CuGeO₃.

for $J_2/J < 0.241$			for $J_2/J > 0.241$		
E_0	E_∞	Δ_g	E_0	E_∞	Δ_g
0	0	1.22	0.15	0.15	1.05
0.1	0	1.31	0.3	0.15	1.2
0.2	0	1.39	0.4	0.15	1.28
0.277	0	1.45	0.474	0.15	1.33

Table 6.1: Complete sets of values in units of [meV].

disordered phase of $2E_\infty = 0.3 \text{ meV}$ [35]. For each case I consider a range of E_0 (see figure 6.2 (b)) within the second-order regime, $E_\infty \leq E_0 \leq E_c$,

$$E_\infty = 0 \text{ meV}; \quad E_0 = 0, 0.1, 0.2, 0.277 \text{ meV} \quad (6.26)$$

$$2E_\infty = 0.3 \text{ meV}; \quad E_0 = 0.15, 0.3, 0.4, 0.474 \text{ meV} \quad (6.27)$$

The largest value of E_0 for each E_∞ corresponds to $E_c(E_\infty)$, compare figure 6.2 (b). The experimental transition temperature $T_{SP} = 14.15 \text{ K}$ of CuGeO₃ then determines the coupling constant Δ_g . The complete sets of parameter values are given in table 6.3.

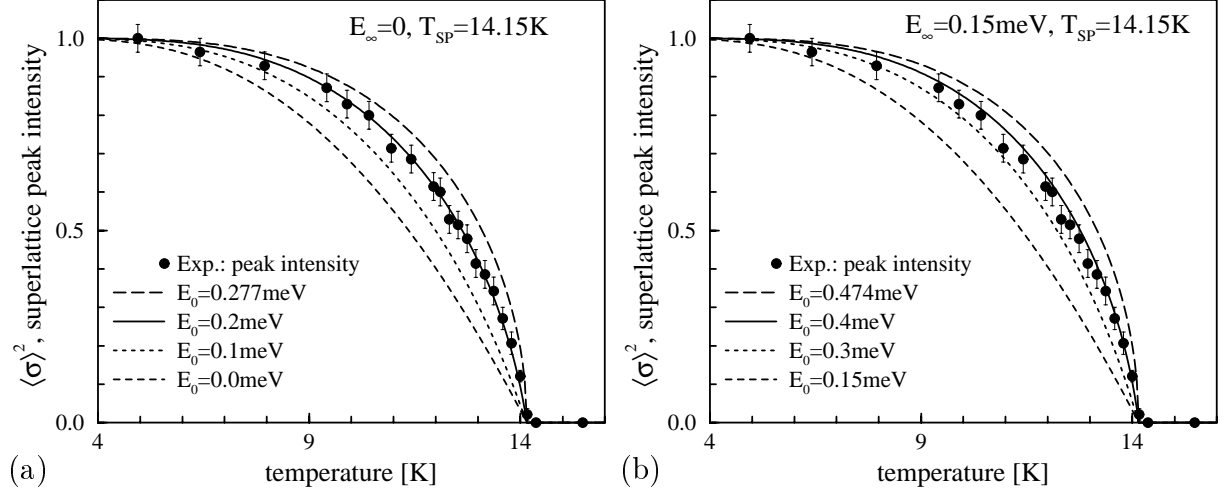


Figure 6.3: The square of the spin-singlet order parameter ($\langle\sigma\rangle^2$, lines) as a function of temperature, for two different values of E_∞ (soliton gap in the disordered phase) and several values of E_0 ($T = 0$ soliton gap). (a): $E_\infty = 0$, i.e., $E_s = E_0\langle\sigma\rangle^2$. (b): $2E_\infty = 0.3$ meV, i.e., $E_s = E_\infty + (E_0 - E_\infty)\langle\sigma\rangle^2$. For comparison I plot the measured (normalized) intensity of an additional superlattice peak (filled circles) [28].

6.3.1 Self-consistency equation

The order parameter $\langle\sigma\rangle$ is determined self-consistently as a function of temperature by setting the derivative of the free energy with respect to $\langle\sigma\rangle$ to zero,

$$\langle\sigma\rangle = \frac{\sinh(\beta\Delta_g\langle\sigma\rangle)}{2\frac{E_0-E_\infty}{\Delta_g\lambda_0}e^{-2\beta E_s} + \sqrt{\sinh^2(\beta\Delta_g\langle\sigma\rangle) + e^{-2\beta E_s}}}. \quad (6.28)$$

In figure 6.3 I show the results for $\langle\sigma\rangle^2$ as a function of temperature for the parameters given in expressions (6.26) and (6.27). I have also plotted the measured intensity of an additional superlattice peak [28], which is proportional to the square of the lattice dimerization. I have normalized the experimental data such that agreement is obtained in the low-temperature regime.

The comparison between theory and the data for CuGeO_3 does not lead to a determination of the frustration J_2/J but indicates closeness to a first-order phase transition, as can be deduced from the closeness of the experimental points in figure 6.3 to the critical curves where $E_0 \approx E_c(E_\infty)$, compare figure 6.2 (b).

6.3.2 Thermodynamics

The Ising model contribution to the entropy s and the specific heat c_V per site are obtained from the free energy (6.18) via

$$s = -\frac{\partial f_{\text{site}}}{\partial T}, \quad c_V = T \frac{\partial s}{\partial T}. \quad (6.29)$$

Entropy

In the disordered phase the entropy is (for $E_\infty = 0$) temperature independent with a value of $k_B \ln(2)$ per dimer. The value per site depends on the soliton width to be discussed below comparing specific heat data. From the derivation of the phonon-induced dimer-dimer interaction term in equation (6.7), which is described here within the Ising model, it is clear that this entropy is both phononic and magnetic. The entropy of the spin 1/2 chain is liberated only on the energy scale of the exchange J contained in the spin part of the partition function Z_s .

Note that the Ising model defined here depends on the existence of well defined dimers. For $T \rightarrow \infty$ the spin-phonon coupling has no effect and the thermodynamic properties are defined by the decoupled contributions Z_s and Z_p . The entropy contribution from the Ising system must thus vanish. This condition can be matched by describing the absence of dimers in the high temperature limit by a diverging soliton width $\lim_{T \rightarrow \infty} \xi_s \rightarrow \infty$. In the presence of dimers the entropy contribution from Z_s is overestimated, since the formation of singlets binds the spins. A better description would be given by Z_δ as defined in section 3.2 with $\langle \sigma \rangle \sim \delta_J$. The implementation can, however, not be done within this simple approach.

Specific heat

In figure 6.4 (a) I present results on $c_V(T)$ for the parameters given by expression (6.26) and in figure 6.4 (b) for the values (6.27). The plots are to be understood per site for the unrestricted model with a soliton width of $\xi_s = 2$ lattice spacings. For small soliton excitation energies the results are typically mean-field like. For values of E_0 approaching the limit of the second-order phase regime the specific heat is strongly enhanced near T_{SP} . It will diverge as the transition becomes first-order. Note that the specific heat is linear in temperature in the limit $T \rightarrow T_{\text{SP}}$ in the second order transition regime, where $E_\infty \leq E_0 < E_c$, and that the jump in the specific heat diverges as $E_0 \rightarrow E_c$ like $(E_c - E_0)^{-1}$. Right at $E_0 = E_c$ the specific heat diverges like $(T_{\text{SP}} - T)^{-1/2}$. Note that a similar divergence $\sim (T_{\text{SP}} - T)^{-0.4}$ has been reported in an early measurement for CuGeO₃ [126] though the exact value of the specific heat critical exponent for CuGeO₃ is still controversial [78, 127, 56].

In the inset of figure 6.4 I present the measured magnetic contribution to the specific heat of CuGeO₃ [56]. The lattice contribution $\sim T^3$ contained in Z_p has been subtracted. Comparing the maximum of the theoretical curves which have a shape comparable to the experiment, i.e., shown by the thick full lines in figure 6.4, the theoretical values are found to be too large by roughly a factor of 5. Introducing a soliton width of $\xi_s \approx 10$ as discussed in section 6.2.1 yields consistency. Note that Lasjaunias *et al.* [56] also find a

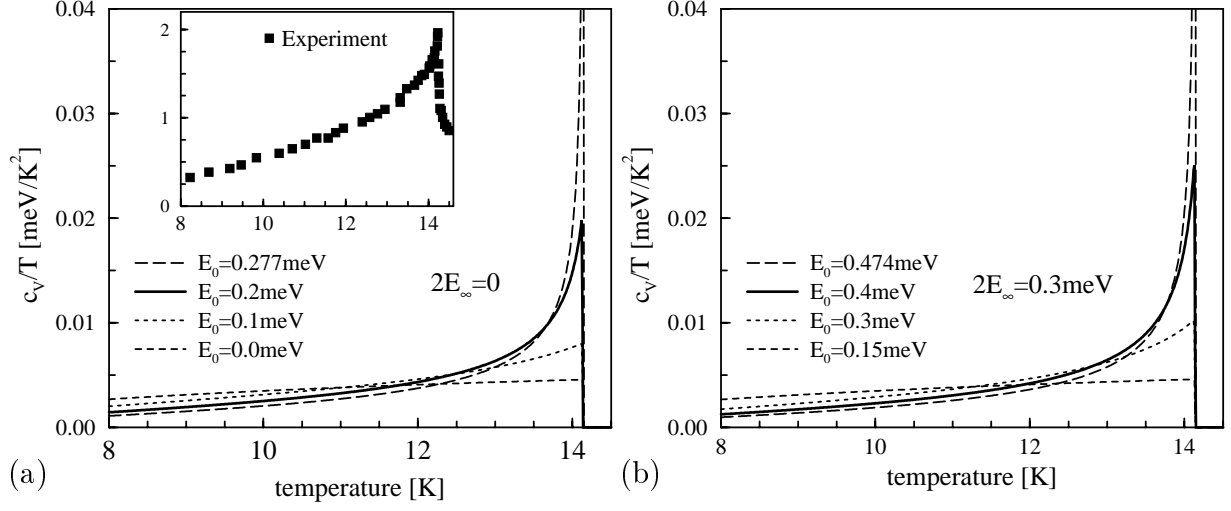


Figure 6.4: Specific heat for different parameters as a function of temperature. (a): $E_\infty = 0$. (b): $2E_\infty = 0.3$ meV. The inset in graph (a) shows the experimental data [56] for c_V/T in units of [mJ/gK²] versus T (10^{-2} meV/K² corresponds to 5.24 mJ/gK²). The lattice contribution $\sim T^3$ has been subtracted.

linear contribution $c_V \sim T$ for $T > T_{\text{SP}}$ which is readily explained as the contribution from Z_s [12].

Susceptibility

Up to now I did not take the spin-degree of freedom of the solitons into account, as they are described by the contribution Z_s of the partition function. An alternative approach is to consider the solitons as spin-1/2 objects in a nonmagnetic background of dimers [85]. Neglecting the magnetic interactions between the spins carried by the solitons, the magnetic susceptibility can be evaluated simply by Curie's law

$$\chi(T) = \frac{g^2 \mu_B^2 S(S+1)}{3k_B T} n(T) \approx 1.16 \frac{\mu_B^2}{k_B T} n(T), \quad (6.30)$$

where $\mu_B = e\hbar/(2m_e v_c)$ is the Bohr magneton, $g = 2.15$ the measured [128, 129] g-factor of the Cu^{2+} ion, $S = 1/2$, and $n(T)$ is the density of thermally activated solitons per site. Here v_c is the speed of light. $n(T)$ is obtained differentiating the free energy with respect to E_s :

$$n(T) = \frac{\partial f_{\text{site}}}{\partial E_s} = \frac{1}{\xi_s \lambda_0} \frac{e^{-2\beta E_s}}{\sqrt{\sinh^2(\beta \Delta_g \langle \sigma \rangle) + e^{-2\beta E_s}}}. \quad (6.31)$$

Above T_{SP} this expression reduces to

$$n(T > T_{\text{SP}}) = \frac{1}{\xi_s} \frac{1}{e^{\beta E_\infty} + 1}. \quad (6.32)$$

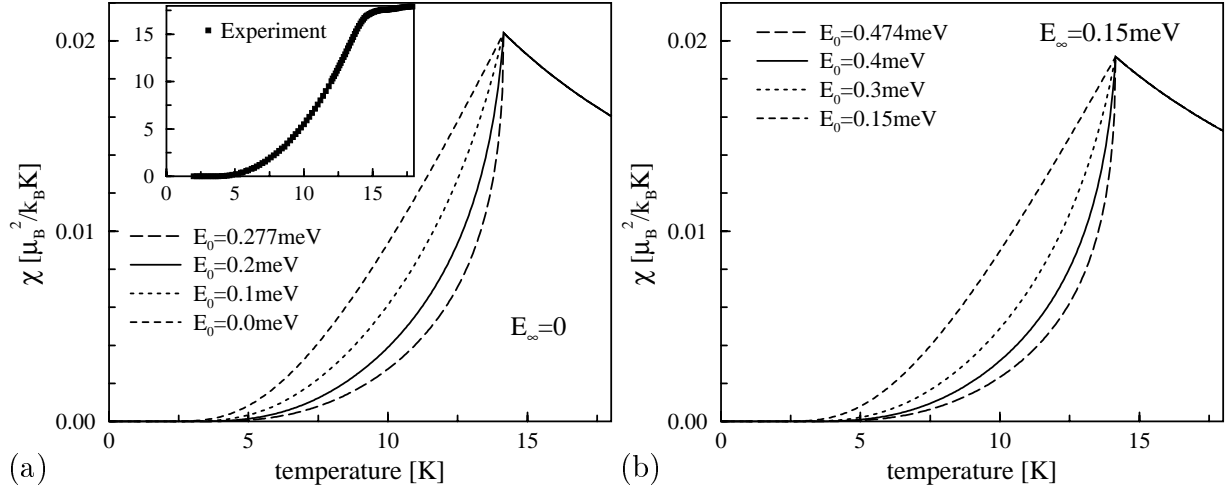


Figure 6.5: Magnetic susceptibility obtained from the simplified model of independent solitons for different parameters as a function of temperature. (a): $E_\infty = 0$. (b): $2E_\infty = 0.3 meV$. The inset in graph (a) shows the experimental data [130] of χ in units of $[10^{-9} m^3/mole]$ versus T ($0.01 \mu_B^2/k_B K$ correspond to $47.12 \cdot 10^{-9} m^3/mole$).

The results for the magnetic susceptibility are shown in figure 6.5 for the unrestricted model, where $\xi_s = 2$. The fast drop of $\chi(T)$ below T_{SP} for larger values of the soliton excitation energy E_0 is again reminiscent of the experimental data for CuGeO₃ [130]. The fast drop is a direct consequence of the opening of the spin gap. The theoretical susceptibility rises though roughly a factor of 5 higher at T_{SP} than the experimental data which might be a direct consequence of the neglected soliton dispersion (6.9). On the other hand, introducing the restriction of a soliton width of $\xi_s = 10$ as discussed in section 6.2.1 restores the consistency between experiment and theory.

Above T_{SP} the Curie-Weiss-like falloff of the susceptibility in figure 6.5 clearly indicates that in the disordered phase the appropriate description of the susceptibility is given by Z_s . Introducing the temperature dependent soliton width $\lim_{T \rightarrow \infty} \xi_s \rightarrow \infty$ discussed in connection with the entropy yields the desired high temperature description of the susceptibility entirely by Z_s .

6.3.3 Singlet-triplet gap

The gap to triplet excitations is given by equation (6.19),

$$\Delta_N = 2(E_\infty + (E_0 - E_\infty)\langle\sigma\rangle^2) + c' v_s \left(\frac{\Delta_g \langle\sigma\rangle}{v_s} \right)^{2/3}, \quad (6.33)$$

with $c' = 2.33$. I use v_s as a fit parameter to adapt $\Delta_N(T = 0)$ to the experimentally observed value of 2.4 meV. The results are given in figure 6.6, together with the measured

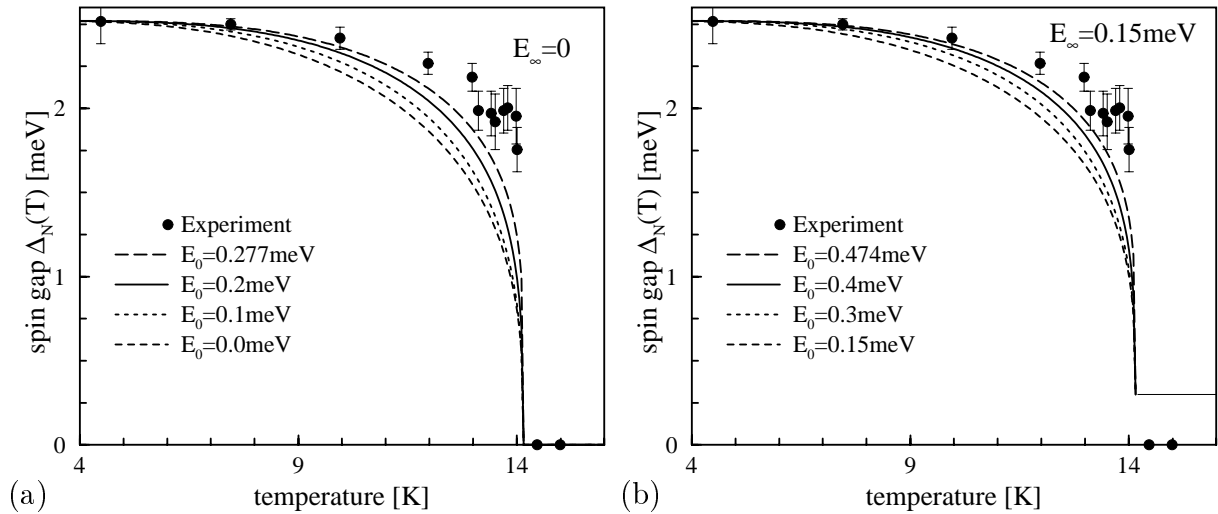


Figure 6.6: The gap to triplet excitations for several parameters as a function of temperature. (a): $E_\infty = 0$. (b): $2E_\infty = 0.3$ meV.

E_0	E_∞	Δ_g	v_s	E_0	E_∞	Δ_g	v_s
0	0	1.22	0.73	0.15	0.15	1.05	0.66
0.1	0	1.31	0.5	0.3	0.15	1.2	0.32
0.2	0	1.39	0.33	0.4	0.15	1.28	0.2
0.277	0	1.45	0.24	0.474	0.15	1.33	0.14

Table 6.2: Complete sets of values in units of [meV].

gap for CuGeO_3 [28]. For $E_\infty = 0$ the contribution from $2E_s$ is rather small.

An upper boundary for the effective nearest neighbor exchange (6.5) is obtained by

$$J_{\text{NN}} < \sum_{\lambda} \frac{2g_{\lambda, q_0}^2}{\hbar\Omega_{\lambda, q_0}} = 28 \text{ K} = 2.4 \text{ meV}, \quad (6.34)$$

where I used the values derived in chapter 2. This result can be used as an estimate for the order of magnitude of the energy scale $v_s < 3$ meV which is consistent with the fitted values given in table 6.3.3. An underestimation of v_s is also possible because the order parameter $\langle \sigma \rangle(T=0) = 1$ in the molecular-field approximation, while it might be smaller than unity for CuGeO_3 .

It should be remarked here that one-dimensional fluctuations leading to a pseudo gap above the three-dimensional transition [119, 120] may induce a value of E_∞ much larger than the one discussed for the next nearest neighbor frustration. Then the experimental spin-gap can be matched even better within this model.

6.3.4 Conclusions

In this chapter I have discussed a simple mean-field theory for spin-Peierls transitions based on the disordering of dimers by solitonic excitations. The theory allows both for a first-order and a second-order spin-Peierls transition, depending on the parameters of the model. I find that the parameters which fit experiments best indicate that CuGeO_3 is close to a first-order phase transition.

The experimental thermodynamical quantities of CuGeO_3 are well reproduced by the theory when including a phenomenological soliton width of $\xi_s \sim 10$ lattice spacings, which is in good agreement with the value given in the literature (see section 6.2.1). It is not possible to determine the magnitude of the frustration parameter J_2/J uniquely from the experimentally measured temperature dependence of the order parameter.

6.4 Appendix: discussion of related topics

In this last section of the chapter I mention a few issues related to the approach of an effective Ising model that are somewhat of less relevance for the discussion above.

6.4.1 Derivation from an electronic model

In our work given in reference [109] we have motivated the effective Ising model via a quasi one-dimensional spin model. The idea at the time was the possibility of an electronically driven transition motivated by the absence of the soft phonon in CuGeO_3 . In our latter work [70], which chapter 5 is based on, it became clear that a phonon driven transition is consistent with the central peak. As a matter of fact, the equivalence of dimer and phonon fields discussed in section 4.1.6 shows that one cannot tell apart the two systems as far as the transition is concerned. Still, there may be a direct interchain-superexchange path J_\perp contributing to the transition, which is shown here to give an effective dimer-dimer interaction equivalent to that in equation (6.7).

Mean-field theory

The effective Hamiltonian for the magnetic excitations for a 2D array of chains in the dimerized state is then [34]

$$H_{2\text{D}} = J \sum_{l_z, l_y} [\mathbf{S}_{l_z, l_y} \cdot \mathbf{S}_{l_z+1, l_y} + \alpha \mathbf{S}_{l_z, l_y} \cdot \mathbf{S}_{l_z+2, l_y}] + J_\perp \sum_{l_z, l_y} \mathbf{S}_{l_z, l_y} \cdot \mathbf{S}_{l_z, l_y+1}. \quad (6.35)$$

The inter-chain coupling having been estimated [123] to be of the order of $J_\perp \approx 0.1J$ allows for a perturbative treatment of $H_\perp = J_\perp \sum_{l_z, l_y} \mathbf{S}_{l_z, l_y} \cdot \mathbf{S}_{l_z, l_y+1}$ in the Hamiltonian (6.35). The contribution of the third dimension is of the order of $J'_\perp \approx 0.01J$ [123] and is neglected. Note that it is likely that the dispersion of the magnetic excitations are at least in part phonon induced, as can be seen from the mapping on the effective spin model in

section 4.1.4 (see also reference [67]). The value of $J_{\perp} \approx 0.1J$ may thus include already spin-phonon coupling effects.

I expand (6.35) up to second order in J_{\perp} by a standard perturbative procedure. It has been shown recently, that a molecular-field decoupling of inter-chain interactions in quasi one-dimensional systems is a good approximation in the strongly anisotropic limit [131]. One may thus decouple the operators of the first order term ($\sim J_{\perp}$) as

$$\begin{aligned} \mathbf{S}_{l_z, l_y} \cdot \mathbf{S}_{l_z, l_y+1} &\rightarrow \mathbf{S}_{l_z, l_y} \cdot \langle \mathbf{S}_{l_z, l_y+1} \rangle \\ &+ \langle \mathbf{S}_{l_z, l_y} \rangle \cdot \mathbf{S}_{l_z, l_y+1} - \langle \mathbf{S}_{l_z, l_y} \rangle \cdot \langle \mathbf{S}_{l_z, l_y+1} \rangle. \end{aligned} \quad (6.36)$$

Since no significant magnetic ordering is expected, i.e., $\langle \mathbf{S}_{l_z, l_y} \rangle \sim 0$, in the absence of an external magnetic field I will neglect this contribution.

The operator product of the second order term ($\sim J_{\perp}^2/J$) is rewritten by Lagrange's theorem.

$$\begin{aligned} (\mathbf{S}_{l_z, l_y} \cdot \mathbf{S}_{l_z, l_y+1}) (\mathbf{S}'_{l_z, l'_y+1} \cdot \mathbf{S}'_{l_z, l'_y}) &= (\mathbf{S}'_{l_z, l'_y+1} \cdot \mathbf{S}_{l_z, l_y+1}) (\mathbf{S}_{l_z, l_y} \cdot \mathbf{S}'_{l_z, l'_y}) \\ &+ (\mathbf{S}_{l_z, l_y} \times \mathbf{S}'_{l_z, l'_y+1}) (\mathbf{S}_{l_z, l_y+1} \times \mathbf{S}'_{l_z, l'_y}) \end{aligned} \quad (6.37)$$

Now a local approximation in space is applied, i.e., only regarding contributions where $l'_z = l_z$ and $l'_y = l_y$. Any spatially constant mean-field decoupling of the cross product terms of (6.37) then vanishes. The mean-field decoupling of the first term on the right hand side of equation (6.37) yields fields of the form $\langle \mathbf{S}_{l_z, l_y} \cdot \mathbf{S}_{l_z+1, l_y} \rangle$. I drop the chain index l for reasons of translational invariance across the chains and define a mean-field inter-chain Hamiltonian

$$H_{\text{mf}} = g \sum_{l_z} \left[\mathbf{S}_{l_z} \cdot \mathbf{S}_{l_z+1} \langle \mathbf{S}_{l_z} \cdot \mathbf{S}_{l_z+1} \rangle - \frac{1}{2} \langle \mathbf{S}_{l_z} \cdot \mathbf{S}_{l_z+1} \rangle^2 \right], \quad (6.38)$$

where $g \sim J_{\perp}^2/J$ is a parameter of the theory. I thus obtain an effective one-dimensional Hamiltonian.

$$H_{\text{spin}} = H_0 + H_{\text{mf}} \quad (6.39)$$

$H_0 = H_{2\text{D}} - H_{\perp}$ is the intra-chain part of the Hamiltonian (6.35). The contribution H_{mf} has essentially the same form as the phonon induced dimer-dimer interaction leading to the dimer contribution of the partition function (6.7) discussed in section 6.1.

6.4.2 Critique: RPA versus Ising

For CuGeO_3 the coupling constants $g_{\lambda, \mathbf{q}}$ have been determined explicitly at the wave vector of the spin-Peierls modulation $\mathbf{q}_0 = (\pi/a, 0, \pi/c)$ and are given in equation (20) of reference [73]. The wave vector dependence will be dominated by the polarization vectors of the four Peierls active phonon modes. When deviating from the high symmetry point \mathbf{q}_0 in the Brillouin zone all 30 modes will couple to the spin system leading to a strong dephazation

and hence to a strong suppression of $g_{\lambda,q}$. The phenomena resulting from spin-phonon coupling will thus be dominated by \mathbf{q}_0 .

For a finite number of phonons coupled to the spin system RPA becomes exact in the thermodynamic limit [116]. The physics that can be extracted from RPA are phenomena local *in reciprocal space*, in our case the collective formation of dimers with diverging correlation length. The sharp peak of $g_{\lambda,q}$ around \mathbf{q}_0 can thus be accounted for the satisfactory description of CuGeO₃ by RPA shown in chapter 5 and the mean-field approaches used in chapter 2 and discussed in section 4.1.2 [57, 63, 73].

The resulting alternating lattice distortion is the starting point for the derivation of the real-space Ising model sketched in figure 6.1. It describes local excitations *in real space*. These excitations lead to the dephazation of the dimer order and thus to the transition to the disordered phase. In this sense the spin-Peierls transition is a order-disorder transition usually approached via Ising models and consistent with the absence of phonon softening [1]. The Ising-like Landau expansion discussed in section 6.4.3 describes the pseudo-gap expected to be present in quasi-one-dimensional systems which is not accessible by the RPA or mean-field approach.

It would be interesting to combine both approaches to have a unified theory describing both the effects of the local fluctuations and the mean-field like aspects modulated with \mathbf{q}_0 . Since both approaches can be derived from the functional integral approach derived in chapter 3 and 4 this might be a promising starting point.

6.4.3 The Ising-Landau approach

I show here the derivation of an effective model which is especially of interest for the discussion of one-dimensional fluctuations leading to a pseudo gap above the three-dimensional transition [119, 120].

When deriving an effective Landau expansion in real space the notion of different phonon modes, which are by definition eigenmodes in reciprocal space (see section 2.1), loses its physical sense. I limit the treatment to one field dropping the index λ . Basis of the analysis is the cumulant expansion equations (4.42) and (4.43) in the static limit, i.e., keeping only the contribution of $\nu = 0$. In the disordered phase considered here $\tilde{\phi}_{\mathbf{q}} \equiv \phi_{\mathbf{q}}$ and I only need to consider even powers in the fields $\phi_{\mathbf{q}}$ which take over the role of the order parameter. Also, $\langle Y_{\mathbf{q}} \rangle = 0$. Performing the cumulant expansion to fourth order in the phonon fields gives the Landau-Ginzburg functional

$$\begin{aligned} \mathcal{S}_i^{(4)} = & \beta \sum_{\mathbf{q}} \Omega_{\mathbf{q}} \phi_{\mathbf{q}}^* \phi_{\mathbf{q}} + \frac{\beta^2}{2!} \sum_{\mathbf{q}} |g_{\mathbf{q}}|^2 (\phi_{-\mathbf{q}}^* + \phi_{\mathbf{q}}) (\phi_{\mathbf{q}}^* + \phi_{-\mathbf{q}}) \frac{\langle Y_{\mathbf{q}} Y_{-\mathbf{q}} \rangle}{N} \\ & + \frac{\beta^4}{4!} \sum_{\mathbf{q}_1 \mathbf{q}_2 \mathbf{q}_3} \frac{\langle \prod_{i=1}^4 Y_{\mathbf{q}_i} \rangle_{\text{cum}}}{N^2} \prod_{i=1}^4 g_{\mathbf{q}_i} (\phi_{-\mathbf{q}_i}^* + \phi_{\mathbf{q}_i}). \quad (6.40) \end{aligned}$$

The spin correlation function in the last line of equation (6.40) assures the conservation of momentum $\mathbf{q}_4 = -\mathbf{q}_1 - \mathbf{q}_2 - \mathbf{q}_3$. I have used definition (3.45) and (3.46) for the static limit of the fields and the dimer operators.

As discussed in section 6.4.2 the physics of the spin-phonon coupled system will be dominated by the wave vector of the spin-Peierls instability \mathbf{q}_0 . To obtain the local models studied in the literature one has to assume that coupling constants, phonon dispersions and dimer correlation functions are well described by expanding up to second order in $\delta\mathbf{q}$ around \mathbf{q}_0 .

$$|g_{\mathbf{q}}|^2 = |g_{\mathbf{q}_0}|^2 + \sum_{\alpha \in \{x,y,z\}} \left. \frac{\partial^2 g_{\mathbf{q}}}{\partial q_{\alpha}^2} \right|_{\mathbf{q}_0} \frac{(\delta q_{\alpha})^2}{2} + \dots \quad (6.41)$$

$$\Omega_{\mathbf{q}} = \Omega_{\mathbf{q}_0} + \sum_{\alpha \in \{x,y,z\}} \left. \frac{\partial^2 \Omega_{\mathbf{q}}}{\partial q_{\alpha}^2} \right|_{\mathbf{q}_0} \frac{(\delta q_{\alpha})^2}{2} + \dots \quad (6.42)$$

$$\langle Y_{\mathbf{q}} Y_{-\mathbf{q}} \rangle = \langle Y_{\mathbf{q}_0} Y_{-\mathbf{q}_0} \rangle + \left. \frac{\partial^2 \langle Y_{\mathbf{q}} Y_{-\mathbf{q}} \rangle}{\partial q_z^2} \right|_{\mathbf{q}_0} \frac{(\delta q_z)^2}{2} + \dots \quad (6.43)$$

The spin correlation function is only a function of q_z in the chain direction.

Usually linear terms vanish for symmetry reasons around \mathbf{q}_0 . It has been pointed out though by Lee *et al.* [119] that one has to be aware of possible linear contributions $\sim |\delta\mathbf{q}|$ from the electronic correlation function. For the approach to the isotropic Heisenberg chain discussed in section 4.3.2 the correlation function (4.94) can be expanded at finite temperatures as

$$\langle Y_{\mathbf{q}} Y_{-\mathbf{q}} \rangle \sim \chi_Y^{\text{CF}}(\mathbf{q}, 0) = -\frac{\chi_0}{k_B T} \left[1 - \chi_2 \left(\frac{v_s |q_z - \pi/c|}{2\pi k_B T} \right)^2 + \dots \right] \quad (6.44)$$

with $\chi_2 = 8.5$, compare equation (5.20). There is thus no linear term in $\delta q_z = q_z - \pi/c$.

Imposing that the spatial order parameter dependence is dominantly given by the quadratic term in equation (6.40) one can attempt to approximate the quartic term by setting the coupling constants $g_{\mathbf{q}}$ and the four-dimer correlation function $\langle \prod_{i=1}^4 Y_{\mathbf{q}_i} \rangle$ constant using their values at $\mathbf{q} = \mathbf{q}_0$. One can then transform equation (6.40) to real space. Introducing the real-space representation for the fields

$$\phi_{\mathbf{q}} = \frac{1}{\sqrt{N}} \sum_{\mathbf{l}} e^{-i\mathbf{q}\mathbf{R}_{\mathbf{l}}} e^{-i\pi l_y} \phi_{\mathbf{l}}, \quad (6.45)$$

the action $\mathcal{S}_1^{(4)}$ in equation (6.40) is transformed to:

$$\begin{aligned} \mathcal{S}_1^{(4)} = & \beta \sum_{\mathbf{l}} \Omega_{\mathbf{l}} |\phi_{\mathbf{l}}|^2 + \frac{\beta^2}{2} \sum_{\mathbf{l}} 4 |g_{\mathbf{q}_0}|^2 \frac{\langle Y_{\mathbf{q}_0} Y_{-\mathbf{q}_0} \rangle}{N} [\text{Re } \phi_{\mathbf{l}}]^2 \\ & + \frac{\beta}{2} \sum_{\mathbf{l}, \alpha} \left[\frac{\partial^2 \Omega_{\mathbf{q}}}{\partial q_{\alpha}^2} \right]_{\mathbf{q}_0} \left| \frac{\partial \phi_{\mathbf{l}}}{\partial \alpha} \right|^2 + \frac{\beta^2}{4} \sum_{\mathbf{l}, \alpha} \frac{\langle Y_{\mathbf{q}_0} Y_{-\mathbf{q}_0} \rangle}{N} \left[\frac{\partial^2 g_{\mathbf{q}}}{\partial q_{\alpha}^2} \right]_{\mathbf{q}_0} \left[\frac{\partial \text{Re } \phi_{\mathbf{l}}}{\partial \alpha} \right]^2 \\ & + \frac{\beta^2}{4} \sum_{\mathbf{l}} |g_{\mathbf{q}_0}|^2 \left[\frac{\partial^2 \langle Y_{\mathbf{q}} Y_{-\mathbf{q}} \rangle}{N \partial q_z^2} \right]_{\mathbf{q}_0} \left[\frac{\partial \text{Re } \phi_{\mathbf{l}}}{\partial z} \right]^2 + \frac{\beta^4}{24} \sum_{\mathbf{l}} \frac{\langle Y_{\mathbf{q}_0}^4 \rangle}{N} |g_{\mathbf{q}_0}|^4 [\text{Re } \phi_{\mathbf{l}}]^4 + \dots \end{aligned} \quad (6.46)$$

This is in principle the Landau functional treated in the Literature [87, 118, 120]. Note that the contributions for $\text{Re } \phi_l$ and $\text{Im } \phi_l$ are decoupled. When considering incommensurability it is essential to expand equations (6.41) – (6.43) to fourth order in q_z to assure stability. Real and imaginary part then are coupled reflecting the order parameter to acquire two components in the incommensurate case.

Given the significance of the approximations made it is tedious to derive ab initio values for the coefficients. They have to be determined phenomenologically. The derivation of the functional from the microscopic model supports its physical relevance, though.

Bibliography

- [1] A. D. Bruce and R. A. Cowley, *Structural Phase Transitions* (Taylor and Francis, London, 1981).
- [2] N. W. Ashcroft and N. D. Mermin, *Solid State Physics* (Saunders College Publishing, Fort Worth, 1976).
- [3] E. Pytte, Phys. Rev. B **10**, 2039 and 4637 (1974).
- [4] J. W. Negele and H. Orland, *Quantum Many-Particle Systems* (Addison-Wesley, New York, 1988).
- [5] T. Lorenz, U. Ammerahl, T. Auweiler, B. Büchner, A. Revcolevschi, and G. Dhalenne, Phys. Rev. B **55**, 5914 (1997).
- [6] M. Braden, E. Ressouche, B. Büchner, R. Keßler, G. Heger, G. Dhalenne, and A. Revcolevschi, Phys. Rev. B **57**, 11497 (1998).
- [7] H. Bethe, Z. Phys. **71**, 205 (1931).
- [8] M. Karbach and G. Müller, Comp. in Phys. **11**, 36 (1997).
- [9] L. Hulthén, Ark. Mat., Astron. Fys. **26A 11**, 1 (1938).
- [10] E. F. Fradkin, *Field Theories of Condensed Matter Systems* (Addison-Wesley, New York, 1991).
- [11] M. Karbach and G. Müller, Comp. in Phys. **12**, 565 (1998).
- [12] A. Klümper, Eur. Phys. J. B **5**, 677 (1998).
- [13] L. N. Bulaevskii, Sov. Phys. JETP **17**, 684 (1963).
- [14] M. C. Cross and D. S. Fischer, Phys. Rev. B **19**, 402 (1979).
- [15] Z. G. Soos, S. Kuwajima, and J. E. Mihalick, Phys. Rev. B **32**, 3124 (1985).
- [16] T. Barnes, J. Riera, and D. A. Tennant, Phys. Rev. B **59**, 11384 (1999).

-
- [17] R. J. Baxter, *Exactly Solved Models in Statistical Mechanics* (Academic Press, London, 1982).
- [18] J. L. Black and V. J. Emery, *Phys. Rev. B* **23**, 429 (1981).
- [19] M. Hase, I. Terasaki, and K. Uchinokura, *Phys. Rev. Lett.* **70**, 3651 (1993).
- [20] J. E. Lorenzo, K. Hirota, G. Shirane, J. M. Tranquada, M. Hase, K. Uchinokura, H. Kojima, I. Tanaka, and Y. Shibuya, *Phys. Rev. B* **50**, 1278 (1994).
- [21] M. Nishi, O. Fujita, and J. Akimitsu, *Phys. Rev. B* **50**, 6508 (1994).
- [22] J. P. Pouget, L. P. Regnault, M. Aïn, B. Hennion, J. P. Renard, P. Veillet, G. Dhalenne, and A. Revcolevschi, *Phys. Rev. Lett.* **72**, 4037 (1994).
- [23] J. Riera and A. Dobry, *Phys. Rev. B* **51**, 16098 (1995).
- [24] K. Fabricius, A. Klümper, U. Löw, B. Büchner, T. Lorenz, G. Dhalenne, and A. Revcolevschi, *Phys. Rev. B* **57**, 1102 (1998).
- [25] M. Arai, M. Fujita, M. Motokawa, J. Akimitsu, and S. M. Bennington, *Phys. Rev. Lett.* **77**, 3649 (1996).
- [26] J. P. Schoeffel, J. P. Pouget, G. Dhalenne, and A. Revcolevschi, *Phys. Rev. B* **53**, 14971 (1996).
- [27] K. Hirota, G. Shirane, Q. J. Harris, Q. Feng, R. J. Birgeneau, M. Hase, and K. Uchinokura, *Phys. Rev. B* **52**, 15412 (1995).
- [28] M. C. Martin, G. Shirane, Y. Fujii, M. Nishi, O. Fujita, J. Akimitsu, M. Hase, and K. Uchinokura, *Phys. Rev. B* **53**, R14713 (1996).
- [29] J. G. Lussier, S. M. Coad, D. F. McMorrow, and D. M. Paul, *J. Phys.: Condens. Mat.* **8**, L59 (1996).
- [30] L. P. Regnault, M. Aïn, B. Hennion, G. Dhalenne, and A. Revcolevschi, *Phys. Rev. B* **53**, 5579 (1996).
- [31] P. H. M. van Loosdrecht, J. P. Boucher, and G. Martinez, *Phys. Rev. Lett.* **76**, 311 (1996).
- [32] G. Els, P. H. M. van Loosdrecht, P. Lemmens, H. Vonberg, G. Güntherrodt, G. S. Uhrig, O. Fujita, J. Akimitsu, G. Dhalenne, and A. Revcolevschi, *Phys. Rev. Lett.* **79**, 5138 (1997).
- [33] T. Sekine, H. Kuroe, J. i. Sasaki, Y. Sasago, N. Koide, K. Uchinokura, and M. Hase, *J. Phys. Soc. Jpn.* **67**, 1140 (1998).

-
- [34] G. Castilla, S. Chakravarty, and V. J. Emery, Phys. Rev. Lett. **75**, 1823 (1995).
- [35] R. Chitra, S. Pati, H. R. Krishnamurthy, D. Sen, and S. Ramasesha, Phys. Rev. B **52**, 6581 (1995).
- [36] V. N. Muthukumar, C. Gros, W. Wenzel, R. Valentí, P. Lemmens, B. Eisener, G. Güntherodt, M. Weiden, C. Geibel, and F. Steglich, Phys. Rev. B **54**, R9635 (1996).
- [37] G. S. Uhrig and H. J. Schulz, Phys. Rev. B **54**, R9624 (1996).
- [38] W. Brenig, Phys. Rev. B **56**, 14441 (1997).
- [39] G. Bouzerar, A. P. Kampf, and G. I. Japaridze, Phys. Rev. B **58**, 3117 (1998).
- [40] M. Braden, G. Wilkendorf, J. Lorenzana, M. Aïn, G. J. McIntyre, M. Behruzi, G. Heger, G. Dhalenne, and A. Revcolevschi, Phys. Rev. B **54**, 1105 (1996).
- [41] H. Völlenkle, A. Wittmann, and H. Nowotny, Monatsh. Chem. **98**, 1352 (1967).
- [42] Y. Fagot-Revurat, H. Horvatić, C. Berthier, J. P. Boucher, P. Ségransan, G. Dhalenne, and A. Revcolevschi, Phys. Rev. B **55**, 2964 (1997).
- [43] W. Geertsma and D. I. Khomskii, Phys. Rev. B **54**, 3011 (1996).
- [44] M. Braden, B. Hennion, W. Reichardt, G. Dhalenne, and A. Revcolevschi, Phys. Rev. Lett. **80**, 3634 (1998).
- [45] H. Takahashi, N. Môri, O. Fujita, J. Akimitsu, and T. Matsumoto, Sol. State Comm. **95**, 817 (1995).
- [46] M. Nishi, O. Fujita, J. Akimitsu, K. Kakurai, and Y. Fujii, Phys. Rev. B **52**, R6959 (1995).
- [47] B. Büchner, U. Ammerahl, T. Lorenz, W. Brenig, G. Dhalenne, and A. Revcolevschi, Phys. Rev. Lett. **77**, 1624 (1996).
- [48] T. Lorenz, Ph.D. thesis, Universität zu Köln, 1998.
- [49] M. Nishi, K. Kakurai, Y. Fujii, M. Yethiraj, D. A. Tennant, S. E. Nagler, J. A. Fernandez-Baca, O. Fujita, and J. Akimitsu, Physica C **241-243**, 537 (1998).
- [50] B. Büchner, H. Fehske, A. P. Kampf, and W. Wellein, Physica B **259-261**, 956 (1999).
- [51] M. Born and K. Huang, *Dynamical Theory of Crystal Lattices* (Oxford University Press, Oxford, 1968).
- [52] H. T. Stokes and D. M. Hatch, *Isotropy Subgroups of the 230 Crystallographic Space Groups* (World Scientific, Singapore, 1988).

-
- [53] M. Braden *et al.*, to be published.
- [54] In the literature the coupling constants often are given with respect to normal coordinates, i.e., set $g_{\text{norm}} = \sqrt{(2\Omega_{\lambda,\mathbf{q}})/\hbar} g_{\lambda,\mathbf{q}}$ in Eq. (2.19). In Eq. (2.25) the transition temperature then is $T_{\text{SP}} \sim g_{\text{norm}}^2/\Omega^2$, consistent with the result of Cross and Fisher [14].
- [55] L. D. Landau and E. M. Lifschitz, *Statistical Mechanics* (Pergamon Press, Oxford, 1988).
- [56] J. C. Lasjaunias, P. Monceau, G. Reményi, S. Sahling, G. Dhalenne, and A. Revcolevschi, *Sol. State Comm.* **101**, 677 (1997).
- [57] A. Klümper, R. Raupach, and F. Schönfeld, *Phys. Rev. B* **59**, 3612 (1999).
- [58] D. Augier and D. Poilblanc, *Eur. Phys. J. B* **1**, 19 (1998).
- [59] G. Wellein, H. Fehske, and A. P. Kampf, *Phys. Rev. Lett.* **81**, 3956 (1998).
- [60] G. S. Uhrig, *Phys. Rev. Lett.* **79**, 163 (1997).
- [61] S. Bräuninger, U. Schwarz, M. Hanfland, T. Zhou, R. K. Kremer, and K. Syassen, *Phys. Rev. B* **56**, R11357 (1997).
- [62] M. Braden, B. Büchner, S. Klotz, W. G. Marschall, J. S. Loveday, M. Behruzi, and G. Heger, preprint (1999).
- [63] R. Raupach, A. Klümper, and F. Schönfeld, preprint (1999).
- [64] H. Winkelmann, E. Gamper, B. Büchner, M. Braden, A. Revcolevschi, and G. Dhalenne, *Phys. Rev. B* **51**, 12884 (1995).
- [65] A. W. Sandvik, R. R. P. Singh, and D. K. Campbell, *Phys. Rev. B* **56**, 14510 (1997).
- [66] M. Poirier, M. Castonguay, A. Revcolevschi, and G. Dhalenne, *Phys. Rev. B* **52**, 16058 (1995).
- [67] G. S. Uhrig, *Phys. Rev. B* **57**, R14004 (1998).
- [68] A. W. Sandvik and D. K. Campbell, preprint, cond-mat/9902230 (1999).
- [69] R. W. Kühne and U. Löw, preprint, cond-mat/9905337 (1999).
- [70] C. Gros and R. Werner, *Phys. Rev. B* **58**, R14677 (1998).
- [71] C. Gros, W. Wenzel, A. Fledderjohann, P. Lemmens, M. Fischer, G. Güntherodt, M. Weiden, C. Geibel, and F. Steglich, *Phys. Rev. B* **55**, 15048 (1997).
- [72] H. J. Schulz, *Phys. Rev. B* **34**, 6372 (1986).

-
- [73] R. Werner, C. Gros, and M. Braden, *Phys. Rev. B* **59**, 14356 (1999).
- [74] W. H. Louisell, *Quantum statistical properties of radiation* (John Wiley & Sons, New York, 1973).
- [75] H. Kleinert, *Path Integrals in Quantum Mechanics, Statistics, and Polymer Physics* (World Scientific, Singapore, 1990).
- [76] G. D. Mahan, *Many-Particle Physics* (Plenum Press, New York, 1981).
- [77] A. L. Fetter and J. D. Walecka, *Quantum Theory of Many-Particle Systems* (McGraw-Hill, New York, 1971).
- [78] X. Liu, J. Wosnitza, H. v. Löhneysen, and R. K. Kremer, *Z. Phys. B* **98**, 163 (1995).
- [79] M. D. Lumsden, B. D. Gaulin, H. Dabkowska, and M. L. Plumer, *Phys. Rev. Lett.* **76**, 4919 (1996).
- [80] V. Kiryukhin, B. Keimer, J. P. Hill, and A. Vigilante, *Phys. Rev. Lett.* **76**, 4608 (1996).
- [81] V. Kiryukhin, B. Keimer, J. P. Hill, S. M. Coad, and D. M. Paul, *Phys. Rev. B* **54**, 7269 (1996).
- [82] Y. Fagot-Revurat, H. Horvatić, C. Berthier, P. Ségransan, G. Dhalenne, and A. Revcolevschi, *Phys. Rev. Lett.* **76**, 4608 (1996).
- [83] T. Lorenz, B. Büchner, P. H. M. van Loosdrecht, F. Schönfeld, G. Chouteau, G. Dhalenne, and A. Revcolevschi, *Phys. Rev. Lett.* **81**, 148 (1998).
- [84] H. Horvatić, Y. Fagot-Revurat, C. Berthier, G. Dhalenne, and A. Revcolevschi, preprint, cond-mat/9812370 (1998).
- [85] F. Schönfeld, G. Bouzerar, G. S. Uhrig, and E. Müller-Hartmann, *Eur. Phys. J. B* **5**, 521 (1998).
- [86] G. S. Uhrig, F. Schönfeld, J. P. Boucher, and M. Horvatić, preprint, cond-mat/9902272 (1999).
- [87] S. M. Bhattacharjee, T. Nattermann, and C. Ronnewinkel, *Phys. Rev. B* **58**, 2658 (1998).
- [88] H. Fröhlich, *Phys. Rev.* **79**, 845 (1950).
- [89] J. Voit, *Eur. Phys. J. B* **5**, 505 (1998).
- [90] H. J. Schulz, cond-mat/9807366 (1998), lecture notes following the summer school lectures in Chia Laguna, Italy, September 1997.

-
- [91] M. J. Rice and S. Strässler, *Sol. State Comm.* **13**, 125 (1973).
- [92] S. T. Chui, T. M. Rice, and C. M. Varma, *Sol. State Comm.* **15**, 155 (1974).
- [93] M. C. Leung, *Phys. Rev. B* **11**, 4272 (1975).
- [94] N. Macris and C.-A. Piguët, *J. Phys. A* in print (1999), preprint, cond-mat/9811376.
- [95] R. L. Stratonovich, *Dokl. Akad. Nauk SSSR* **115**, 1097 (1957).
- [96] R. L. Stratonovich, *Sovjet Phys. – Doklady* **2**, 416 (1958), engl. transl.
- [97] J. Hubbard, *Phys. Rev. Lett.* **3**, 77 (1958).
- [98] R. Kubo, *J. Phys. Soc. Jpn.* **17**, 1100 (1962).
- [99] H. E. Stanley, *Introduction to Phase Transitions and Critical Phenomena* (Oxford University Press, Oxford, 1971).
- [100] G. Beni and P. Pincus, *J. Chem. Phys.* **57**, 72 (1972).
- [101] C. K. Majumdar, *J. Phys. C* **3**, 911 (1970).
- [102] B. S. Shastry and B. Sutherland, *Phys. Rev. Lett.* **47**, 964 (1981).
- [103] K. Fabricius and U. Löw, *Phys. Rev. B* **57**, 13371 (1998).
- [104] C. H. Mak, R. Egger, and H. Weber-Gottschick, *Phys. Rev. Lett.* **81**, 4533 (1998).
- [105] A. M. Tsvelik, *Phys. Rev. B* **45**, 486 (1992).
- [106] J. Zang, A. R. Bishop, and D. Schmeltzer, *Phys. Rev. B* **52**, 6723 (1995), and *Phys. Rev. B* **54**, 9556 (1996).
- [107] F. D. M. Haldane, *Phys. Rev. B* **25**, 4925 (1981).
- [108] M. Mostovoy and D. I. Khomskii, *Z. Phys. B* **103**, 209 (1997).
- [109] R. Werner and C. Gros, *Phys. Rev. B* **57**, 2897 (1998).
- [110] I. Affleck, in *Dynamic Properties of Unconventional Magnetic Systems* (Kluwer Academic Publishers, Dordrecht, 1998), p. 123.
- [111] H.-J. Mikeska and M. Steiner, *Ann. Phys.* **40**, 191 (1991).
- [112] M. Abramovitz and I. Stegun, *Handbook of Mathematical Functions* (Dover Publications, New York, 1972).
- [113] J. A. Hertz, *Phys. Rev. B* **14**, 1165 (1976).

-
- [114] D. A. Tennat, R. A. Cowley, S. E. Nagler, and A. M. Tsvetik, Phys. Rev. B **52**, 13368 (1995).
- [115] M. Braden, private communication.
- [116] U. Brandt and H. Leschke, Z. Phys. **271**, 295 (1974).
- [117] A. Fledderjohann and C. Gros, Europhys. Lett. **37**, 189 (1997).
- [118] R. H. McKenzie, Phys. Rev. B **51**, 6249 (1995).
- [119] P. A. Lee, T. M. Rice, and P. W. Anderson, Phys. Rev. Lett. **31**, 462 (1973).
- [120] R. H. McKenzie, Phys. Rev. B **52**, 16428 (1995).
- [121] A. Dobry and J. A. Riera, Phys. Rev. B **56**, R2912 (1997).
- [122] J. Zang, S. Chakravarty, and A. R. Bishop, Phys. Rev. B **55**, R14705 (1997).
- [123] D. I. Khomskii, W. Geertsma, and M. Mostovoy, Czech. Journ. of Phys. **46**, 3239 (1996).
- [124] L. N. Bulaevskii, E. L. Nagaev, and D. I. Khomskii, Sov. Phys. JETP **27**, 836 (1968).
- [125] A change of variable $x \rightarrow B^{1/(2+\gamma)}x$ for the stationary Schrödinger equation $-\Psi''(x) + B|x|^\gamma\Psi(x) = E\Psi(x)$ leads to $E \sim B^{2/(2+\gamma)}$. Here $\gamma = 1$.
- [126] S. Sahling, J. C. Lasjaunias, P. Monceau, and A. Revcolevschi, Sol. State Comm. **92**, 423 (1994).
- [127] M. Weiden, J. Köhler, G. Sparn, M. Köppen, M. Lang, C. Geibel, and F. Steglich, Z. Phys. B **98**, 167 (1995).
- [128] B. Pilawa, J. Phys.: Condens. Mat. **9**, 3779 (1997).
- [129] A. K. Hassan, L. A. Pardi, G. B. Martins, G. Cao, and L.-C. Brunel, Phys. Rev. Lett. **80**, 1984 (1998).
- [130] V. N. Muthukumar, C. Gros, R. Valentí, M. Weiden, C. Geibel, F. Steglich, P. Lemmens, M. Fischer, and G. Güntherodt, Phys. Rev. B **55**, 5944 (1997).
- [131] K. M. Kojima *et al.*, Phys. Rev. Lett. **78**, 1787 (1997).